2016

A Theoretical Study of Polymer based Drug Delivery Systems

Ebtisam Abdullatif Aldaais
University of South Carolina

A Theoretical Study of Polymer Based Drug Delivery Systems

by

Ebtisam Abdullatif Aldaais

Bachelor of Science
King Faisal University 1999

Master of Science
University of South Carolina 2012

Submitted in Partial Fulfillment of the Requirements

for the Degree of Doctor of Philosophy in

Biomedical Engineering

College of Engineering and Computing

University of South Carolina

2016

Accepted by:

Mark J. Uline, Major Professor

Tarek Shazly, Committee Member

Melissa A. Moss, Committee Member

David Tedeschi, Committee Member

Lacy Ford, Senior Vice Provost and Dean of Graduate Studies

Dedication

I dedicate my dissertation work to my late father who passed away 11 years ago, yet whose encouraging words have remained to be my inspiration to complete this work. I am indebted to the foundation he has laid in my life and am grateful for his love and faith in me.

I also dedicate my dissertation to my husband along with our four children: Shahd, Abdulaziz, Nayef and Saud. My loving husband has been a pillar of strength and encouragement throughout my academical journey. My daughter, Shahd, has particularly been the carrier of many family responsibilities to relieve the pressure on me, which she has done without complaint. She is more than a just daughter to me, even a friend.

Acknowledgments

I would like to express my gratitude to my advisor Dr. Mark Uline who has been a source of constant advice to me in the development of this Ph.D., and to whom I will continue to seek input from in my future research. He has been exceedingly generous with his time and expertise in the process of developing this dissertation.

I am also thankful to my committee members: Prof. David Tedeschi, Dr. Melissa Moss, and Dr. Tarek Shazly. I thank Prof. Tedeschi who was my advisor at the Masters level and has continued to be a source of wisdom and counsel. Thanks must also be given to Dr. Moss, who has been my program director for the four years I have spent in the department, as well as Dr. Shazly, the graduate director. They have both helped me navigate through a number of situations during that time. Thank you for allowing me to continue my research and to make all assistance available to me.

I also wish to thank my group of colleagues who have been a source of vibrant discussions and have become my friends. I wish to express my thanks to my supportive family: my mother, mother in law, brothers and sisters who kept me always in their prayers. Lastly, I am grateful to my husband and my children: my daughter, Shahd, and my three sons, Abdulaziz, Nayef and Saud for the unceasing encouragement, support and attentiveness.

Abstract

Polymer nanostructured materials for drug delivery applications have witnessed tremendous progress in recent years due to their vast potential. One-end-grafted polymers can form grafted micelles with specific mechanical properties. Biological conditions can alter these properties resulting in the protection or release of drugs. Charged surfactants can also form micelles in an aqueous solution, which can also be manipulated through special conditions. On the micellar surface, self-organized polyelectrolytes can be stimulated to extend their attached ligands and thus increase the probability of binding to targeted receptors. This thesis focuses on modeling polymer-based drug delivery systems by studying the physical interactions between polymer segments under several biological conditions.

Temperature, pH, salt concentrations, electrostatic charges and other biological conditions have been used as stimuli for polymer-based drug delivery applications. Different stimuli trigger multiple physical interactions (e.g. steric, van der Waals and electrostatic interactions), which are coupled with each other. The complex coupling between the physical interactions is studied by modeling thermodynamic systems composed of grafted polymers in a biological solution.

A cubic lattice geometry has been used for modeling all studied thermodynamic systems. For each model, polymer self-organization is determined by generalizing a molecular theory based on a mean-field approach. These molecular theories determine the molecular organizations and the polymers aggregations in one or three-dimensional (1D or 3D) calculations. The theories are shown to form a design guideline for the creation of therapeutic polymer-based drug delivery devices.

Table of Contents

List of Tables

List of Figures

Chapter 1

Introduction

1.1 Polymers

A polymer or a *macromolecule* is a large size molecule that can be described as a chain of covalently bonded elementary units called *monomers*. These *monomers* can be joined in a simple linear skeletal structure or a more complex non-linear skeletal structure (see Figure 1.1). For example, *Cyclic polymers* have no ends, *Branched polymers* have side chains, and *Network polymers* have three-dimensional structures where each chain is connected to the others by an arrangement of junction points. In this study, we focus on modeling polymers with linear skeletal structures only.

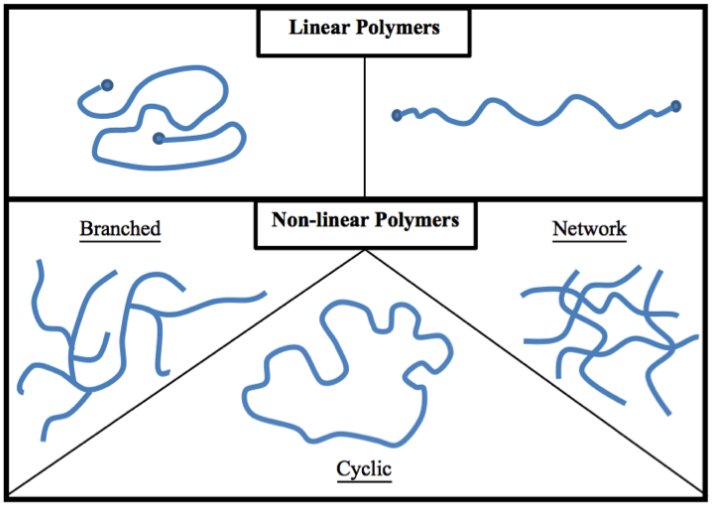

Figure 1.1: The linear and non-linear skeletal structures of polymers.

Polymers are also characterized according to their internal structure. *Homopoly-*

mers have a structure represented by repetition of a single monomer A. *Copolymers* are macromolecules that contain two different repeated units (A and B). Copolymers can be further categorized into three combinational forms: textitalternating, *random*, or *block* (see Figure 1.2). Differences in the arrangement of the bonded units give rise to major differences in properties of the copolymers. The properties of polymers can thus be manipulated for specific applications [13].

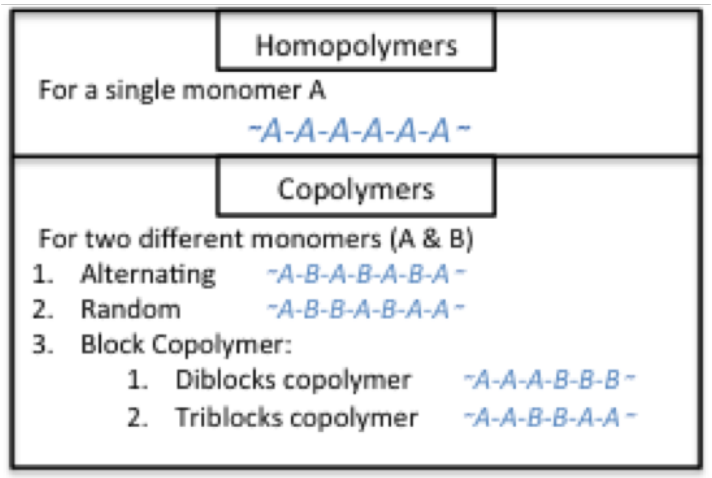

Figure 1.2: Characterizing polymers according to their internal structure.

A single polymer can adopt many different configurations. Each polymer configuration represents a spatial structure determined by the relative location of all the monomer units. Which configuration the polymer adopts depends on three characteristics: flexibility of the chain, interactions between the polymer segments on the chain, and interaction between the chain and the surroundings including other polymer segments.

The flexibility of a polymer is determined by the nature of its conformations, or to the relatively unhindered rotations around carbon-carbon single bonds in the polymer backbone. The ease of rotation is described by the energy spectrum of the polymer. Each configuration has a specific potential energy as shown on the energy spectrum graph for polyethylene (Figure 1.3).

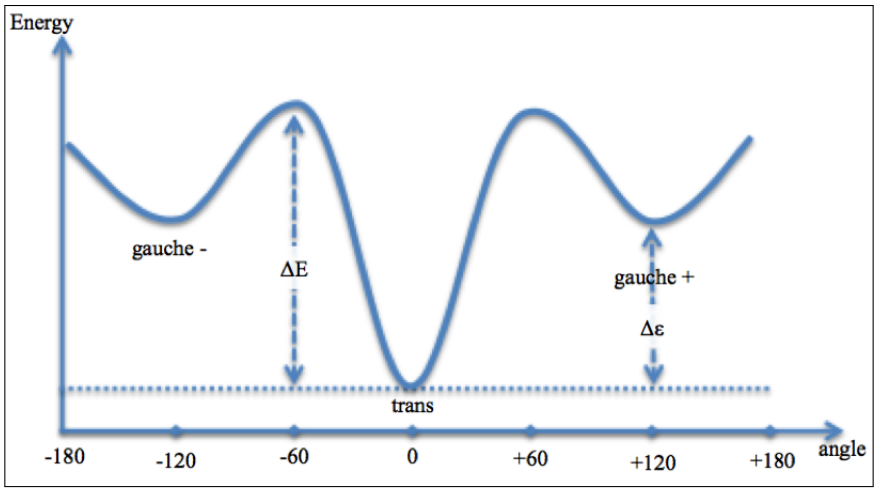

Figure 1.3: The energy spectrum of the three principle conformations.

There are three minima corresponding to three principle conformations: *trans*, *gauche*$^+$, and *gauche*$^-$ [1]. $\Delta\varepsilon$ represents the energy difference between the minima. ΔE represents the energy barrier that separates the minima. When the energy difference between minima, $\Delta\varepsilon$, is smaller than the thermal energy, K_BT, the chain is considered to be highly flexible [16] (meaning that there is not a preference conformation). When $\Delta\varepsilon > K_BT$, the trans state will be energetically more favorable and the chain will be rigid. For a chain with total length L, and degree of polymerization N [2], the flexibility parameter x is given by:

$$x = \frac{l_p}{L} \cong \frac{1}{N}\exp(\frac{\Delta\varepsilon}{K_BT}) \quad [3]$$

where l_p is called the *persistence length*. The persistence length is a characteristic length quantifying the chain flexibility.

[1] Trans state of the torsion angle $\phi_i = 0°$ represents the lowest energy state between three neighboring carbon atoms. Gauche ($\pm$) states correspond to the torsion angle $\phi_i = \pm 120°$ [44].

[2] The degree of polymerization is the number of monomer units on a polymer chain.

[3] Notice the usage of the following signs: 1- ($=$) sign indicates exact equality including all numerical coefficients. 2- ($\cong$) sign states only a scaling law with all dimensional factors, and ignoring numerical coefficients. 3- ($\sim$) sign stresses only the power law without taking into account the dimensional factors or the numerical coefficients.

There can be either attractive or repulsive interactions between the polymer segments from the same chain, different chains, and the surrounding molecules, such as solvent molecules. These interactions, such as electrostatic, van der Waals, and steric interactions, affect the polymer configurations. [1] We will use statistical mechanics to predict these configurations.

1.2 Polymer's conformational structure

The total length of an unfolded polymer chain with a polymerization number N, is $L = Nb$, where b is the length of the chemical bond between two monomers and is independent of the chemical structure of the solvent [13]. The average distance between two ends of a polymer chain over all the possible conformational states of that polymer is called the root-mean-squared-end-to-end distance of a polymer chain $R = \sqrt{\left\langle \mathbf{R}^2 \right\rangle} = \sqrt{\langle \mathbf{R} \cdot \mathbf{R} \rangle}$, where $\mathbf{R}$ is the end-to-end vector. The value of this parameter depends on the configurational structure of the chain, where it increases as the chain stretches and decreases when the chain is compressed. Chain configurations depend on the interactions between the neighboring monomers, *short-ranged interferences*, and monomers separated by large distances, *long-ranged interferences* (see Figure 1.4).

Numerous interferences affect the polymer configurations and accordingly its self-energy. In a simple statistical model, the long-ranged interactions between the far apart monomers in the chain are ignored even if they approach each other in space. This is called an *Ideal Chain*, and can be modeled via the *Random Walk* lattice model. In the Random Walk lattice model the next step may proceed toward any of the nearest neighbor lattice sites with equal statistical probabilities (Figure 1.5 (A)). The mean-squared-end-to-end distance of an Ideal chain is linearly related to its polymerization number N. The universal relation for a Random Walk on a periodic

[1] We will spend some time talking about each of these interactions in details.

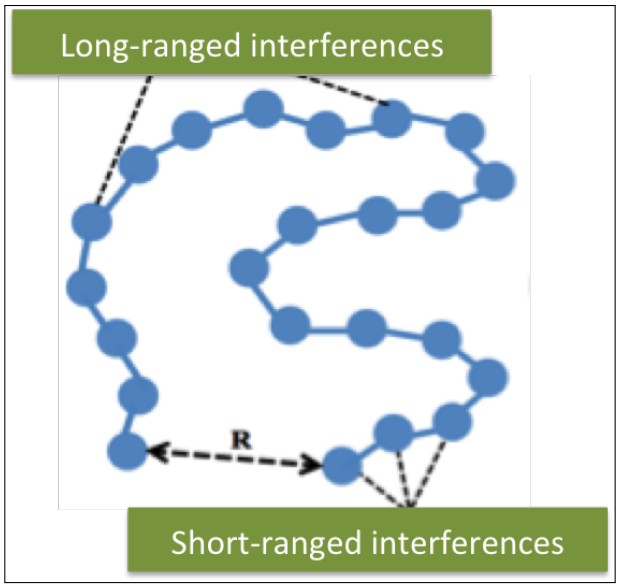

Figure 1.4: Linear skeletal model of a polymer shows two different kinds of interactions between its monomers (R represents the end-to-end distance vector).

lattice model that describes ideal chains is:

$$\left\langle R^2 \right\rangle \sim a^2 N$$

The **Kuhn Length** (a) is the effective length of the freely jointed bonds on a polymer chain. It is a constant that depends on the chemical structure of both the polymer and the solvent.

Real chains interact via long and short-ranged interferences. Real chain models consider direct monomer-monomer interactions between neighboring monomers and monomers that are far apart on the polymer backbone. These models also take into account the interaction with the surrounding molecules, such as solvent molecules. Real chains in a good solvent have the same universal features as *Self-avoiding Walks* (SAWs) in a lattice. The SAW is a random walk model that never visits the same site more than once (see Figure 1.5(B)). Thus, the statistical probabilities are not equal for each step. The mean-squared-end-to-end distance for a real chain is proportional

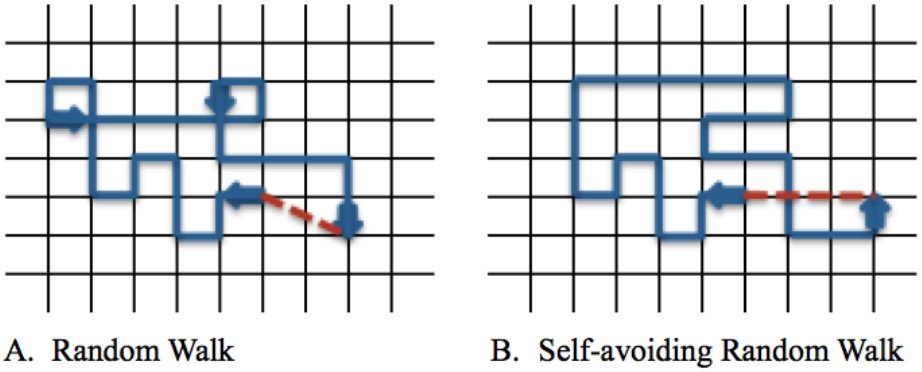

Figure 1.5: Statistical models for Random walk and Self-avoiding random walk. The two models represent 27 steps, and the red lines show the end-to-end distance, which looks shorter in the random walk than the self-avoiding walk, as the statistical calculations predict.

to the number of monomers in the chain via the following relation:

$$\left\langle R^2 \right\rangle \sim a^2 N^{\nu} \tag{1.1}$$

Flory computed a universal value of the exponent ν (see Appendix A), which is called the excluded volume parameter. The value of this parameter depends on the number of dimensions at which we study the SAW ($\nu_3 \cong 6/5, \nu_2 \cong 3/2, \nu_1 \cong 2$) [16]. In Equation 1.1, (a) depends on both the chemical structure of the polymer and the solvent. By using the SAW technique, Domb [12] was able to calculate the prefactor for this relation ($Constant \cdot a$). He called it $A(N)$, where $A(N) = \frac{<R^2>}{N^{6/5}}$, and he found that for a three-dimensional simple cubic lattice system $A(N > 10) = 1.061097$. Dumb's system only characterizes the case of a perfectly good solvent. Thus, for the same system and different solvent quality this prefactor would differ to reflect the appropriate interactions for a polymer mixture. Hence, the SAW model has been used to describe real chain behavior.

1.3 Polymer Solutions

Polymer mixtures have several characteristic properties that make them unique among fluid mixtures. These properties can be broken up into three categories. First, polymers tend not to mix with different polymers, but instead blended polymers typically separate to form, either little spherical bulbs, layer-by-layer structure (LBL) or undefined shapes (see Figure 1.6).

A. Spherical blobs morphology.

B. Sheetlike layers or layer-by-layer (LBL) morphology.

C. Undefined shape.

Figure 1.6: Different polymer blends provide singular phase morphologies.

Second, a polymer molecule is typically much larger than a solvent molecule. This causes non-idealities of polymer solutions. To overcome the non-ideality problem, Flory and Huggins assumed that each polymer segment (monomer) has the same size as a solvent molecule. Thus, they treated each monomer equivalent to a solvent molecule to calculate the entropy of a polymer solution. Third, due to the conformational degree of freedom of a polymer molecule, liquid polymers, polymer solutions, and solid polymers are rubbery in nature. They are viscous and have an elastic behavior, so they are viscoelastic materials. All the properties of polymer solutions are produced due to the short-ranged and the long-ranged interactions and the interactions between monomers and the surrounding molecules.

A real polymer chain in a solvent, behaves as an ideal chain at a temperature that is called the *theta temperature* (T_θ). At the theta temperature the attractive

interactions between polymer segments compensate for the repulsive interactions due to the excluded volume effect, and lead to the chain acting if it was an ideal chain. At any temperature below T_θ, polymer segments attract each other to form collapsed conformations, and the solvent at this temperature is called a *poor solvent*. Vise versa, polymers at temperatures higher than T_θ show more extended conformations due to the repulsive interaction between the polymer segments, and the solvent at this temperature is known as a *good solvent*. Figure 1.7 shows the effect of the temperature on the behavior of a real chain and how the θ temperature leads to an ideal chain behavior.

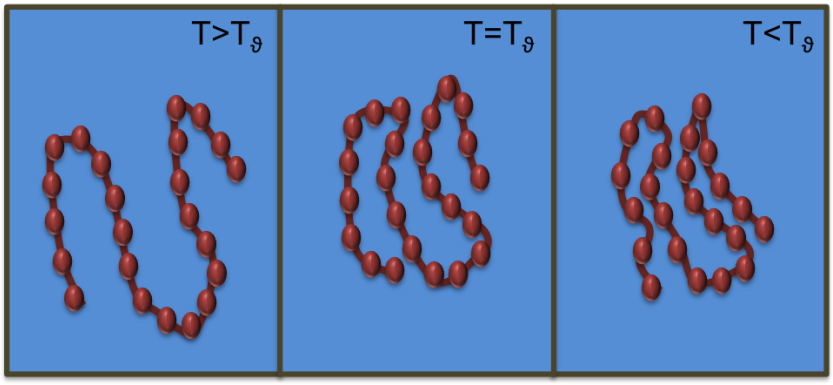

Figure 1.7: The effect of T_θ on polymers conformational structure.

1.3.1 Polyelectrolytes' Solutions

Polyelectrolytes are macromolecules that are capable of dissolving or reacting in a polar solvent depending on their chemical groups, to generate charged species. Poly-anions with acidic groups along their backbone are able to dissolve to release free counterions, leaving bound residues with negatively charged species [13]. In contrast, Poly-cations with basic groups along their backbone are able to react with free solvent ions, generating bound residues with positively charged species. For example, each monomer in Poly(acrylic acid) (PAA) has a COOH group that gives rise to acidic

functionality. In a polar solvent, usually water at neutral pH, COOH groups dissociate to release hydrogen ions, H^+, leaving negatively charged residues along the chain backbone (COO). Figure (1.8) represents polybase (Poly-cation), such as polyamine polymer, that is able to react with hydrogen ions of water solution at a wide range of pH, leaving charged monomers a long the polymer chain.

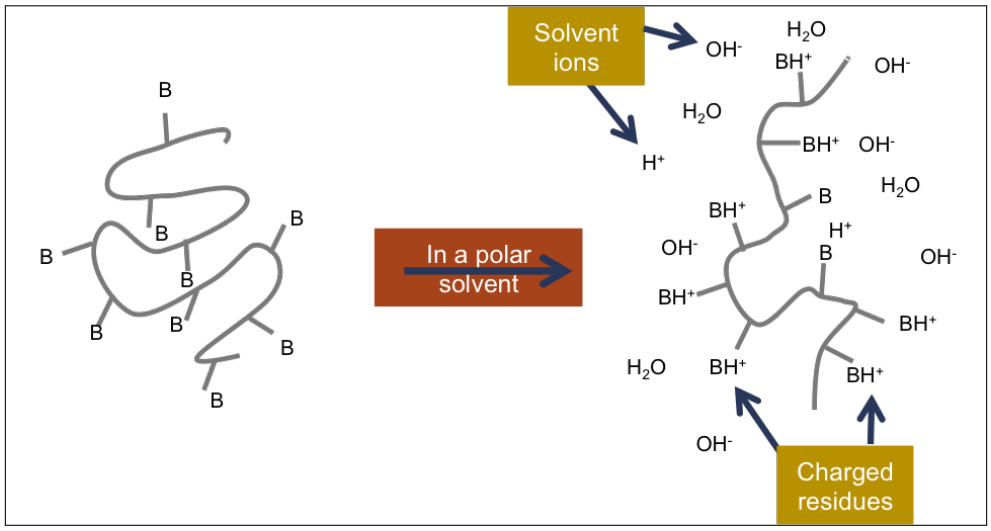

Figure 1.8: Poly-cation (polybase) reaction in an aqueous solution.

Polyelectrolytes can be classified as *weak* and *strong* (*also known as quenched*) according to the concentration of the dissociated groups. If the number of the dissociated-groups in a polyelectrolyte is fixed under different environmental conditions, such as salt concentration and pH, this polyelectrolyte is called a quenched polyelectrolyte. However, in weak polyelectrolytes, salt concentration and pH are used to control the ionic properties of the chain through the amount of dissociation. Weak polyelectrolytes can be synthesized carefully to control their functionality at the desired location, which makes them a great component for synthesizing targeted drug delivery device.

A polymer's conformational structure in a solution is controlled by several interactions in the system. In addition to the polymer architecture and the solvent affinity, electrostatic interactions play very important roles in polyelectrolyte's con-

formational structure. Polyelectrolytes tend to swell due to the repulsive interaction between their charged bound residues. In the case of the weak polyelectrolytes, one can generate more collapsed conformations by increasing salt concentration. In this environment, salt ions screen the charged polymer segments giving rise to more collapsed conformations. Moreover, changing the salt concentration or the pH in the system can affect the dissociation, and therefore change the fractional charge of the polyelectrolyte chain. In brief, one can control the polyelectrolytes aggregation by controlling the salt concentration and the pH in the system.

There are several bio-polyelectrolytes in nature. Deoxyribonucleic acid (DNA) is an example of a biological polyelectrolyte molecule. DNA is composed of two pairs of ionisable phosphate groups. Synthesized polyelectrolytes can be used for different biological and medical applications due to their solubility in water. In this study we will be focusing on using polyelectrolytes for drug delivery applications. The behavior of free and one end-tethered polyelectrolytes enables us to study different drug delivery systems and micellar aggregations.

1.4 Polymer's interactions

There can be either attractive or repulsive interactions between the polymer segments from the same chain, different chains, and the surrounding molecules, such as solvent molecules. These interactions affect the polymer conformations. In this study, we will explore electrostatic, van der Waals, and steric interactions and their effect on polymer conformations. We will use statistical mechanics to predict these configurations.

A polymer's degree of flexibility arises from the covalent bonds between its monomers, which represents the short-ranged interferences. Long-ranged interferences between polymer segments that are separated by large distance along the polymer chain backbone, are responsible for determining the prevalence of certain polymer conformations. The *excluded volume effect* is an indicator of long-ranged interferences that

constraint two polymer segments from occupying the same location in space. In a mixture, the *Incompressibility* constraint restricts the sum of the volume fractions of all molecular species in the system to be equal to one. Van der Waals interactions between polymer segments play a central role in the polymer entanglement. Van der Waals interactions also appear between two polymer segments from two different polymers. In a polymer solution, the van der Waals attraction or repulsion forces between the solvent-solvent and solvent-monomer molecules affect the polymer conformational structure. In some systems with different salt concentrations and pH, the electrostatic interactions significantly control the polymers' aggregation. The competition between all these altered interactions determines the polymer conformational structure.

1.4.1 Excluded volume

The excluded volume for any molecule in a space is the volume surrounding this molecule that excludes the presence of all other molecules. In any system, it's known that "Like" molecules attract each other unless there is an electrostatic repulsion between them. Thus, in a polymer solution, monomer molecules tend to attract each other at a distance larger than the excluded volume. Within the excluded volume, there is a repulsion interaction caused by the steric effect. This effect prevents two monomers from overlapping. To explain this kind of behavior, we consider a potential energy $U(r)$ between two monomers separated by distance r [44]. This energy is equal to the work done to bring one of the monomers from ∞ to be within a distance r from the other one. Figure 1.9 sketches the potential energy $U(r)$ as a function of r. The hard-core barrier in the potential energy plot represents the repulsive interaction between the two monomers within the excluded volume, and the attractive well corresponds to the interactions between similar molecules.

The probability of finding two monomers separated by distance r is proportional

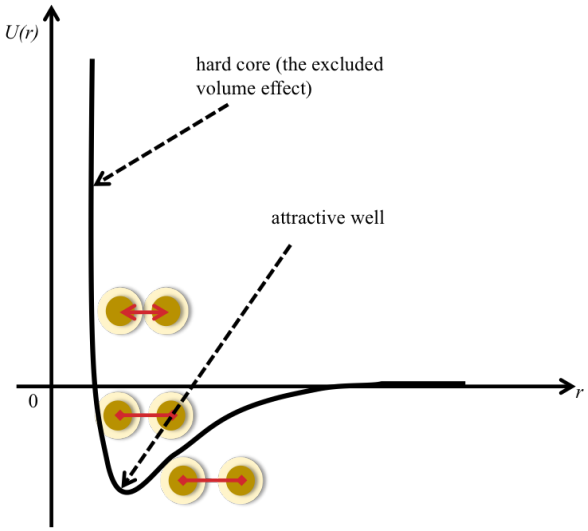

Figure 1.9: Lennard-Jones potential plot shows the effective excluded volume interaction between two neighboring monomers in a solution.

to the thermal energy, K_BT, where K_B is **Boltzmann** factor and T is the absolute temperature of the system.

$$P(r) = \exp\left(-\frac{U(r)}{K_BT}\right) \tag{1.2}$$

Subtracting this probability from the total probabilities ($\sum P(r) = 1$) gives **Mayer f-function** ($f(r)$). Mathematically the excluded volume V is defined as the negative integral of Mayer f-function over the whole volume in space.

$$V = -\int f(r)d^3r = -\int \left[\exp\left(-\frac{U(r)}{K_BT} - 1\right)\right] d^3r \tag{1.3}$$

The excluded volume depends on the potential attractive energy and the absolute temperature of the mixture. The relative strength of the excluded volume interaction, for a specific mixture, depends strongly on the temperature. At a definite temperature called the *theta-temperature* (T_θ), the excluded volume effect on the conformations goes to zero, cancelling the net penalty of monomer-monomer contact. In this situation, the polymer chain has approximately ideal conformations. Thus, the solvent at T_θ is known as *theta-solvent*. The excluded volume interactions increase in their intensity, at temperatures higher than the theta temperature. At this point, beside

the monomer-monomer attractions there are monomer-solvent attractions, leading to a *good-solvent* environment. In contrast, at temperature below theta temperature, the monomer-monomer attraction energy is dominant and the solvent is considered as *poor-solvent*. Figure 1.7 shows a polymer chain in a good solvent, θ-solvent, and poor solvent.

Considering a specific lattice system, which is the case in most of our study, implicitly takes care of the excluded volume effect. In such a system, each lattice site is occupied with only one molecular species. Thus, summing over all volume fractions of molecular species (ϕ_i) on the system, goes to one.

$$\sum \phi_i(r) = 1$$

This constraint, known as the compressibility constraint, accounts for the excluded volume effect within any lattice system.

1.4.2 Van der Waals interaction

The **van der Waals** attraction between molecules is due to the presence of induced electric dipole moments on a nearby non-polar molecule, corresponding to an effective formation of separated charges within the molecule [25]. Induced polar molecules tend to attract each other to form special types of interactions. These interactions can be seen in a polymer mixture between two unbound monomers or between a monomer and a solvent molecule. Normal thermal molecular motion disrupts the ordering imposed by the van der Waals forces in the system. The thermal motion diminishes as the temperature decreases, thus van der Waals forces become more effective at ordering the molecules at lower temperature, and may cause a condensation of the polymers.

In a polymer solution, polymer molecules are much larger than solvent molecules. For this reason, Flory and Huggins used the cubic lattice model to study the van der Waals interactions between solvent molecules and polymer segments (monomers).

The Flory- Huggins model will be covered in the next chapter as a useful statistical mechanical model in studying the thermodynamic properties of polymer solutions.

1.4.3 Electrostatic interactions

Consider a polymer solution system composed of charged molecules (polyelectrolyte) and mobile salt ions. Charged polymers attract oppositely charged mobile ions, which are called *counterions*, and repel mobile ions that have the same polarity, called *co-ions*. Both counterions and co-ions are distributed in the system with a total density ρ_q that is generating an electric potential field $\psi(z)$ at distance z away from a charged surface. The distribution of mobile salt ions is controlled by coulomb interaction and molecular diffusion. The presence of counterions in the system shields the electric repulsion between the charged polymer segments, which reduces the electric potential field.

To understand the electrostatic interaction of a polymer solution first we need to determine the Lagrangian of the system by studying its electrodynamics [47]. Then, since we study the system at an equilibrium state, we should eliminate the magnetic energy terms that are generated by the molecular dynamics. Hence, the following relation describes the electrostatic energy of a canonical ensemble [1].

$$U_{elec} = \int dV \left[\rho_q \psi(\boldsymbol{r}) - \frac{1}{2}\epsilon(\nabla\psi(\boldsymbol{r}))^2\right] \tag{1.4}$$

Note that ϵ is the permittivity of the medium, and $\nabla\psi(\boldsymbol{r})$ is the gradient of the electric potential field that equates to the negative electric field $\boldsymbol{E}(r)$ of the system.

$$\boldsymbol{E}(r) = -\nabla\psi(\boldsymbol{r}) \tag{1.5}$$

By taking the divergence of the electric filed we get **Poisson's equation**:

$$\nabla \cdot \boldsymbol{E}(r) = -\nabla^2\psi(\boldsymbol{r}) = \frac{\rho_q}{\epsilon} \tag{1.6}$$

[1] Canonical ensemble represents various possible states of a closed system with unchanged volume, temperature, and number of compositions. These ensembles differ in their total energy.

where ∇^2 is called *Laplacian operator*, and it varies for different coordinate systems; see Appendix C.

Poisson's equation allows us to calculate the electric potential of a specific system that is made of an identified dielectric media by knowing the charge distribution of a fixed number of charged molecules. The charge distribution is calculated using the **Boltzmann distribution** equation [9].

$$f(z) = Ae^{-\beta E} \tag{1.7}$$

where, A: is a normalized constant.

β: is the inverse of thermal energy.

E: is the energy.

Equation 1.7 can be applied to the distribution of all ion concentrations of i *species* in the system, $C_i(z)$, that has C_∞ bulk concentration.

$$C_i(z) = C_\infty e^{-\beta \Delta E_i} \tag{1.8}$$

Then, we can write the charge density as follow:

$$\rho_q(z) = \sum_i Z_i e C_\infty \exp\left(-\beta Z_i e \psi(z)\right) \tag{1.9}$$

where Z_i: is the charge valance.

e: is the elementary charge.

In such a system, the **Poisson-Boltzmann** model is used to study the charge screening and colloidal stability against aggregation. This model was developed by combining Poisson's equation and the Boltzmann distribution equation. In the case where the surface of a charged colloidal particle is described as a plane, one can solve Poisson- Boltzmann equation to get the electric potential as (see Appendix D).

$$\psi(z) = \frac{\sigma_q \lambda_D}{\epsilon} \exp(-\frac{z}{\lambda_D}) \tag{1.10}$$

where σ is the charge density on the surface, and $\lambda_D = \sqrt{\frac{\epsilon}{2\beta e^2 Z^2 C_\infty}}$, is **Debye length**, which is a screening distance. However, solving the same equation for a spherical surface gives the following relation:

$$\psi(r) = \frac{Qe^{R/\lambda_D}}{4\pi\epsilon\left(1+\frac{R}{\lambda_D}\right)}\frac{e^{-r/\lambda_D}}{r} \tag{1.11}$$

Note that $Q = 4\pi R^2\sigma_q$, is the total charge on the surface of a sphere with radius R.

Chapter 2

Statistical Models and Methods

In this chapter, we use statistical mechanical methods to study thermodynamic behavior. Statistical mechanics is a branch of theoretical physics that enables us to understand the natural phenomena of macroscopic systems by analyzing their microscopic and molecular behavior. Macroscopic systems are composed of numerous particles that naturally fluctuate on the molecular length and time scale. Statistical thermodynamics is a branch of statistical mechanics used for studying the equilibrium states of a system. One branch of statistical thermodynamics studies the molecular interactions between micro-molecules in the system explicitly. This branch is able to deal with the most challenging problems such as the existence of the first-phase order transition. Another branch of statistical thermodynamics simplifies the problems by approximating some of the molecular interactions. In our study of polymer solutions, we are devoted to methods that simplify the intermolecular interactions using the *mean-field approximation*.

The study of thermodynamics is governed by the choice of the set of macroscopically observable variables. At statistical equilibrium, different macroscopic constraints define different kinds of statistical ensembles. The*Micro-canonical ensemble* is a statistical ensemble that has all its macroscopic states at equilibrium when the energy, the volume of the ensemble, and the number of molecules are fixed (E, V, N) . The *Canonical ensemble* is defined by the constraints of a fixed volume, number of molecules and temperature (T, V, N). The *Grand Canonical ensemble* is defined by the constraints of a fixed volume, temperature and chemical potential (E, V, μ°).

In this study, we will be dealing with a polymer solution under biological conditions, which can be described as a container of a fluid system whose walls allows for both heat and mass transfer. Our systems in this study are treated as being in a class called the *Semi-grand canonical ensembles*, where the system can be defined as a statistical ensemble existing between the canonical and the grand canonical ensembles constraints. Some of the molecules in the Semi-grand canonical ensemble have a fixed number while other molecules have fixed chemical potentials [36].

Statistical mechanical theories and methods that can be applied to thermodynamic problems in order to greatly simplify them will be further explored. The specific techniques that apply to the models of this study are: the Flory-Huggins theory of the thermodynamics of polymer solution, the mean-field approximation and the use of the numerical methods for studying polymer solutions and the Monte Carlo methods and Rosenbluth technique.

2.1 Flory-Huggins model of polymer solution

Flory and Huggins used the cubic lattice system to model polymer solutions. Because polymer molecules in polymer solution systems are much larger than solvent molecules, they used the cubic lattice model to study the variety of ways to arrange polymer segments for n_p number of polymer molecules and n_s solvent molecules. In the cubic lattice model, polymer segments and all other molecules in the system are considered to be virtually identical in size. They studied all possible polymeric configurations in the system by using self-avoiding random walks to build the polymer chain, (see section 1.2) and filled the empty sites randomly with solvent molecules. Most of the modeling in this study is of grafted polymers; therefore the possible number of configurations of a polymer with polymerization number N is reduced. In the cubic lattice model, polymer segments and all other molecules in the system are

considered to be virtually identical in size.

The system under study is composed of n_s number of solvent molecules and n_p number of polymer molecules. Each polymer molecule has N segments. Flory defined a lattice system containing M number of lattice sites where,$M = Nn_p + n_s$, and he defined the molar fraction for each molecular species in the system as [44]:

$$\phi_p = \frac{Nn_p}{M} \quad and \quad \phi_s = \frac{n_s}{M}$$

For a system that contains two different species only, we can denote the volume fraction for each species as follows:

$$\phi_p = \phi \quad and \quad \phi_s = (1 - \phi)$$

To study van der Waals interactions, Flory calculated the change in energy for each monomer solvent contact (see Appendix B). This energy difference is giving by the following relation:

$$\Delta u_{ms} = \frac{1}{2}(2u_{ms} - u_{mm} - u_{ss})$$

The intensive change of energy for the mixture per site is given by:

$$\Delta \bar{U}_{mix} = \frac{z}{2}\phi(1 - \phi)(2u_{ms} - u_{mm} - u_{ss}) \tag{2.1}$$

where z represents the number of nearest neighbors, which is the coordination number of the lattice.

Flory introduced his dimensionless **interaction parameter** or **Chi-parameter** (χ) to measure the strength of the interaction energy between two neighboring species in the system.

$$\chi \equiv \frac{z}{2}\frac{(2u_{ms} - u_{mm} - u_{ss})}{K_B T} \tag{2.2}$$

Thus, we can rewrite the intensive energy for a mixture per lattice site as:

$$\Delta \bar{U}_{mix} = \chi\phi(1 - \phi)K_B T \tag{2.3}$$

which is the mean-field description of the internal energy of a mixture.

2.2 Mean-Field Theory

The idea of particle-to-field transformation is commonly used in polymer physics and is described in Fredrickson's book [13]. In particle-to-field transformation, the effect of the direct interactions among polymer segments is replaced by decoupling the interaction between those segments with one or two auxiliary fields. The statistical field theories approach expresses the relevant partition function as a grand canonical partition function. The partition function describes the statistical properties of the system at thermodynamic equilibrium as a functional integral over the auxiliary potential fields ($w(\mathbf{r})$).

$$q = \int \mathfrak{D}_w \exp(-H[w])$$

And correspondingly the average sum of an observable Φ can be written as:

$$\langle \Phi[w] \rangle = q^{-1} \int \mathfrak{D}_w \Phi[w] \exp(-H[w]) \tag{2.4}$$

where the notation $\int \mathfrak{D}_w$ indicates a functional integral [1] over all possible potential fields in the system, and $H[w]$ is the effective Hamiltonian, which depends on the particular interaction and the chain model used to construct the field theory.

The *mean-field-approximation* assumes that a single field configuration ($w^*(\mathbf{r})$) dominates the functional integrals, meaning that all configurations of the potential field are neglected except for the particular configuration (w^*). In other words, the effective Hamiltonian is stationary with respect to variations in ($w(\mathbf{r})$).

$$\left. \frac{\partial H[w]}{\partial w(\boldsymbol{r})} \right|_{w=w^*} = 0$$

This assumption allows us to obtain the "mean-field potential" $w^*(\mathbf{r})$. Thus, we can write the following relations:

$$q \approx \exp(-H[w^*]) \qquad \langle \Phi[w] \rangle \approx \Phi[w^*] \tag{2.5}$$

[1] Functional integration is a collection of results in mathematics and physics, where the domain of an integral is no longer a region of space, but a space of functions. So, it is a path integral where its contour is a space.

The mean-field approximation neglects the atomic scale fluctuations, which makes it a poor approximation to study atomic or small molecular fluids. This limitation is negated by the fact that the lattice model of polymer solution assumes that each monomer occupies a single lattice cell. Furthermore, the mean field approximation method includes only the fluctuations that occur within a lattice cell and neglects all fluctuations extending beyond that scale length. Although this procedure is not exact, it can often be very accurate. It also has the benefit of greatly simplifying the numerical intractability of the problem.

2.3 Numerical methods

This study aims to study polymers behavior in continuous biological systems. The complexity of these systems draws us to use *numerical methods* in calculating the partition function and the potential fields in the system. Numerical techniques are well suited to solve "field-theory" based problems by converting continuous variables into discrete counterparts. This can be achieved in a finite system by defining a computational grid of discrete points at which potential fields vary. This study covers both simple numerical calculations of homogeneous polymer solutions where the potential field varies in one direction only, and more complex cases in which we consider variation on the potential field at each point in three-dimensional space.

In our numerical calculations, we apply the *finite difference method*[1]. By applying this method in simple one-dimensional calculations, we assume that our system is homogeneous on the $x - y$ plane and differs on the z axis only. Let us consider a finite system that goes from 0 to L in the z axis. The numerical approach allows us to discretize the system into L_z number of equally spaced layers that have thickness Δ. This thickness is called the *grid spacing*, where $L_z = \frac{L}{\Delta}$. The next step in the finite difference method, is using the *forward Euler difference approximation* to define

[1] see Fredrickson [13]

the first derivative of the potential field function at polymer configuration α, with respect to z, $(w(\alpha, z))$ as:

$$\frac{\partial w(\alpha, z)}{\partial z} = \frac{w(\alpha, z + \Delta) - w(\alpha, z)}{\Delta} + O(\Delta)$$

By using the *centered space difference approximation* to define the second derivative of the potential field, we get:

$$\frac{\partial^2 w(\alpha, z)}{\partial z^2} = \frac{w(\alpha, z + \Delta) - 2w(\alpha, z) + w(\alpha, z - \Delta)}{\Delta^2} + O(\Delta^2)$$

Note that, the error in the second derivative, $O(\Delta^2)$, diminishes as we increase the discretization and decrease the size of grid spacing Δ. Only the second derivative is used to solve the numerical equations. We use Poisson and Poisson-Boltzmann equations to solve for the electric potential in the system, using as an input the charge density function. This allows us to neglect the error function in the equations while getting very accurate results.

The last step in the numerical methods, is to impose the boundary conditions at the boundary points: $z = 0$ and $z = L$. In most of our calculations, we inflect the boundary conditions based on the electric potential properties in the system (see Section 1.4.3). After applying these numerical methods, we end up with a set of N_e nonlinear equations that describe the chemical equilibrium and the physical interactions of polymer molecules in the system. That set of equations has N_ν of unknown variable, where N_ν should be less than N_e. Then, we use the variation of Newton's method to find the zeroes of continuously differentiable functions, giving a reasonable initial guess. The algorithm uses the generalized inverse of the Jacobian matrix [1] instead of the inverse Jacobian to solve the nonlinear equations [26].

[1]Generalized inverse Jacobian matrix is the inverse of the multiplication of the transposition Jacobian matrix and the Jacobian matrix itself is multiplied by the transposition Jacobian matrix $(J_F^+ = ((J_F^T J_F)^{-1}) J_F^T)$

This numerical approach has been used to solve the nonlinear equations that describe our systems. KINSOL [1] solver for Fortran90 language, and fsolve function in MATLAB programming language have been selected to solve these nonlinear equations. Both the solvers use a variation of Newton's method with a finite different approximation that depends on a good initial guess. Their performance depends on using iterative techniques to find values for the unknown variables that allow the equations of the entire system to approach zero. Poorly chosen starting points could affect the accuracy of the outputs, thus understanding the system's behavior is critical for accurate results.

2.4 Monte Carlo Methods

Monte Carlo (MC) method is a computational algorithm that uses random sampling of different possible states of a system to generate a diagram, which describes the behavior of the system from a probability distribution function [44]. It is also a useful method for solving optimization and numerical integration problems. This method allows for the evaluation of an average value of a specific variable (e.g ϕ) by generating a very large number N_{con} of random field configurations.

$$\langle \Phi(\boldsymbol{w}) \rangle \approx \frac{1}{N_{con}} \sum_{i=1}^{N_{con}} \Phi(\boldsymbol{w}^i)$$

The approximated average becomes closer to exact by increasing the number of random configurations. Monte Carlo methods restrict the generation of the random field configurations with probability distribution function $P(\boldsymbol{w})$ and the approximation of this is defined as follows:

$$\langle \Phi(\boldsymbol{w}) \rangle \equiv \int d_{\boldsymbol{w}} P(\boldsymbol{w}) \Phi(\boldsymbol{w}) \tag{2.6}$$

[1] The solver is a one of SUNDIALS solvers (SUite of Nonlinear and DIfferential/ALgebraic equation Solvers) [49]

where,

$$P(\boldsymbol{w}) \equiv \frac{\exp(-H(\boldsymbol{w}))}{\int d_{\boldsymbol{w}} exp(-H(\boldsymbol{w}))}^{1}$$

This definition is normalized so that $\int d_{\boldsymbol{w}} P(\boldsymbol{w}) = 1$. Such a definition is suitable for a probability weight function that we will use for Rosenbluth weighting technique in the next section.

The random field sequence of configurations that the MC methods adopt can be generated starting with an initial state i. The Probability distribution for the system to be in state i is P_i, where $P_i = P(\boldsymbol{w}^i)$. The probability of the system moving to state j is P_j. The dynamics of the system at time t can be described by the *master equation*:

$$\frac{\partial P_i(t)}{\partial t} = \sum_{j(\neq i)} [M_{ij} P_j(t) - M_{ji} P_i(t)] \tag{2.7}$$

where M_{ij} is a matrix that translates the system from state j to state i and vise versa for matrix M_{ji}. Equation 2.7 indicates that there is a gain or loss in the probability of state i, due to the translation from or to the same state with the corresponding matrix. Considering the steady state solution of the system causes the *master equation* to go to zero. Accordingly, and by assuming that the forward and the reverse probability between the two states i and j are in exact balance (that is called microscopic reversibility), one can write the following:

$$M_{ij} P_j(t) = M_{ji} P_i(t)$$

The *Metropolis Monte Carlo* form of transition rates is the most popular form of the translational matrix.

$$M_{ij} = \begin{cases} \alpha \exp(-\Delta E_{ij}) & \Delta E_{ij} > 0 \\ \alpha & \Delta E_{ij} < 0 \end{cases} \tag{2.8}$$

[1]Note that we consider a discrete approximation over the real contribution of the Hamiltonian only (see Fredrickson [13] P.327 for more detailes)

where α represents the number of transitions between the two states that have energy E_i and E_j . And $(\Delta E_{ij} \equiv E_i - E_j)$ is the difference between the energy of the two states in units of $K_B T$.

2.5 Rosenbluth Technique

Monte Carlo methods depend on generating a very large number of random samples in order to properly describe a specific state. Thus, MC methods have been used to generate all possible configurations of short ideal or real chains that are described by random walk or self avoiding random walk models respectively (see section 1.2 for more information). Note that in a cubic lattice, there are 6^N different states or configurations with a fixed starting point for an ideal chain of N number of monomers. Due to the magnitude of the permutations, it is clear that sampling all the states of a long chain is impossible. A MATLAB script was used to generate all possible configurations for a free chain at a fixed point and for a one-end grafted chain. With the available computing power and memory, it took approximately one full day to collect all possible configurations for a chain with a maximum length of 11 monomers (see listing 2.1).

Listing 2.1: A MATLAB script collects all possible configurations for SAW

```
1 %%%%%%%%%%%%%%%%%%%%%%%%%%%%%%%%%%%%%%%%%%%%%%%%%%%%%%%%%%%%%%%%%%%%%%%%
2 % In the name of Allah, The most Gracious and Merciful  %
3 % All SAW Configurations in A Cubic Lattice             %
4 % By Ebtisam Aldaais                                    %
5 % BMEN | University of South Carolina                   %
6 % January 2014                                          %
7 %%%%%%%%%%%%%%%%%%%%%%%%%%%%%%%%%%%%%%%%%%%%%%%%%%%%%%%%%%%%%%%%%%%%%%%%
8 clc
9 clear
```

```
t       = tic;
time    = [];
Num_steps = 0;          % Total number of steps
x=int8(0);              % (0,0,0) is the starting point
y=int8(0);
z=int8(0);
count           = int64(0);
old_count       = int64(0);
total_conf      = int64(0);
% A Matrix to store the seps for each confirmation
steps = int8([x;y;z]);
current_file        = matfile('RW_0.mat','Writable',true);
current_file.steps  = steps;
current_file.count  = 1;
for Num_monomers= 1:Num_steps;    % Number of steps
    file_name = ['RW_',num2str(Num_monomers),'.mat'];
    if(2==exist(file_name,'file'))
        disp([file_name,' Exist'])
    else
        current_file    = matfile(file_name,'Writable',true);
        old_file        = matfile(['RW_',num2str(Num_monomers-1)...
                          ,'.mat'],'Writable',true);
        old_count       = old_file.count;
        total_conf      = 0;    % Counter for possible configurations
        piece_size      = 10240;
        % Due to memory shortage we divide data into pieces.
        for p = 1:(ceil(old_count/piece_size))
            count=0;  % Counter for possible configurations
                      % for current piece.
            % Reading a piece of Data from a file.
            a = 1+(piece_size*(p-1));
            b = min(piece_size*p,old_count);
            old_steps = old_file.steps(:,(a:b));
```

```
43              [m,n]=size(old_steps);
44              steps_big = zeros(m+3,n*6, 'int8');
45              for i=1:n;
46                  x=old_steps(m-2,i); % Column n-2 should have x value.
47                  y=old_steps(m-1,i); % Column n-1 should have y value.
48                  z=old_steps(m,i);   % Column n should have z value.
49                      Trajectory  = [x+1 y z;x-1 y z;x y+1 z;...
50                                     x y-1 z;x y z+1;x y z-1];
51                  % Check matrix converts rows to columns
52                  check=reshape(old_steps(:,i),3,m/3)';
53                  position=setdiff(Trajectory,check,'rows');
54                  [n_row,n_col]=size(position);
55                  if (n_row ≠0)                % Places not visited yet
56                      steps_big(1:(3*(Num_monomers+1)),count+1:count...
57                             + n_row)=[repmat(old_steps(:,i),...
58                              1,n_row);position'];
59                      count = count + n_row;
60                  end
61              end
62              current_file.steps(1:(3*(Num_monomers+1))...
63                      ,total_conf+1:total_conf+count) = ...
64                      steps_big(:,1:count);
65              total_conf  = total_conf + count;
66          end
67          current_file.count = total_conf;
68          disp([Num_monomers,total_conf]);
69      end
70      temp = toc (t);
71      time =  [time; temp];
72      h = plot(time,'--rs','LineWidth',2);
73      xlabel ( 'Number of steps' )
74      ylabel ( 'Time' )
75      title  ( 'Time Graph' )
```

```
76      saveas(h,['SARW_',num2str(Num_monomers)], 'png');
77  end
```

At this point, two constraints were found to be limiting in terms of modeling longer chains. First, the code was taking a very long time to collect the configurations, which was linked to the computer and the script performance. Second, the number of configurations required a large amount of memory to save all possibilities. An assumption could be made that we were able to improve the performance of the code and the computer specifications so that it would take five seconds to collect all possible configurations for a 9-monomer length chain, and 5 bytes to store all the configurations. Even with these unreasonable assumptions, it was found that 756 thousand centuries would be required to collect the configurations of a 30-monomer length chain, and 2168 TB of memory would be required to store the data (see Table 2.1 and Table 2.2).

Using these methods, it would literally be impossible to obtain all possible configurations of a long chain.

However, Marshall and Arianna Rosenbluth (RB) developed a technique that allows one to approximate all of the possible configurations of a real chain in a cubic lattice, by using a system of weights [43]. Their paper is very clear and contains several illustrative sketches to explain their idea. They started a self-avoiding random walk (SAW) at point $(0, 0, 0)$, and chose the second step to be $(1, 0, 0)$. The first step is thus specified for the walker. For the second step, the walker has only five possible positions to choose from randomly. For every next step, the walker should check the possible choices. The number of available positions (n) divided by the total possible directions in three-dimensional systems (5) represents the weight of the step. Therefore the total weight of the chain, according to Rosenbluth and Rosenbluth, can be written as follows:

$$W_{N+1} = \left(\frac{n}{5}\right) W_N \tag{2.9}$$

Table 2.1: Estimating the time needed to collect self-avoiding configurations for up to 30-monomers chain, when the code performance was improved to get all 9-monomers chain configurations in 5 seconds.

No. Steps	Time needed to collect all configurations in:					
	Seconds	Minutes	Hours	Days	Years	Centuries
9	5.00E+00	8.33E-02	1.39E-03	5.79E-05	1.59E-07	1.59E-09
10	2.50E+01	4.17E-01	6.94E-03	2.89E-04	7.93E-07	7.93E-09
11	1.25E+02	2.08E+00	3.47E-02	1.45E-03	3.96E-06	3.96E-08
12	6.25E+02	1.04E+01	1.74E-01	7.23E-03	1.98E-05	1.98E-07
13	3.13E+03	5.21E+01	8.68E-01	3.62E-02	9.91E-05	9.91E-07
14	1.56E+04	2.60E+02	4.34E+00	1.81E-01	4.95E-04	4.95E-06
15	7.81E+04	1.30E+03	2.17E+01	9.04E-01	2.48E-03	2.48E-05
16	3.91E+05	6.51E+03	1.09E+02	4.52E+00	1.24E-02	1.24E-04
17	1.95E+06	3.26E+04	5.43E+02	2.26E+01	6.19E-02	6.19E-04
18	9.77E+06	1.63E+05	2.71E+03	1.13E+02	3.10E-01	3.10E-03
19	4.88E+07	8.14E+05	1.36E+04	5.65E+02	1.55E+00	1.55E-02
20	2.44E+08	4.07E+06	6.78E+04	2.83E+03	7.74E+00	7.74E-02
21	1.22E+09	2.03E+07	3.39E+05	1.41E+04	3.87E+01	3.87E-01
22	6.10E+09	1.02E+08	1.70E+06	7.06E+04	1.94E+02	1.94E+00
23	3.05E+01	5.09E+07	8.48E+06	3.53E+05	9.68E+02	9.68E+00
24	1.52E+11	2.54E+09	4.24E+07	1.77E+06	4.84E+03	4.84E+01
25	7.62E+11	1.27E+10	2.12E+08	8.83E+06	2.42E+04	2.42E+02
26	3.81E+12	6.36E+10	1.06E+09	4.42E+07	1.21E+05	1.21E+03
27	1.90E+13	3.18E+11	5.30E+09	2.21E+08	6.05E+05	6.05E+03
28	9.53E+13	1.59E+12	2.65E+10	1.10E+09	3.02E+06	3.02E+04
29	4.76E+14	7.95E+12	1.32E+11	5.52E+09	1.51E+07	1.51E+05
30	2.38E+15	3.97E+13	6.62E+11	2.76E+10	7.56E+07	7.56E+05

where W_{N+1} represents the weight for step number $N+1$. The Rosenbluths indicate that by calculating the average weight $\langle W_N \rangle$ for the $3D$ SAW, one should find the number of all possible configurations using the following formula:

$$N_{con} = (5)^{N-1} \langle W_N \rangle \tag{2.10}$$

Using the Rosenbluth's method, we were able to write a MATLAB script to calculate all possible configurations for long chains (see listing 2.2). That script, as with any SAW script, terminates the chain when there is no empty neighboring position (dead-ended chain).

Table 2.2: Estimating the memory needed to collect all self-avoiding configurations for up to 30-monomers chain, when the computer capacity was improved to collect all 9-monomers chain configurations at 5 bytes only.

No. Steps	Memory needed to save all configurations in:				
	Bytes	KBs	MBs	GBs	TBs
9	5.00E+00	4.88E-03	4.77E-06	4.66E-09	4.55E-12
10	2.50E+01	2.44E-02	2.38E-05	2.33E-08	2.27E-11
11	1.25E+02	1.22E-01	1.19E-04	1.16E-07	1.14E-10
12	6.25E+02	6.10E-01	5.96E-04	5.82E-07	5.68E-10
13	3.13E+03	3.05E+00	2.98E-03	2.91E-06	2.84E-09
14	1.56E+04	1.53E+01	1.49E-02	1.46E-05	1.42E-08
15	7.81E+04	7.63E+01	7.45E-02	7.28E-05	7.11E-08
16	3.91E+05	3.81E+02	3.73E-01	3.64E-04	3.55E-07
17	1.95E+06	1.91E+03	1.86E+00	1.82E-03	1.78E-06
18	9.77E+06	9.54E+03	9.31E+00	9.09E-03	8.88E-06
19	4.88E+07	4.77E+04	4.66E+01	4.55E-02	4.44E-05
20	2.44E+08	2.38E+05	2.33E+02	2.27E-01	2.22E-04
21	1.22E+09	1.19E+06	1.16E+03	1.14E+00	1.11E-03
22	6.10E+09	5.96E+06	5.82E+03	5.68E+00	5.55E-03
23	3.05E+10	2.98E+07	2.91E+04	2.84E+01	2.78E-02
24	1.53E+11	1.49E+08	1.46E+05	1.42E+02	1.39E-01
25	7.63E+11	7.45E+08	7.28E+05	7.11E+02	6.94E-01
26	3.81E+12	3.73E+09	3.64E+06	3.55E+03	3.47E+00
27	1.91E+13	1.86E+10	1.82E+07	1.78E+04	1.73E+01
28	9.54E+13	9.31E+10	9.09E+07	8.88E+04	8.67E+01
29	4.77E+14	4.66E+11	4.55E+08	4.44E+05	4.34E+02
30	2.38E+15	2.33E+12	2.27E+09	2.22E+06	2.17E+03

Listing 2.2: A MATLAB script collects all possible configurations for SAW using RB methods

```
%%%%%%%%%%%%%%%%%%%%%%%%%%%%%%%%%%%%%%%%%%%%%%%%%%%%%%%%%%
% In the name of Allah, The most Gracious and Merciful%
% Using Rosenbluth method in a cubic lattice to       %
% calculate the number of configurations              %
% Ebtisam Aldaais                                     %
% USC (BMEN)/ Spring 2014                             %
%%%%%%%%%%%%%%%%%%%%%%%%%%%%%%%%%%%%%%%%%%%%%%%%%%%%%%%%%%
clc
```

```
clear
clf
Num_walks=10000;    % Nymber of trails
Num_steps=0;
all_Num_steps = zeros(Num_steps,1);
for ii=1:Num_steps+1;
    StateFun   = zeros(Num_walks,1);
    disp(ii)
    tot_W_RB=0;       % Final RB weighting function for a walker
    for j=1:Num_walks
        coolrun = false;
        while (¬coolrun)
            x=int16(0);
            y=int16(0);
            z=int16(0);
            steps = zeros(ii,3);
            W_RB=1;              % RB weighting for the first step
            coolrun = true;
            for i=1:ii;
                steps(i,:)    = [x y z];
                Trajectory    = [x+1 y z; x-1 y z; x y+1 z; ...
                                 x y-1 z; x y z+1; x y z-1];
                position      = setdiff(Trajectory,steps,'rows');
                [n_row,n_col] = size(position);
                if(n_row ≠ 0)
                    index = 1 + floor(n_row*rand);
                    x = position(index,1);
                    y = position(index,2);
                    z = position(index,3);
                    W_RB_i=n_row/5;   % See RB paper
                    W_RB=W_RB*W_RB_i;
                else
                    disp(['break at step number ',...
```

```
42                          num2str(i),' of ',num2str(j),' walk'])
43                      coolrun = false;
44                      break;
45                  end
46              end
47          end
48          tot_W_RB    = tot_W_RB+W_RB;
49      end
50      avg_W_RB = tot_W_RB/Num_walks;    % Calculate Avrerage W_RB.
51      Num_conf  = avg_W_RB*(5)^(ii-1); % Total number of configurations
52  end                                   % as mentioned in RB paper.
```

In 2000, D. MacDonald and his group used a different logarithm that uses the critical point of a chain to calculate the possible number of configurations for chains of up to 26-monomers in length [34]. We refer to their number of configurations as exact in Table 2.3. Then, we compared the results of Rosenbluths' numerical methods and the exact numbers to find the error percentage. Notice that the error percentage increases with the number of monomers in the chain. However, the error percentage never exceeded 7% for a 26-monomers chain, even with number of trails as low as $10,000$. The $10,000$ trails, for a 26-monomers chain, is about 10^{-14} fraction of the total number of configurations, which is 4.21204×10^{17}.

These results give us the confidence to use the RB weighting function in modeling the configurations of polymers. In complex systems where we couldn't get the number of trials above $10,000$, we used polymer chains that have 25 or less monomers to keep the error percentage as low as possible. Multiplying the RB statistical weight by the probability of each configuration improves the statistics, and provides a sample of all possible configurations. This statistical weight works exactly as the weight function

[1]These numbers are calculated using equation 2.10 and the weighting function in Rosenbluth paper ($\langle W \rangle = 1.46(0.941)^N$) [43].

[2]The error percentage is between exact number of configurations and RB analytical calculations.

Table 2.3: Comparison between Rosenbluth technique and MacDonald's logarithm in calculating the number of configurations of a real chain in a cubic lattice.

	Calculating the number of configurations			
No. steps	Exact	RB Numerical [1]	RB Analytical	Error % [2]
0	1.00E+00	1.37E+00	1.20E+00	0.0
1	6.00E+00	6.46E+00	6.00E+00	0.0
2	3.00E+01	3.04E+01	3.00E+01	0.0
3	1.50E+02	1.43E+02	1.45E+02	3.3
4	7.26E+02	6.73E+02	7.06E+02	2.8
5	3.53E+03	3.17E+03	3.38E+03	4.3
6	1.69E+04	1.49E+04	1.63E+04	3.9
7	8.14E+04	7.01E+04	7.77E+04	4.6
8	3.88E+05	3.30E+05	3.71E+05	4.4
9	1.85E+06	1.55E+06	1.76E+06	5.2
10	8.81E+06	7.30E+06	8.42E+06	4.5
11	4.19E+07	3.44E+07	3.98E+07	5.0
12	1.99E+08	1.62E+08	1.88E+08	5.5
13	9.44E+08	7.61E+08	8.89E+08	5.8
14	4.47E+09	3.58E+09	4.21E+09	5.9
15	2.12E+10	1.68E+10	2.01E+10	5.2
16	1.00E+11	7.92E+10	9.50E+10	5.1
17	4.74E+11	3.73E+11	4.46E+11	5.9
18	2.24E+12	1.75E+12	2.12E+12	5.1
19	1.06E+13	8.25E+12	9.95E+12	5.9
20	4.99E+13	3.88E+13	4.69E+13	6.1
21	2.36E+14	1.83E+14	2.22E+14	5.7
22	1.11E+15	8.60E+14	1.05E+15	5.6
23	5.25E+15	4.04E+15	4.91E+15	6.3
24	2.47E+16	1.90E+16	2.31E+16	6.6
25	1.17E+17	8.95E+16	1.09E+17	6.9
26	5.49E+17	4.21E+17	5.20E+17	5.3

in equation 2.6. Thus, we can define any averaged variable as:

$$\langle \Phi(\alpha, r) \rangle = \frac{\int dr \ \Phi(\alpha) W_\alpha P(\alpha)}{\int dr \ W_\alpha P(\alpha)} \tag{2.11}$$

where $P(\alpha)$ represents the probability of configuration α.

Chapter 3

Decoupling The Mean Field Theory

Polymeric tissue materials attract much scientific interest due to their very useful biomedical applications ranging from drug delivery systems and adhesive materials to their regulatory effect on enzymes and gene expressions [3, 58]. Understanding the competition between intermolecular interactions is vital to engineer "smart" nanostructured materials. The complex coupling of van der Waals, electrostatic, and steric interactions influences the thermal and electrical response of a polymer's molecular structure. In some highly detailed molecular field theories, the attractive interactions between polymer segments are determined via exact calculations of the intra-molecular interactions, while the inter-molecular interactions are treated with the mean field approximation, which leads to double counting. This chapter presents a modification of the three-dimensional (3D) mean field approximation in order to correct for the double counting of the inter-molecular interactions that occurs in the standard mean field approach. The new approach is applied on a system with **thermoresponsive polymers** and **polyelectrolytes**. The free energy of one end grafted polymers in a cubic lattice system with a coordination number of six is determined for both the standard mean field approach and the modified mean field. The results section shows a comparison between the standard mean field approach and the modified mean field approach.

3.1 Polymer Biomaterials Applications

Thermoresponsive polymeric materials represent one of the most exciting and promising classes of materials, especially for biomedical applications. Thermoresponsive polymers show configurational or phase changes with the variation of temperature. This property manipulation has been used in numerous biomedical applications [3, 58] (see Figure 3.1). The usage of the thermoresponsive polymeric drug delivery matrix can improve the drug release at the site of action under the desired biological conditions [18]. Thermoresponsive polymeric vectors are very interesting tools for gene delivery [55]. In addition, there is a new trend to use thermoresponsive materials in designing a local radiotherapy system [19]. These applications are achieved through manipulation by the collapse and expansion of the thermoresponsive polymers.

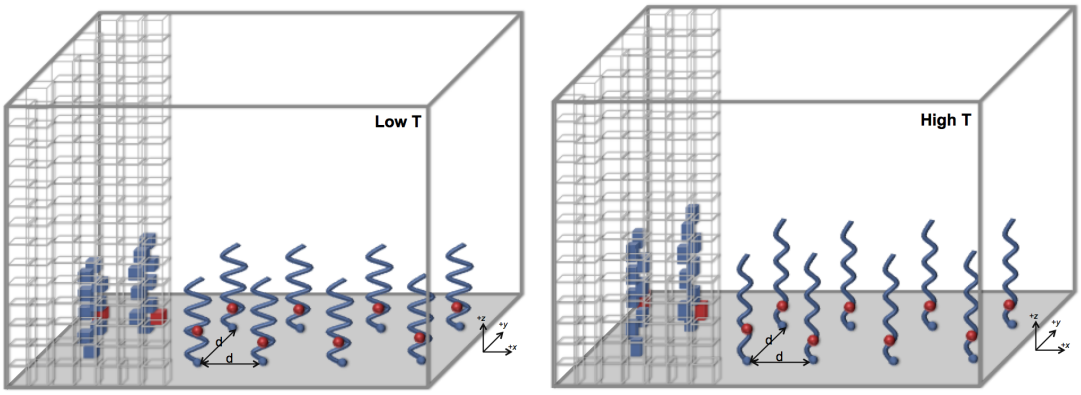

(a) UCST polymers at low T (b) UCST polymers at high T

Figure 3.1: A 3D cubical and continuous illustration of UCST grafted polymers at low and high temperature (the red spheres that are attached to the polymers characterize drug molecules).

Thermoresponsive polymers are divided into two main types: (1)Those that present at Low Critical Solution Temperature (LCST). Below this temperature they and the solvent are completely miscible. (2) Those that present at Upper Critical Solution Temperature (UCST). Above this temperature they and the solvent are completely miscible [58]. Thermoresponsive polymers with an LCST of about 32°, such

as poly(N-isopropylacrylamide) (PNIPAm), have been used to protect a drug until it gets inside the body. Interestingly, their transition from hydrophilic material below LCST to hydrophobic material above this temperature can be controlled. Specific changes to the synthesis of the thermoresponsive material of (PNIPAm) polymer can increase its LCST to be close to the body temperature. Moreover, incorporation of PNIPAm into a cross-linked polymer gel leads to a more sustainable drug release in comparison to the intravenous injection [3]. LCST cross-linked gels that are loaded with the desired drug swell below LCST, which is modified to be around the body temperature. Inside the body where the temperature is above the LCST point, the gel shrinks gradually causing the drug to leave the gel matrix.

In contrast, UCST polymers have been used to control drug release by stretching the UCST matrix while increasing the temperature. The UCST polymer's matrix holds the drug at temperatures below the UCST by forming a tight polymeric net around the drug. Above the UCST, polymers stretch allowing the drug to escape from the polymeric matrix. For example, interpenetrating network hydrogels grafted to β-cyclodextrin have been used to release a drug at temperatures above 35° [58].

Thermoresponsive UCST type polymers are considered as potential drug carriers for cancer treatment, such as methoxy-poly(ethylene glycol)-block-poly(acrylamide-co-acrylonitrile) (mPEG-b-P(AAm-co-AN)) amphiphilic copolymer [20]. The first part of this chapter models homopolymers where the UCST lies close to the body temperature. The polymers under study become hydrophobic (collapse) below the UCST and hydrophilic (expand) above the UCST.

Polyelectrolyte nanostructured materials for therapeutic applications have reconstructable surfaces that allow tailoring of permeability, as well as mechanical and adhesive properties [48]. Polyelectrolytes are capable of dissolving in an aqueous solution generating charged monomers (see Section (1.3)). Figure 3.2 illustrates the behavior of grafted polyelectrolytes in a solvent at low and high salt concentration.

Notice that at low salt concentration the charged monomers on the polyelectrolytes repel each other causing the polymer chain to stretch. In contrast, at high salt concentration, the salt ions screen the charged monomers on the polymer chains allowing them to shrink.

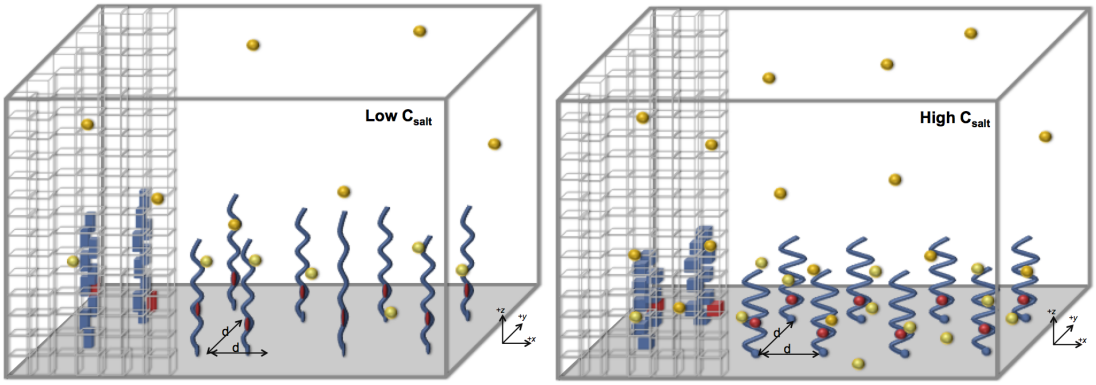

(a) Polyelectrolytes at low C_{salt} (b) Polyelectrolytes at high C_{salt}

Figure 3.2: A 3D cubical and continuous illustration of grafted polyelectrolytes at low and high salt concentration.

The glucose-sensitive insulin-releasing system, which is still under development, is an example of a Polyelectrolyte nanostructured material [14]. The therapeutic system is an insulin loaded matrix that contains pH-sensitive polymers and glucose oxidase. The presence of glucose in the system causes its oxidation into a gluconic acid and hence decreases the pH. As a result, pH-sensitive polymers shrink allowing the release of insulin. Another example of a Polyelectrolyte therapeutic nanostructed material is a wound healing hybrid biomaterial. Ito and colleagues designed a novel sheet-shaped poly(ethylene glycol) (PEG) grafted chitosan hydrogel (PEG-*g*-chitosan) with cross-linkable polymeric micelles that carry a drug [23]. The drug release mechanism depends on the degradation of the polymeric network and the diffusion of the compounds through the hydrogel. Recently, a graphene-based nanosheet material has been designed for specific co-delivery of an anticancer drug, Doxorubicin (DOX) [24]. The nano-carrier is administrated intravenously and accumulates at the tumor site

through passive and active affects, where it internalizes into the tumor cell through endocytosis. The acidic environment triggers the DOX release into the endosome where it causes DNA damage and an apoptosis of the cancer cell. Figure 3.1 illustrates the general three-dimensional architecture of Polyelectrolyte nanostructured materials.

3.2 Limitations of The Conventional Mean-Field

The ability to control the molecular organization of tethered polymers, and correspondingly to reconstruct the surface of polymeric nanomaterials, is critical to further development of a design platform for tissue biomaterials and therapeutic devices. Polymeric molecular organization in highly inhomogeneous biological systems strongly depends on the complex coupling between van der Waals, electrostatic, and steric interactions in the system. Most theoretical studies simplify the complexity of the system by using the mean-field approximation, in which the direct interactions between the molecules in the system are modeled with interactions between the system's supplementary fields. The attractive intra-molecular interactions, which are the interactions between two unbound polymer segments from the same polymer, are calculated exactly while building the polymer chain using self avoiding random walk techniques. The attractive inter-molecular interactions, which are the interactions between two unbound monomers from two different polymers, are determined with the mean field approximation [51, 56, 52]. The standard mean field approach studies the interactions between the segments of the polymer under study and the segments of all polymers in the system including the polymer under study itself. Including the segments of the polymer under study produces an over-counting, and accordingly an inaccuracy in the calculations of the inter-molecular interactions.

The decoupled mean field should improve the understanding of the molecular interactions in a highly inhomogeneous system by modifying the mean field approxima-

tion required in calculating the attractive inter-molecular interactions. The modified mean field approximation is applied by studying one end-grafted polymers in a cubic lattice system with a coordination number of six. Two highly inhomogeneous systems are modeled and studied:

- A system of end grafted thermoresponsive polymers with a UCST of approximately 37°. Such polymers collapse below the UCST and stretch above the UCST.
- A system of grafted polyelectrolytes that are effected not only by the temperature of the system, but also by the salt concentration and the pH of the solvent.

3.3 The Study of Grafted Thermoresponsive Polymers

The modification in the mean-field approach to calculate the inter-molecular interactions is examined in a designed thermoresponsive therapeutic tissue material system. The tissue material design is that of one end-grafted polymers to a solid surface. To mimic this design, the polymers are modeled in a solvent (water) (see Figure 3.1). In such a system, polymers self assembly is affected by the temperature of the system only.

3.3.1 The Model

The system is modeled as a controlled cubic lattice system at which the X and Y coordinates go from $-x : +x$ and $-y : +y$, while the Z coordinate goes from $0 : +z$. On the surface of the cubic lattice (at $Z = 0$), a number of Np grafted polymer chains with a polymerization number N are generated. Polymers are generated at equally spaced points in the two principle directions of the plane of the surface. In other words, the grafting points are placed symmetrically in a square pattern, and d is the distance in the two orthogonal directions that separate the grafted points (see Figure

(3.1)). The density of polymers on the solid surface is σ_p, where $\sigma_p = \frac{N_p}{A}$, and A is the area of the solid surface.

The cubic lattice model is discretized into equally spaced points (i, j, k) allowing the system variables to change at each point. Hence, our system has a total number of $(i \times j \times k)$ sites, where i, j, and k characterize the number of units at the X, Y, and Z axes respectively. The system is enforced under periodic boundary conditions in the planar surface direction, to insure that all polymers segments are inside the $(i \times j \times k)$ lattice sites, and that the system is continuous.

The *self avoiding random walk* (SAW) technique is used to generate the grafted polymers. Starting with the first polymer, N_{con} number of configurations are generated. Then, the exact same configurations are applied on all the grafting points at the surface. Each polymer ii $(ii = 1 : N_p)$ has a probability $P_{ii}(\alpha)$ to be at configuration α, where α goes from $1 : N_{con}$. Rosenbluth weighting method is used to improve the statistics efficiency on calculating the probabilities. The following is the Rosenbluth weighting function that is used to account for all configurations [43]:

$$W_{RB} = \prod_{m=1}^{N} \left(\frac{D}{5}\right) \tag{3.1}$$

The weighting function is calculated while building each polymer chain ii, which has N number of monomers $(m = 1 : N)$. The variable D is the number of available positions for the next monomer. The actual position is chosen randomly. To calculate the probability of having the monomer at any specific position, the number D should be divided by $five$, which is the maximum number of available positions for a self avoiding random walk in a simple cubic lattice system [43].

The temperature effect on the polymer configurations is tested by calculating the end-to-end distance at different temperatures. The average end-to-end distance squared for N_{con} number of configurations (α) of polymers that have N number of

monomers is given by:

$$\langle R^2 \rangle = \frac{\sum_{\alpha=1}^{N_{con}} R^2 \; W_{RB} \; \exp(-\beta E_{intra}(\alpha))}{\sum_{\alpha=1}^{N_{con}} W_{RB} \; \exp(-\beta E_{intra}(\alpha))} \tag{3.2}$$

where $(E_{intra}(\alpha))$ is the intra-molecular energy for each configuration (α), and is given in the inverse thermodynamic energy unit, β (see section (3.3.2) for more details on how we calculate $E_{intra}(\alpha)$). In the system, β is chosen carefully to insure that the polymers are collapsed away from the site of action. Plot (3.3) shows the relation between the average end-to-end distance square $(\langle R^2 \rangle)$ for end grafted polymers and the length of the chain (N) at different temperatures $(\beta = \frac{1}{K_B T})$. At $K_B T \approx 3$ the (3.3) plot shows a linear relation between $\langle R^2 \rangle$ and the number of monomers as in the case of an ideal chain model. Thus, we consider the temperature at this point to be T_θ.

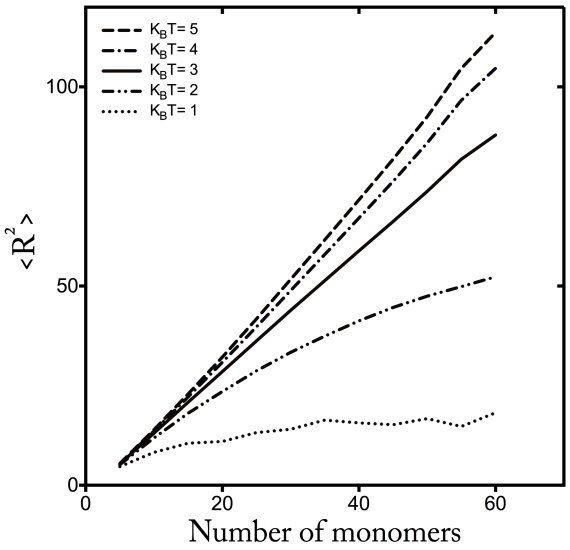

Figure 3.3: Effect of temperature on the chain end-to-end distance.

The tethered polymers are presented in an aqueous solution. The model assumes that polymer segments and solvent molecules have the same volume (see Figure (3.1)) and are therefore subject to steric and van der Waals forces [1]. The repulsive steric

[1]See section 1.3 for more details.

interactions are accounted for through the cubic lattice geometry and the assumption of a good solvent. The van der Waals interactions are accounted for through the intra and inter-molecular interactions. Figure (3.4) shows two polymers of different configuration surrounded by solvent molecules in a 2D SAW model. The green arrows indicate the intra-molecular interactions between the unbound nearby monomers from the same polymer. The blue arrows indicate the inter-molecular interactions between the unbound nearby monomers from two different polymers. The values of these two short-ranged attractive interactions, (ε_{intra} and ε_{inter}), have been chosen carefully so they don't affect the solubility of the solvent in the system. The model demonstrates the physical interactions between all molecules in the system that effect polymer configuration due to thermal variations.

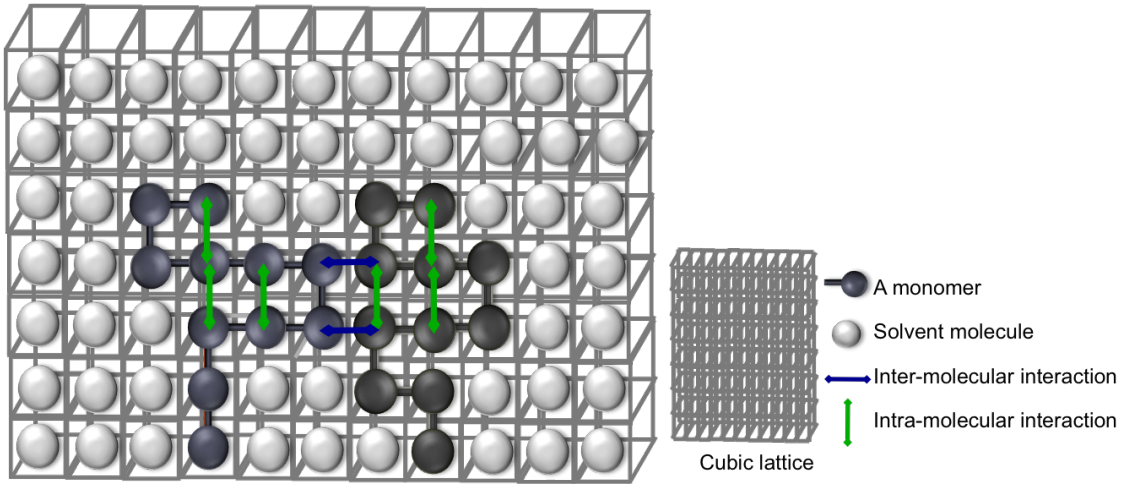

Figure 3.4: A 2D SAW model of two polymers in a cubic lattice, with different configurations and surrounded by solvent molecules. The green and the blue arrows represent the intra and inter-molecular interactions respectively.

3.3.2 Theoretical Approach

To calculate the free energy of the system, a theoretical approach that is developed from a single chain mean field theory (SCMF) is used. SCMF theory explicitly considers the shape, size, charge, configurations, and charge distribution of each individual

molecule in the system. The theory describes the interactions of a single molecule with the surrounding mean molecular field (MF) by determining the most probable configurations of the molecule through the probabilities of each individual molecule. For each configuration (α), one can calculate the polymer intra-molecular interaction energy $E_{intra}(\alpha)$ explicitly by triggering the monomers position(x, y, z) within the polymer chain (see Figure 3.5).

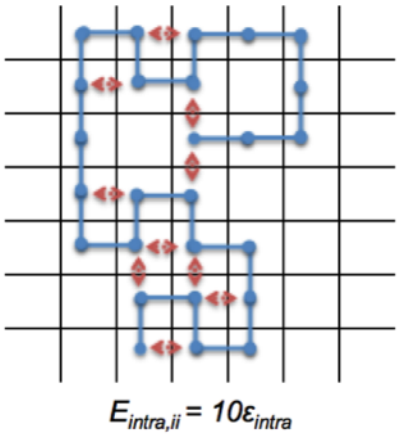

Figure 3.5: Calculating the intra-energy for a specific configuration.

Each monomer in the chain is mapped by calculating the distance between monomer i and monomer $i + 3$ and placing a constraint on that distance. This constraint should be equal to one to add an intra interaction. Thus, we define $E_{intra}(\alpha)$ for a specific configuration α mathematically as:

$$E_{intra}(\alpha) = -\varepsilon_{intra} \sum_{n=1}^{N_m} \sum_{m=n+3}^{N_m} \delta(r) \tag{3.3}$$

where ε_{intra} represents the elementary intra attractive energy, n and m are the monomers under study, and $\delta(r)$ is a Kronecker delta function that equals 1 when $r = 1$ and *zero* otherwise, where r is defined as:

$$r = \sqrt{(x(n) - x(m))^2 + (y(n) - y(m))^2 + (z(n) - z(m))^2} \tag{3.4}$$

In an incompressible system the inter-molecular interaction is modeled by determining the effective attractions between polymer chains. The mean field approach has been used to calculate the average inter-molecular interactions ($E_{inter}(\alpha)$) in most theoretical studies of polymers [50, 42, 46]. The conventional mean-field approach determines the average intermolecular attraction through the interactions between the average volume fractions of each point in space and its neighbors. The average intermolecular interaction is defined mathematically as follows:

$$\langle E_{inter}(\alpha)\rangle = -\frac{\varepsilon_{inter}}{2}\sum_{ii=1}^{N_P}\sum_{i}\sum_{j}\sum_{k}\langle\phi_p(i,j,k)\rangle\langle\phi_p^{int}(i,j,k)\rangle \tag{3.5}$$

where ε_{inter} represents the elementary inter-attractive energy, which is divided by two to correct for the double counting of the interactions. The average volume fraction at point (i,j,k) in a space is defined as follows:

$$\langle\phi_p(i,j,k)\rangle = \sum_{ii}^{N_p}\sum_{\alpha}P_{ii}(\alpha)n_{p,ii}(\alpha,i,j,k) \tag{3.6}$$

where $n_{p,ii}(\alpha,i,j,k)$ is the Kronecker delta function that equals 1 at configuration α, when a polymer segment of polymer ii occupies the (i,j,k) position. $\langle\phi_p^{int}(i,j,k)\rangle$ is what is called by Oversteegen and his colleagues the contact fraction, and is defined as follows [41]:

$$\langle\phi_p^{int}(i,j,k)\rangle = \frac{1}{D}\sum_{i=l,-l}\Big(\phi(i+l,j,k)+\phi(i,j+l,k)+\phi(i,j,k+l)\Big) \tag{3.7}$$

where D is the number of coordination in the system. Notice that $\frac{1}{D}$ represents a weighting function of possible interactions around point (i,j,k), which is equal to $\frac{1}{6}$ for all neighbors in $3D$ system.

The decoupled mean-field approach increases the efficiency of calculating the inter-molecular interaction. Thus, all possible inter-molecular interactions for each monomer are collected while building the chain using SAW technique. While building the chain, each additional monomer will have a number of possible positions, one of

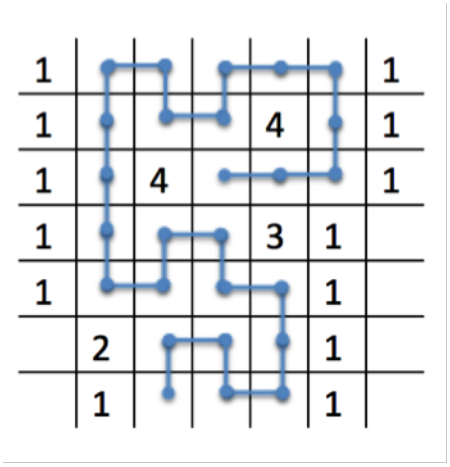

Figure 3.6: Calculating the number of intermolecular interactions at several sites for specific configuration $\eta^*_{ii}(\alpha, i, j, k)$.

which is chosen for a specific configuration while the others are counted as possible inter-molecular interaction sites $\eta^*_{ii}(\alpha, i, j, k)$ (see Figure 3.6).

In the decoupled mean-field approach the average inter-molecular interaction energy is defined as follows:

$$\langle E_{inter}(\alpha)\rangle = -\frac{\varepsilon_{inter}}{2}\sum_{ii=1}^{N_P}\sum_{i}\sum_{j}\sum_{k}\langle\eta^*_{ii}(i,j,k)\rangle\langle\phi^*_{ii}(i,j,k)\rangle \tag{3.8}$$

where $\langle\eta^*_{ii}(i,j,k)\rangle$ is the average number of inter-molecular interactions at site (i,j,k) due to polymer ii, and $\langle\phi^*_{ii}(i,j,k)\rangle$ is the average volume fraction at site (i,j,k) due to all polymers in the system except polymer ii. The mathematical definitions of these two quantities are as follows:

$$\begin{aligned}\langle\eta^*_{ii}(i,j,k)\rangle = \frac{1}{D}\sum_{\alpha}P_{ii}(\alpha)\sum_{l=1,-1}\left(1-\sum_{i}\sum_{j}\sum_{k}n_{p,ii}(\alpha,i,j,k)\right)\\ \left[n_{p,ii}(\alpha,i+l,j,k)+n_{p,ii}(\alpha,i,j+l,k)+n_{p,ii}(\alpha,i,j,k+l)\right] \qquad (3.9)\\ \langle\phi^*_{ii}(i,j,k)\rangle = \sum_{jj\neq ii=1}^{N_P}\sum_{\alpha}P_{jj}(\alpha)n_{p,jj}(\alpha,i,j,k)\end{aligned}$$

where we use $(\frac{1}{D} = \frac{1}{6})$ as the weighting function of the decoupled inter-molecular interactions fraction.

The total free energy function of a system of thermoresponsive polymers, is defined as the sum of the polymer's free energies that are caused by the intra and the inter-molecular interactions. Notice that the steric energy is embedded in the cubic lattice model. Thus, the free energy function per unit area can be written as follows:

$$\Omega = \beta \left[\langle E_{intra} \rangle + \langle E_{inter} \rangle \right] + \frac{1}{A} \sum_{ii}^{N_p} \left(\sum_{\alpha} P_{ii}(\alpha) \ln P_{ii}(\alpha) \right) \tag{3.10}$$

The first term in the free energy function denotes the effect of the intra and the inter-molecular attractive energies between polymer chains. The second term denotes the conformational entropy of polymer chains, where $P_{ii}(\alpha)$ refers to the probability of having chain ii at configuration α.

The system under study is subject to the incompressibility constraint, where each lattice site must be occupied by a monomer or water molecule. This constraint is expressed mathematically as follows:

$$\langle \phi_p(i,j,k) \rangle + \phi_w(i,j,k) = 1 \tag{3.11}$$

The first term in the incompressibility constraint accounts for the average volume fraction of all polymer segments in the system, and the second term denotes the volume fraction of water molecules. To solve the incompressibility constraint equation, the average polymer volume fraction is written in terms of the probability of having a polymer ii at configuration α. This probability can be expressed by minimizing the free energy function with respect to the polymer's occupation fraction, and introducing the Lagrange multipliers $\pi(i,j,k)$.

$$P_{ii}(\alpha) = \frac{w_{RB}(\alpha)}{q_{ii}} \exp\Big(-\beta \Big[E_{intra,ii}(\alpha) - E_{inter,ii}(\alpha) \Big] \Big) \tag{3.12}$$

where q_{ii} is a state function for polymer ii, ensuring that $\sum_{\alpha} P_{ii}(\alpha) = 1$. Here, $w_{RB}(\alpha)$ is the Rosenbluth weighting function that should improve the statistical efficiency. Also note that, $v_{p,ii}(\alpha,i,j,k) = n_{p,ii}(\alpha,i,j,k) v_w$. Minimizing equation (3.23) gives us

the following definition for the density of water molecules at point (i, j, k):

$$\rho_w(i, j, k)v_w = \exp(-\beta\pi(i, j, k)v_w) \tag{3.13}$$

The volume of the water molecule is chosen to symbolize the volume of polymer segments. Equation (3.13) emphasizes the physical meaning of Lagrange multipliers by relating these values to the osmotic pressure that keeps the chemical potential constant at any specific position, while the number of particles at the same position fluctuates [1].

3.4 The Study of Grafted Polyelectrolytes

Grafted polyelectrolytes are used to examine the modification of the mean-field theory. The model mimics a tissue material that is made of polyelectrolytes. As the polyelectrolytes dissolve in the biological solution, they produce charged functional groups (see Section 1.3). Polymer's self-organization is affected not only by the temperature, but also by the surface charge density, the salt concentration of the solvent and the pH of the surrounding. The model and the theoretical approach for this model are described below.

3.4.1 The Model

The model of the grafted polyelectrolytes is similar to the inhomogeneous model of thermoresponsive polymers (see Subsection 3.3.1), but with the addition of salt ions and charged polymer segments that are distributed in the lattice sites (see Figure 3.7).

The model contains grafted polybases in a biological solution. The choice of polybase should serve in increasing the attractive interaction between the drug delivery

[1]For more information on the osmotic pressure $\pi(i, j, k)$ reed the Tethered Polymer Layers chapter from Advances in Chemical Physics [50].

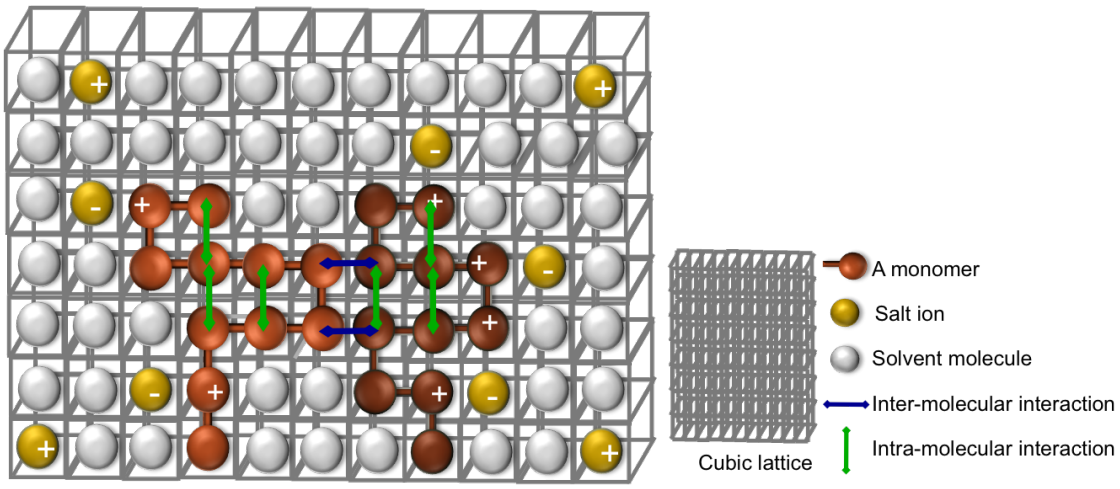

Figure 3.7: A 2D SAW model of two polyelectrolytes in a cubic lattice with two different configurations surrounded by solvent molecules and salt ions.

device and the negatively charged surface of the cell [1, 6]. The basic polyelectrolytes contain monomers that are able to either ionize to positively charged molecules or stay neutral through the interaction $\mathrm{B} + \mathrm{H}^+ \rightleftharpoons \mathrm{BH}^+$. The equilibrium dissociation constant K_d of the interaction is given by:

$$K_d = \frac{[B][\mathrm{H}^+]}{[\mathrm{BH}^+]} \tag{3.14}$$

This constant can be determined by the change in the standard state Gibbs free energy of the reaction, $\triangle G^0 = \mu^0_{\mathrm{B}} + \mu^0_{\mathrm{H}^+} - \mu^0_{\mathrm{BH}^+}$, where μ^0_i is the standard chemical potential, and $K_d = C \exp(-\beta \triangle G^0)$. C is a dimensional constant, and β is the inverse thermodynamic temperature $\left(\beta = \frac{1}{K_B T}\right)$.

The aqueous solution has dissociated monovalent salt molecules ($\mathrm{NaCl} \longrightarrow \mathrm{Na}^+ + \mathrm{Cl}^-$) (see Figure 3.1). The bulk salt concentration is C_{salt}. In this study, water molecules are able to dissociate to protons H^+ and hydroxyl ions OH^-. The study covers a pH range of 5.8 : 7.6, which is consistent with therapeutic tissue materials that target malignant tissues [54].

This model assumes that there is no change in the volume of the ionized and neutral monomers. Hence, the volume of both B and BH^+ is equal, and it is identical

to the volume of all molecules in the system. Another considered assumption, is that the activities of all species in the system are given by their concentrations. These two assumptions are the same assumptions used by Uline in modeling DNA molecules [56].

All molecules in the system are subject to different kinds of forces, such as steric, van der Waals and electrostatic forces. The repulsive steric interactions are modeled with the assumption that the system contains a good solvent and by employing a cubic lattice model. The van der Waals interactions are accounted for through the intra and inter-molecular interactions as discussed in the study of thermoresponsive polymers (see Section 3.3.1 and Figure 3.4). The values of the two short-ranged attractive interactions, (ε_{intra} and ε_{inter}), have been chosen carefully so they don't affect the solubility of the solvent in the system. The electrostatic interactions between two charged molecules in the system are influenced by several variables. This model studies the effect of the surface charge coverage; or the number of charged elements per unit area (σ_q), the salt concentration (C_{salt}) in the system, and the bulk pH on the electrostatic interactions as well as the temperature effect on the polymers aggregations. Different electrostatic interactions cause different configurations and accordingly, different intra and inter-molecular interactions. The model demonstrates the complexity of the chemical equilibrium and the physical interactions between all molecules in the system.

3.4.2 Theoretical Approach

Building on the thermoresponsive model, we write the total free energy function as the sum of the free energies that are caused by all possible interactions between polymer segments, solvent and ion salt molecules in the system.

$$F = F_{polymer} + F_{elect} + F_{if} + F_{chem} + F_{mix} \tag{3.15}$$

The first term accounts for the polymers self energy that is caused by intra and

inter-molecular interactions, and the polymers conformational entropy. The decoupled MF approach that is discussed in the previous section (see Section 3.3.2) is used to calculate the inter-molecular interactions in the system.

$$F_{polymer} = \langle E_{intra} \rangle + \langle E_{inter} \rangle + TS_{poly} \tag{3.16}$$

The second term accounts for the electrostatic interactions between all molecular species in the system:

$$F_{elec} = \sum_i \sum_j \sum_k \left[\langle \phi_q(i,j,k) \rangle \, \psi(i,j,k) - \frac{\epsilon}{2} \left(\nabla \psi(i,j,k) \right)^2 \right] \tag{3.17}$$

where, $\psi(i,j,k)$ is the electric potential at point (i,j,k), and ϵ is the medium permittivity that is held to be constant in the system. The expression $(\nabla\psi(i,j,k))^2$ characterizes the gradient of the electric potential in a Cartesian coordinate system squared. We define $\langle \phi_q(i,j,k) \rangle$ as the average occupation fraction of charges at position (i,j,k) , and it is stated mathematically as follows:

$$\langle \phi_q(i,j,k) \rangle = f_{\mathrm{H}^+}(i,j,k) q_p \, \langle \phi_p(i,j,k) \rangle + \sum_i q_i \, \langle \phi_i(i,j,k) \rangle \tag{3.18}$$

where $f_{\mathrm{H}^+}(i,j,k)$ is the fraction of protonated monomers along the polymer chains. Also, q_i and $\langle \phi_i(i,j,k) \rangle$ are the charge and the occupation fraction of ion $i (i = \mathrm{H}^+, \mathrm{OH}^-, \mathrm{Na}^+, \mathrm{Cl}^-)$ respectively. $\langle \phi_p(i.j.k) \rangle$ is the average occupation fraction of the polymers at point (i,j,k), and it is given by the following relation:

$$\langle \phi_p(i,j,k) \rangle = \sum_{ii}^{N_p} \sum_{\alpha} P_{ii}(\alpha) n_{p,ii}(\alpha,i,j,k) \tag{3.19}$$

The expression $(\Delta\psi(i,j,k))^2$ characterizes the gradient of the electric potential in a Cartesian Coordinate system squared, which provides a scalar (see Appendix C).

The third term incorporates the ion formation free energy for water;

$$F_{if} = \sum_i \sum_j \sum_k \left(\phi_{H^+}(i,j,k) \mu^{\circ}_{\mathrm{H}^+} + \phi_{OH^-}(i,j,k) \mu^{\circ}_{\mathrm{OH}^-} \right) \tag{3.20}$$

The fourth term represents the free energy caused by the chemical interaction;

$$\begin{aligned} F_{chem} =& \frac{1}{\beta}\sum_i\sum_j\sum_k\langle\phi_p(i,j,k)\rangle\Big\{ f_{\mathrm{H}^+}(i,j,k)\Big[\ln f_{\mathrm{H}^+}(i,j,k)+\beta\mu^{\circ}_{\mathrm{BH}^+}\Big] \\ &+\Big(1-f_{\mathrm{H}^+}(i,j,k)\Big)\Big[\ln\Big(1-f_{\mathrm{H}^+}(i,j,k)\Big)+\beta\mu^{0}_{\mathrm{B}}\Big]\Big\} \end{aligned} \tag{3.21}$$

The fifth term is the free energy due to mixing all species in the system;

$$\begin{aligned} F_{mix} =& \frac{1}{\beta}\sum_i\sum_j\sum_k[\phi_w(i,j,k)(\ln\phi_w(i,j,k)-1)]+[\phi_{\mathrm{H}^+}(i,j,k)(\ln\phi_{\mathrm{H}^+}(i,j,k)-1)] \\ &+[\phi_{\mathrm{OH}^-}(i,j,k)(\ln\phi_{\mathrm{OH}^-}(i,j,k)-1)]+[\phi_+(i,j,k)(\ln\phi_+(i,j,k)-1)] \\ &+[\phi_-(i,j,k)(\ln\phi_-(i,j,k)-1)] \end{aligned} \tag{3.22}$$

Accordingly, the free energy function per unit area for a semi-grand canonical ensemble is given as follows:

$$\begin{aligned} \Omega =& \beta\Big[\langle E_{intra}\rangle+\langle E_{inter}\rangle\Big]+\frac{1}{A}\sum_{ii}^{N_p}\left(\sum_\alpha P_{ii}(\alpha)\ln P_{ii}(\alpha)\right) \\ &+\beta\sum_i\sum_j\sum_k\left[\langle\phi_q(i,j,k)\rangle\,\psi(i,j,k)-\frac{\epsilon}{2}\left(\nabla\psi(i,j,k)\right)^2\right] \\ &+\sum_i\sum_j\sum_k\langle\phi_p(i,j,k)\rangle\left[f_{\mathrm{H}^+}(i,j,k)\left[\ln f_{\mathrm{H}^+}(i,j,k)+\beta\mu^0_{\mathrm{BH}^+}\right]\right. \\ &\left.+(1-f_{H+}(i,j,k))\left[\ln(1-f_{H+}(i,j,k))+\beta\mu^0_{\mathrm{B}}\right]\right] \\ &+\sum_i\sum_j\sum_k\left[\Big[\phi_w(i,j,k)(\ln\phi_w(i,j,k)-1)\Big]\right. \\ &+\Big[\phi_{\mathrm{H}^+}(i,j,k)(\ln\phi_{H^+}(i,j,k)-1+\beta\mu^0_{\mathrm{H}^+})\Big] \\ &+\Big[\phi_{\mathrm{OH}^-}(i,j,k)(\ln\phi_{\mathrm{OH}^-}(i,j,k)-1+\beta\mu^0_{\mathrm{OH}^-})\Big] \\ &\left.+\Big[\phi_+(i,j,k)(\ln\phi_+(i,j,k)-1-\beta\mu_+)\Big]+[\phi_-(i,j,k)(\ln\phi_-(i,j,k)-1-\beta\mu_-)]\right] \end{aligned} \tag{3.23}$$

The first term in the free energy function accounts for the intra and the intermolecular attractive energies of polymer chains. The second term denotes the conformational entropy of polymer chains, where $P_{ii}(\alpha)$ refers to the probability of having

chain ii at configuration α. The third term accounts for the electrostatic interactions, which have been clarified previously.

The fourth term in the free energy function represents the acid base equilibrium, while the fifth term accounts for the translational entropy of all molecular species in the system and the formation of anions. Here, μ_i^0 and μ_i represent the standard chemical potential and the bulk chemical potential of specie i respectively.

The system under study is subject to the incompressibility constraint, where each lattice site must be occupied by a monomer, counterion, water, or salt ion molecule. This takes care of the excluded volume interactions through the following relation:

$$\begin{aligned} \langle \phi_p(i,j,k) \rangle + \phi_w(i,j,k) + \phi_{\mathrm{H}^+}(i,j,k) + \phi_{\mathrm{OH}^-}(i,j,k) \\ + \phi_+(i,j,k) + \phi_-(i,j,k) = 1 \end{aligned} \tag{3.24}$$

The first term in the incompressibility constraint denotes the average volume fraction of charged polymer segments along with those which are bound to counterions. The other terms in the constraint equation represent the volume fraction of the water (solvent), proton, hydroxyl ion, cation, and anion molecules respectively. Notice that free counter ions are considered in the anion volume fraction $\phi_-(i,j,k)$. To solve the incompressibility constraint equation, the average polymer volume fraction is written in terms of the probability. Another set of equations is needed to learn more about the system, thus we extremitize the free energy function with respect to the electric potential $\psi(i,j,k)$ to get Poisson's equation.

$$\Delta\psi(i,j,k) = -\frac{\langle \phi_q(i,j,k) \rangle}{A\epsilon} \tag{3.25}$$

where the simple Δ symbolizes the Laplacian or the divergent of the gradient of the electrical potential ($\Delta = \nabla \cdot \nabla$), and for the computational analysis we use the centered space difference approximation method, which we mentioned in section 2.3.

We consider two boundary conditions in order to solve Poisson's equation. The first condition enforces the surface charge coverage to be equal to a given value σ_q

(Meaning that the surface potential is constant at the surface), and the second one insures that there are no charges at a distance far away from the grafted surface. These two boundary conditions are expressed mathematically as follows:

$$\begin{cases} \psi(i,j,k=0) = \psi_0 \quad \Rightarrow \quad \nabla_k \, \psi(i,j,k=0) = 0 \\ \lim\limits_{k\to\infty} \psi(i,j,k) = 0 \end{cases} \tag{3.26}$$

By minimizing the free energy function with respect to the polymers occupation fraction, and introducing the Lagrange multipliers, $\pi(i,j,k)$, one can get the following expression for the probability of having a polymer ii at configuration α:

$$P_{ii}(\alpha) = \frac{w(\alpha)}{q_{ii}} \exp\Bigg(-\beta\Big[E_{intra,ii}(\alpha) - E_{inter,ii}(\alpha)\Big] - \sum_i \sum_j \sum_k v_{p,ii}(\alpha,i,j,k) \Big[\beta q_p \psi(i,j,k) + \ln f_{\mathrm{H}^+}(i,j,k) - \beta\pi(i,j,k)\Big]\Bigg) \tag{3.27}$$

where q_{ii} is a state function for polymer ii, ensuring that $\sum_\alpha P_{ii}(\alpha) = 1$. Here, $w(\alpha)$ is the Rosenbluth weighting function. Also, $v_{p,ii}(\alpha,i,j,k) = n_{p,ii}(\alpha,i,j,k)v_w$. By minimizing equation (3.23), we get the following definitions for all the molecular species' densities in the system, where $\rho_i(i,j,k) = \frac{\phi_i(i,j,k)}{v_w}$, and v_w is the volume fraction of the water molecule.

$$\begin{aligned} \rho_+(i,j,k)v_w &= \exp(\beta\mu_+ - \beta\pi(i,j,k)v_+ - \beta q_+\psi(i,j,k)) \\ \rho_-(i,j,k)v_w &= \exp(\beta\mu_- - \beta\pi(i,j,k)v_- - \beta q_-\psi(i,j,k)) \\ \rho_{\mathrm{H}^+}(i,j,k)v_w &= \exp(-\beta\mu^0_{\mathrm{H}^+} - \beta\pi(i,j,k)v_w - \beta q_{\mathrm{H}^+}\psi(i,j,k)) \\ \rho_{\mathrm{OH}^-}(i,j,k)v_w &= \exp(-\beta\mu^0_{\mathrm{OH}^-} - \beta\pi(i,j,k)v_w - \beta q_{\mathrm{OH}^-}\psi(i,j,k)) \\ \rho_w(i,j,k)v_w &= \exp(-\beta\pi(i,j,k)v_w) \end{aligned} \tag{3.28}$$

where $\rho_+(i,j,k)$ and $\rho_-(i,j,k)$ are the densities of the cations and the anions segments at (i,j,k) position. The volume of the water molecule is chosen to symbolize the volume of all molecular species in the system. Importantly, the last equation emphasizes the physical meaning of Lagrange multipliers by relating these values to the

osmotic pressure that keeps the chemical potential constant at any specific position, while the number of particles at the same position fluctuates.

Moreover, we obtain the value of the protonation fractions, $f_{\mathrm{H^+}}(i,j,k)$, by minimizing the free energy with respect to that variable to get the following relation:

$$\frac{f_{\mathrm{H^+}}(i,j,k)}{\Big(1-f_{\mathrm{H^+}}(i,j,k)\Big)} = \frac{\phi_{\mathrm{H^+}}(i,j,k)}{K_d^0 \phi_w(i,j,k)} \tag{3.29}$$

where the dissociation equilibrium constant (K_d^0) is defined as the negative exponential of Gibbs free energy in K_BT units;

$$K_d^0 = \exp(-\beta \Delta G^0) = \exp\Big(-\beta(\mu_{\mathrm{B}}^0 + \mu_{\mathrm{H^+}}^0 - \mu_{\mathrm{BH^+}}^0)\Big) \tag{3.30}$$

3.5 Results and Discussion

The system understudy is composed of nine grafted polymers with a polymerization number of 25. The elementary intra and inter-molecular interactions are set to be equal to -1 during all calculations ($\varepsilon_{intra} = \varepsilon_{inter} = -1$). We compare the standard MF approach with the decoupled MF at several thermodynamic temperatures (K_BT), and separation grafted distance (d) values. The 3D complex system is solved using KINSOL solver from the SUNDIALS library with the SPGMR interface. In the case at which we apply the standard MF, we solve the system for one set of unknowns, which is the solvent volume fraction ($\phi_w(i,j,k)$). By applying the decoupled MF, we increase the number of unknowns in the system. These unkowns are as follows:

- Nine sets of the average volume fraction of all polymers in the system accept the polymer under study, $\langle \phi_{ii}^*(i,j,k) \rangle$.
- Nine sets of the average inter-molecular interaction of the polymer under study, $\langle \eta_{ii}^*(i,j,k) \rangle$.
- One set of solvent volume fraction, $\phi_w(i,j,k)$.

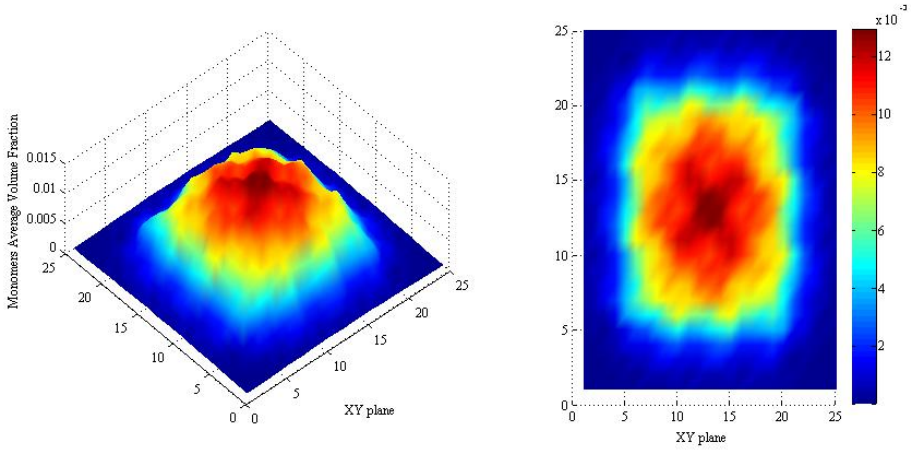

Figure 3.8: An illustration of the average volume fraction ($\langle\phi_p(i,j,k)\rangle$) that is used to calculate the inter-molecular interactions in the standard MF approach

Figure (3.8) represents the average volume fraction function ($\langle\phi_p(i,j,k)\rangle$) at $k = 8$ that is used in the standard MF approach to calculate the inter-molecular interactions through the following relation:

$$\langle E_{inter}(\alpha)\rangle = -\frac{\varepsilon_{inter}}{2}\sum_{ii=1}^{N_P}\sum_{i}\sum_{j}\sum_{k}\langle\phi_p(i,j,k)\rangle\langle\phi_p^{int}(i,j,k)\rangle$$

where ($\langle\phi_p^{int}(i,j,k)\rangle$) is the contact fraction of the same function at point (i,j,k) (see Section 3.3.2). The system is tested at $K_BT = 2$ and $d = 5$. One expects a double counting by multiplying the two functions; the average volume fraction function and the contact fraction of the same function.

The decoupled MF approach is tested at the same previous parameters. Figures (3.9), (3.10), and (3.11) represent the average volume fractions ($\langle\phi_{ii}^*(i,j,k)\rangle$) and the corresponding average inter-molecular interaction functions ($\langle\eta_{ii}^*(i,j,k)\rangle$) that is used to calculate the inter-molecular interactions in the decoupled MF approach for each polymer in the system. The figures show the eighth layer ($k = 8$) in the system. Notice that the polymer itself is not included in the average volume fraction function $\langle\phi_{ii}^*(i,j,k)\rangle$. The decoupled approach corrects for the double counting that appears in the standard approach. The decoupled MF inter-molecular interaction is calculated

by summing the multiplication values of $\langle \phi^*_{ii}(i,j,k) \rangle$ and $\langle \eta^*_{ii}(i,j,k) \rangle$ for all polymers in the system.

To track the double counting, we compare the free energy of the standard MF and the decoupled MF for the same system under symmetrical conditions. Figure (3.12) shows the free energy values that are calculated with the standard MF and the decoupled MF at separation distance $d = 3$, and different K_BT values. This figure represents the double counting that is caused by the standard MF approach. At low temperature the free energy values that are calculated with standard MF is more negative, meaning that it has more attractive energy than those calculated with the decoupled MF. Hence, at low temperature, the chains are more collapsed, which is causing the system to be more dense. At dense systems the inter-molecular interactions are dominant. Thus, the double counting effect in the standard MF approach becomes more distinct. As the thermodynamic temperature of the system increases, the chains stretch leading to a more relaxed system. At relaxed systems the inter-molecular interactions are trivial. At low thermodynamic temperature, the free energy values that are calculated with the standard MF become very close to the free energy values that are calculated with decoupled MF.

The double counting that is caused by the standard MF approach is expected to effect the calculated average values in the system, such as the average end-to-end distance value ($\langle R \rangle$). At symmetrical condition, we compare the average end-to-end distance value $\langle R \rangle$ for the middle polymer (polymer number 5) using both approaches at $d = 3$ and $K_BT = 1 : 0.5 : 3$. Figure (3.13) shows that the end-to-end distance value that is calculated with the decoupled MF approach is higher than that calculated with the standard MF approach. As mentioned earlier, the double counting that is caused by the standard MF causes an increase in the attractive free energy of the system. This increase in the attractive energy reveal collapsed chains. Therefore, the $\langle R \rangle$ values that are calculated with standard MF approach are less

than the $\langle R \rangle$ values that are calculated with decoupled MF approach. The decoupled MF approach gives a more accurate values for the average end-to-end distance $\langle R \rangle$ as it corrects for the double counting.

Here we use the decoupled MF approach to study how the nine grafted thermo-responsive polymers interact with each other to form a micelle. We study the effect of the thermodynamic temperature on the micelle formation when the separation distance between the grafted polymers is $d = 5$. Figure (3.14) and (3.15) represent the average volume fraction of polymer segments at each layer in the system at $K_BT = 1$. At this low temperature the polymers shrink and the system becomes very dense. Thus, a rough micellar shape starts to appear at the second layer in the system. Increasing the thermodynamic temperature causes the UCST polymers to stretch. Figure (3.16) and (3.17) represent the average volume fraction of polymer segments at $K_BT = 3$, where a smooth micellar shape appears at the sixth layer with maximum average volume fraction of 0.07.

One can notice that changing the thermodynamic temperature does not effect the average volume fraction of polymer segments at the first layer. The first layer in Figure (3.14) and Figure (3.16) shows the grafted polymer segments for the nine polymers. Starting from the second layer, one can notice the effect of increasing the thermodynamic temperature on the average volume fraction of polymer segments. As the polymers collapse at low temperature such as $K_BT = 1$, Figure (3.15) shows no monomers after the 12th layer. However, Figure (3.17) shows that at $K_BT = 3$ only the 16th layer has no monomers.

We also study the effect of the separation distance d on the micelle formation at constant K_BT. We notice that the polymers' separation distance affects the micelle formation. Figures (3.18) and (3.19) represent the average volume fraction of polymer segments at $K_BT = 2$ and $d = 3$ at each layer in the space of the studied system. In this dense system we see that a smooth micelle starts to appear at the fourth

layer. This is compared to the smooth micelle that starts to appear at the sixth layer in a system with $K_BT = 2$ and $d = 5$ (see Figure (3.20)). However, at the same thermodynamic temperature and separation distance $d = 7$ one can see no micelle formation (see Figure (3.22) and Figure (3.23)).

The micelle formation is affected not only by the thermodynamic temperature, it is also affected by the separation distance between polymers as well as the length of polymers. At specific polymers' length, if the value of the separation distance between polymers is approximately equal to the average end-to-end distance ($\langle R \rangle$) of these polymers, micelle can not form. In order for a set of polymers to form a micelle, the separation distance between these polymers should be less than the ($\langle R \rangle$). Figure (3.13) shows that the studied system contains polymers with average length (end-to-end distance ($\langle R \rangle$)) approximately equals to eight cubic lattice sites at $K_BT = 2$.

In conclusion, the decoupled MF approach corrects the double counting of the inter-molecular interactions that is caused by the standard MF approach. The double counting that is caused by the standard MF approach increases in the condense system at low thermodynamic temperature. The double counting affects the average end-to-end distance values of the polymers in the system. Accordingly, it may affect the value of all average variables in the system. This effect is expected to increase in a more complex system that has electrostatic interactions beside the steric and the van der Waals interactions.

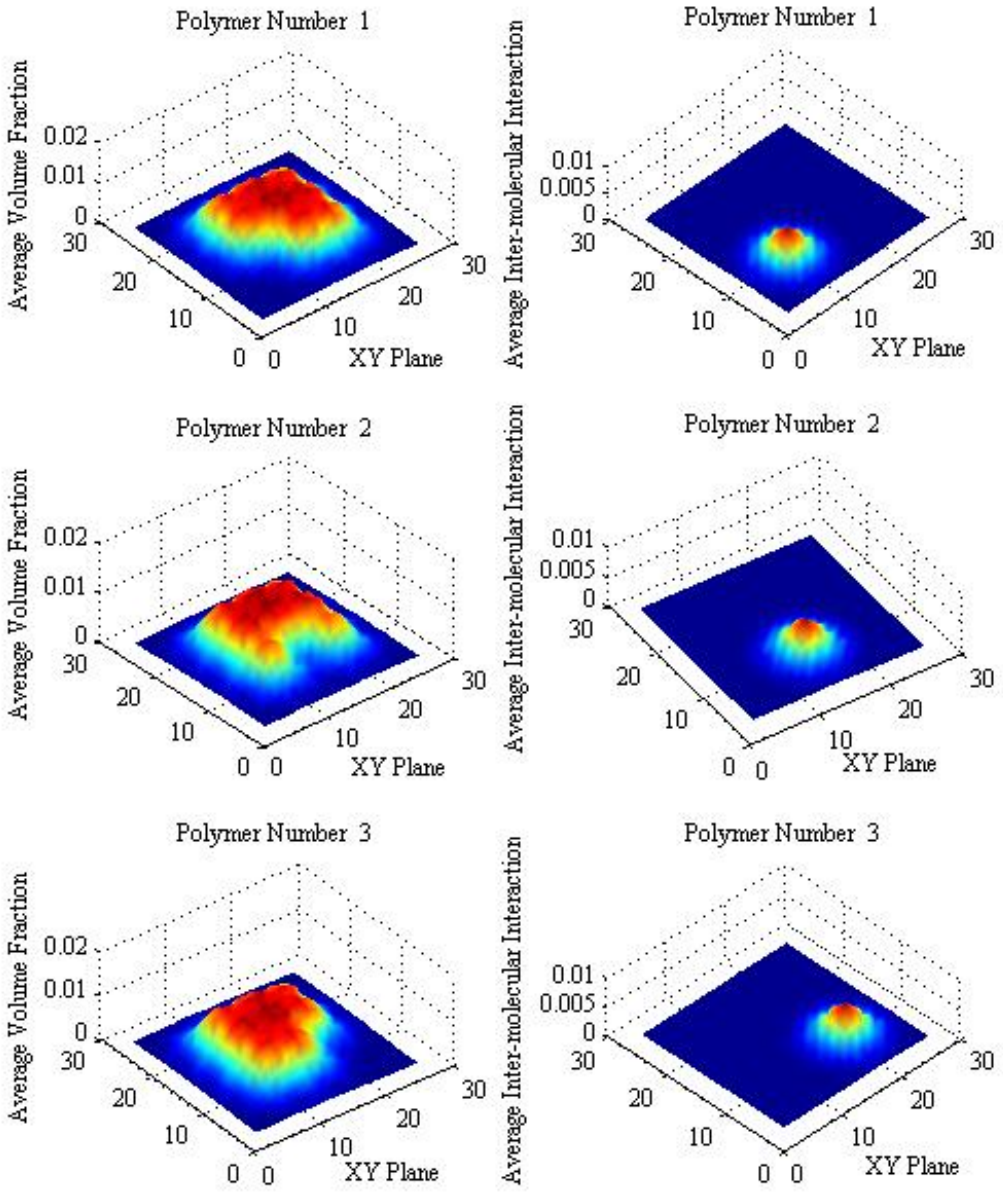

Figure 3.9: An illustration of the average volume fraction function $\langle \phi^*_{ii}(i,j,k) \rangle$ and the corresponding average inter-molecular interaction functions ($\langle \eta^*_{ii}(i,j,k) \rangle$) that is used to calculate the inter-molecular interactions for polymers (1-3) in the standard MF approach.

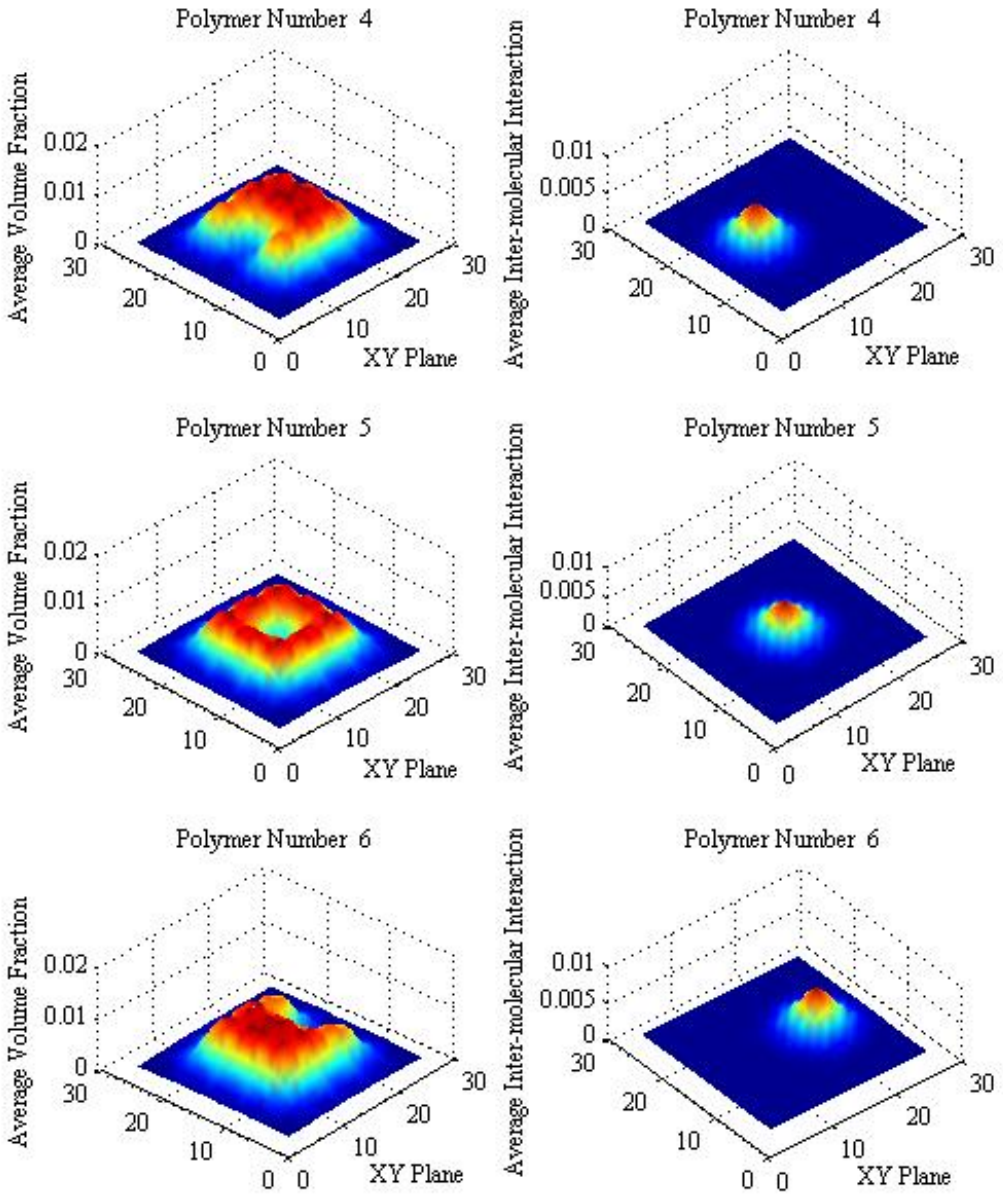

Figure 3.10: An illustration of the average volume fraction function $\langle \phi^*_{ii}(i,j,k) \rangle$ and the corresponding average inter-molecular interaction functions ($\langle \eta^*_{ii}(i,j,k) \rangle$) that is used to calculate the inter-molecular interactions for polymers (4-6) in the standard MF approach.

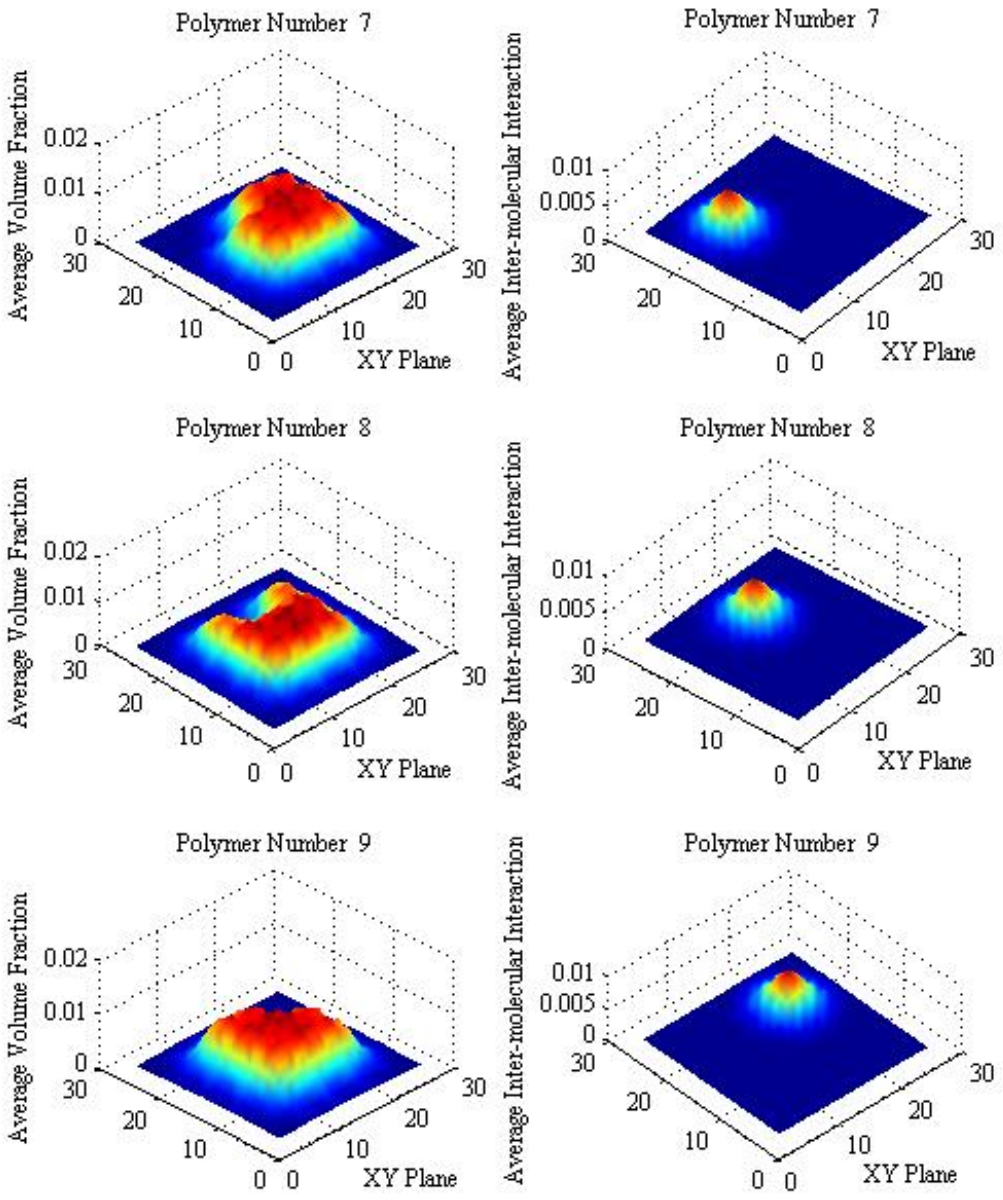

Figure 3.11: An illustration of the average volume fraction function $\langle \phi^*_{ii}(i,j,k) \rangle$ and the corresponding average inter-molecular interaction functions ($\langle \eta^*_{ii}(i,j,k) \rangle$) that is used to calculate the inter-molecular interactions for polymers (7-9) in the standard MF approach.

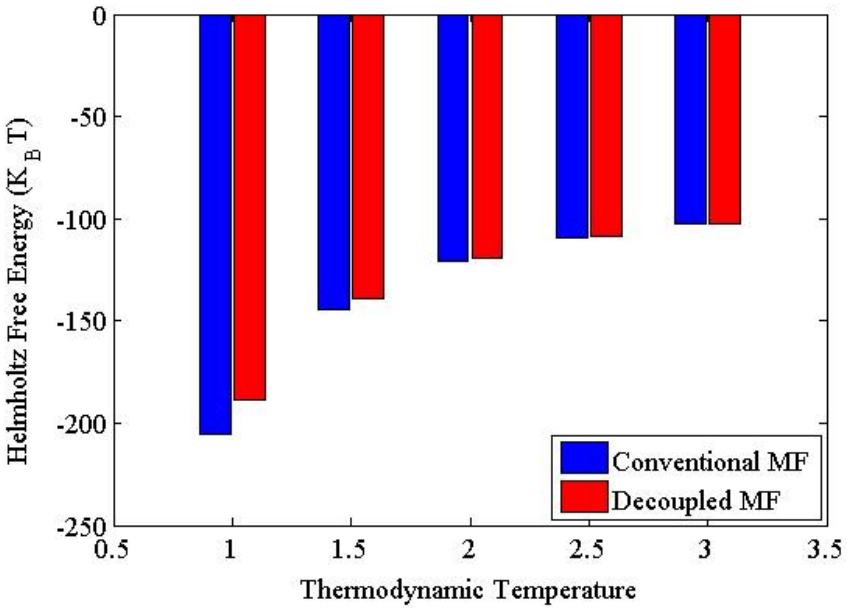

Figure 3.12: A diagram represents the Helmholtz free energy for the standard and the decoupled MF approaches at different K_BT values when the separation distance between the grafted polymers $d = 3$

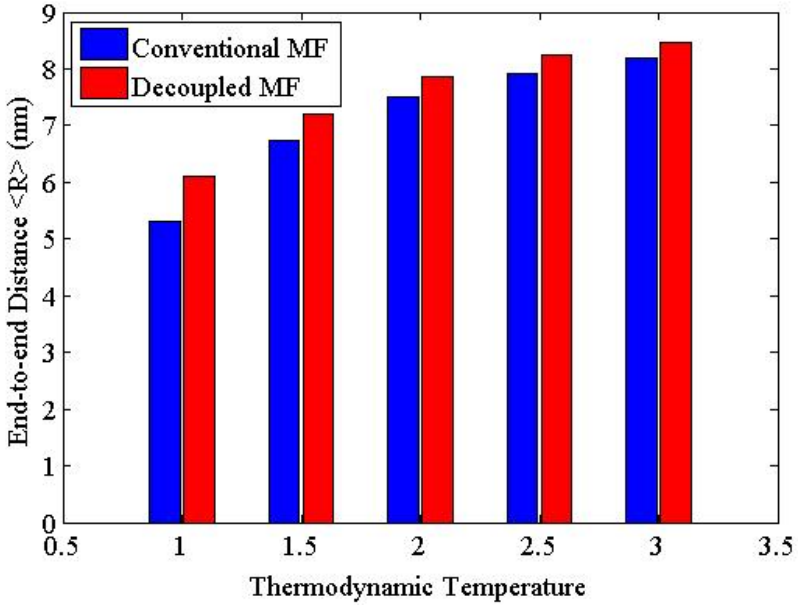

Figure 3.13: A diagram represents the end-to-end distance that is calculated with the standard and the decoupled MF approaches at different K_BT values when the separation distance between grafted polymers $d = 3$

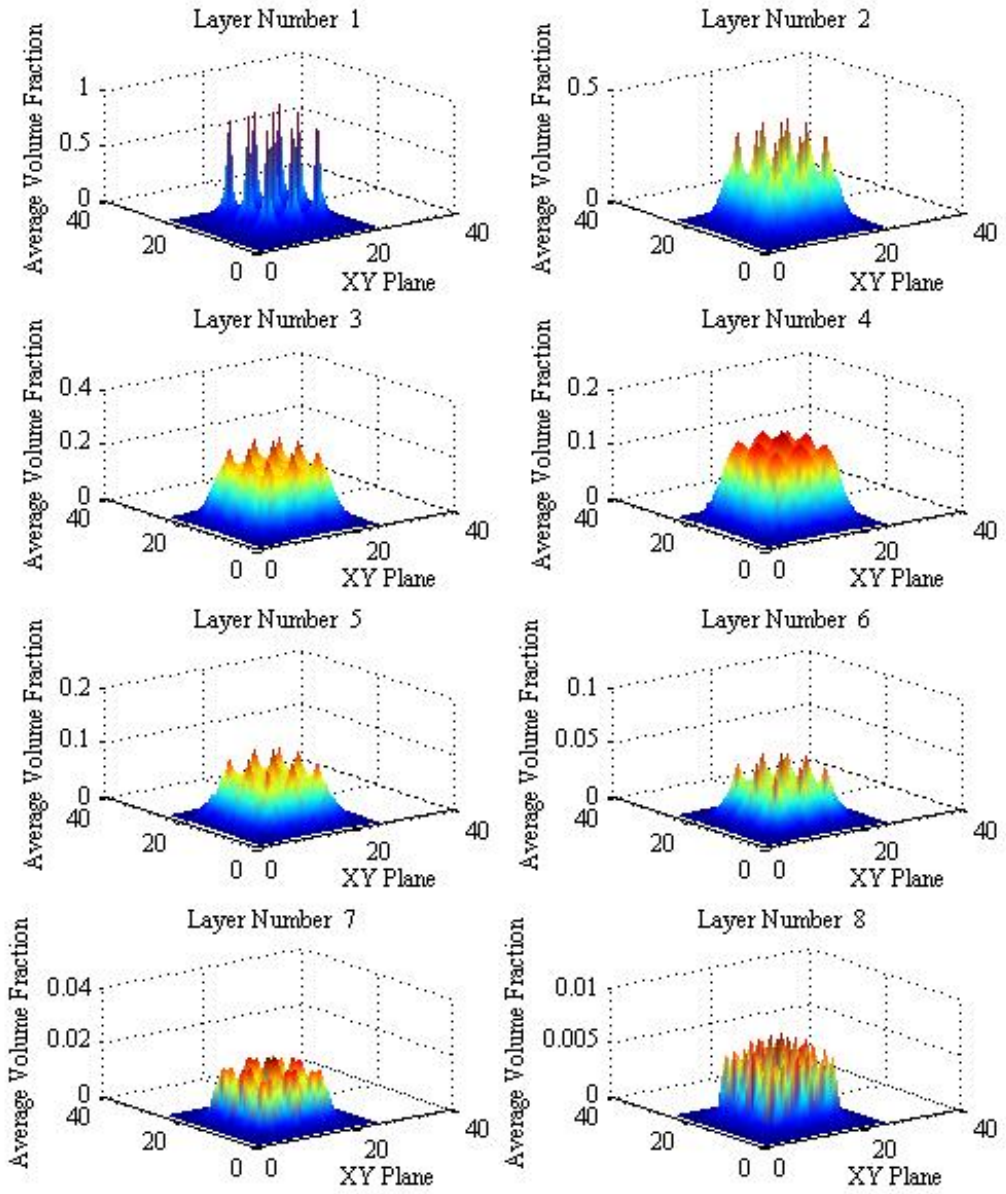

Figure 3.14: The average volume fraction of polymer segments at layers (1-8) in the system at separation distance $d = 5$ and $K_BT = 1$.

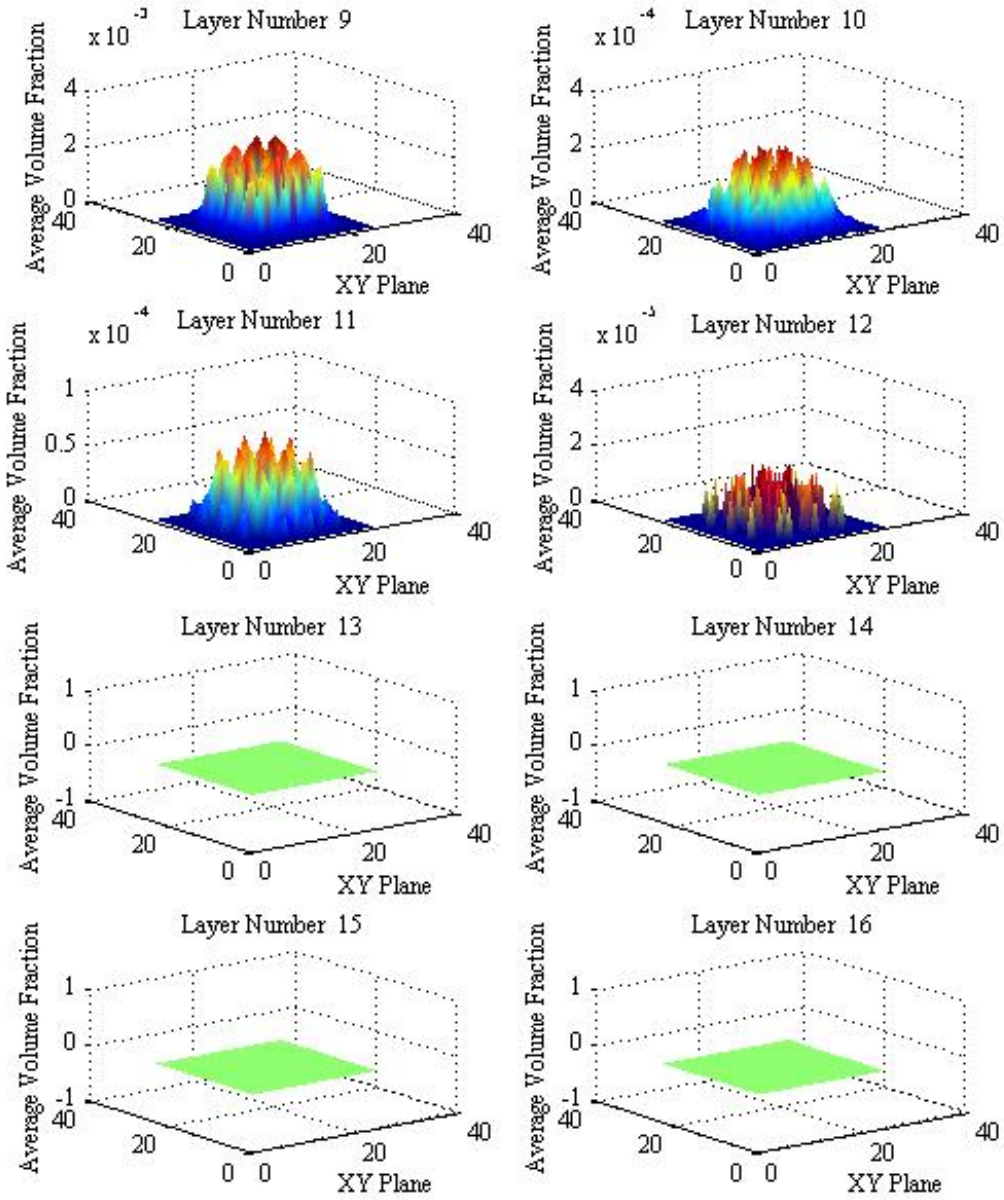

Figure 3.15: The average volume fraction of polymer segments at layers (9-16) in the system at separation distance $d = 5$ and $K_BT = 1$.

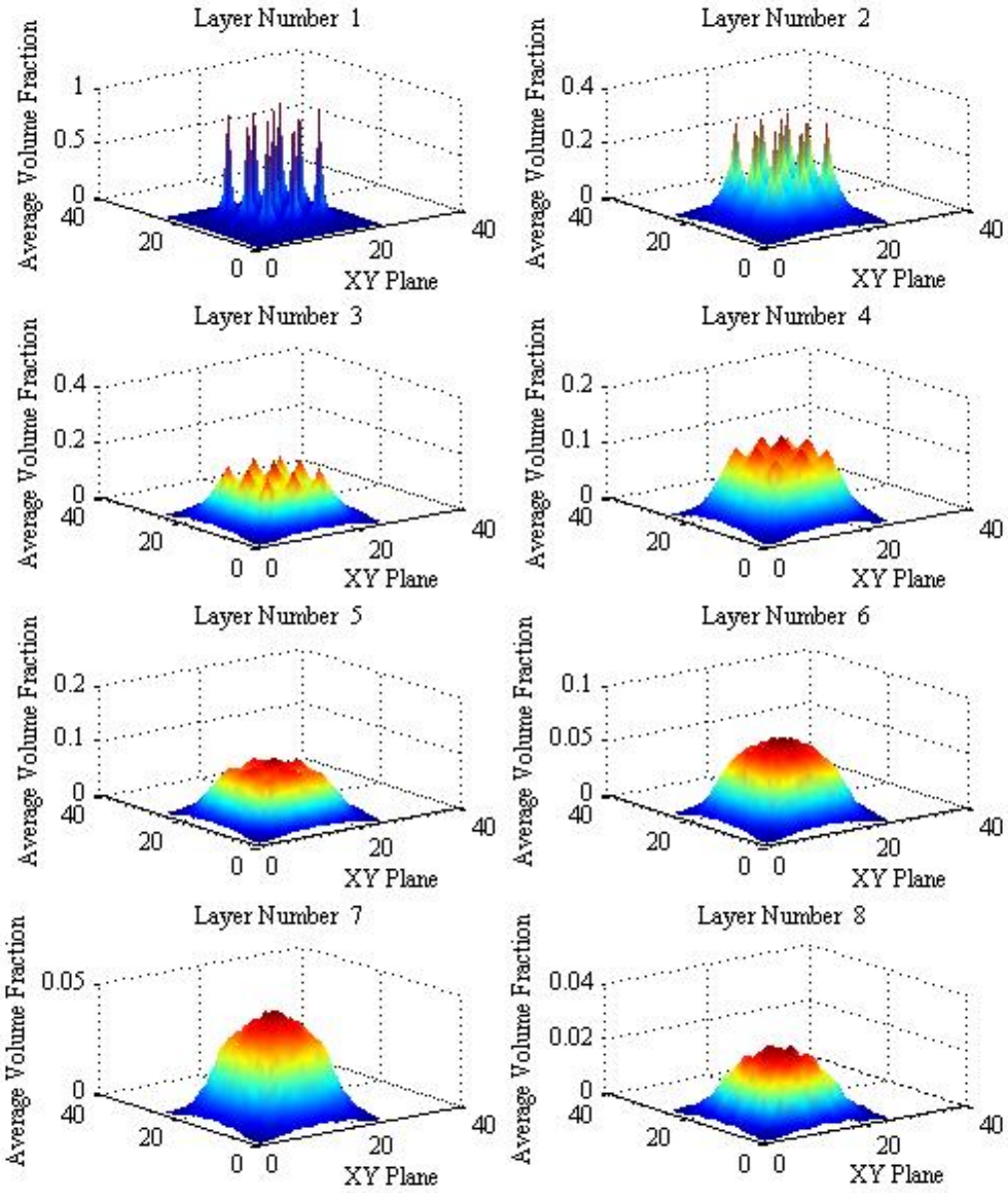

Figure 3.16: The average volume fraction of polymer segments at layers (1-8) in the system at separation distance $d = 5$ and $K_BT = 3$.

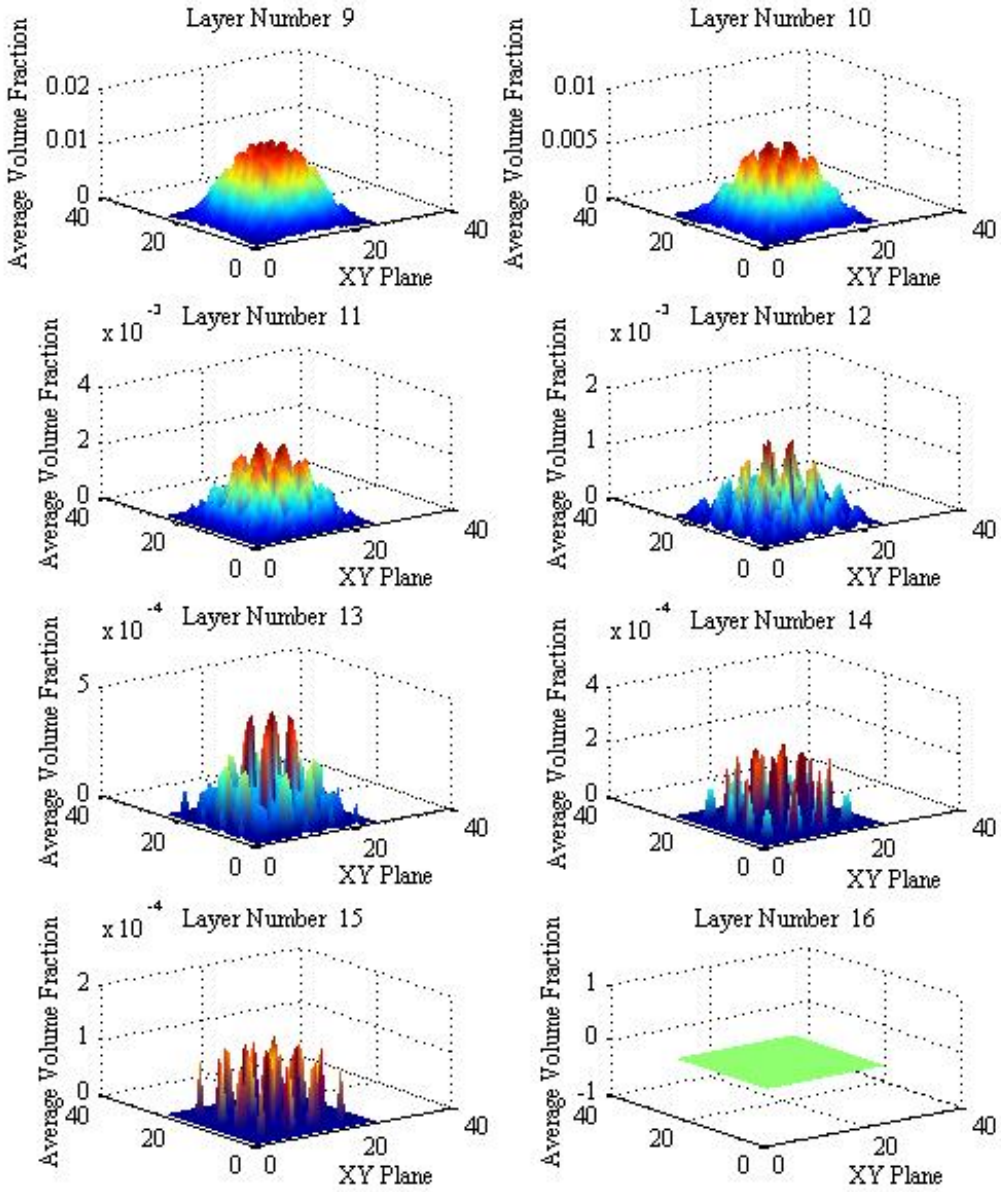

Figure 3.17: The average volume fraction of polymer segments at layers (9-16) in the system at separation distance $d = 5$ and $K_BT = 3$.

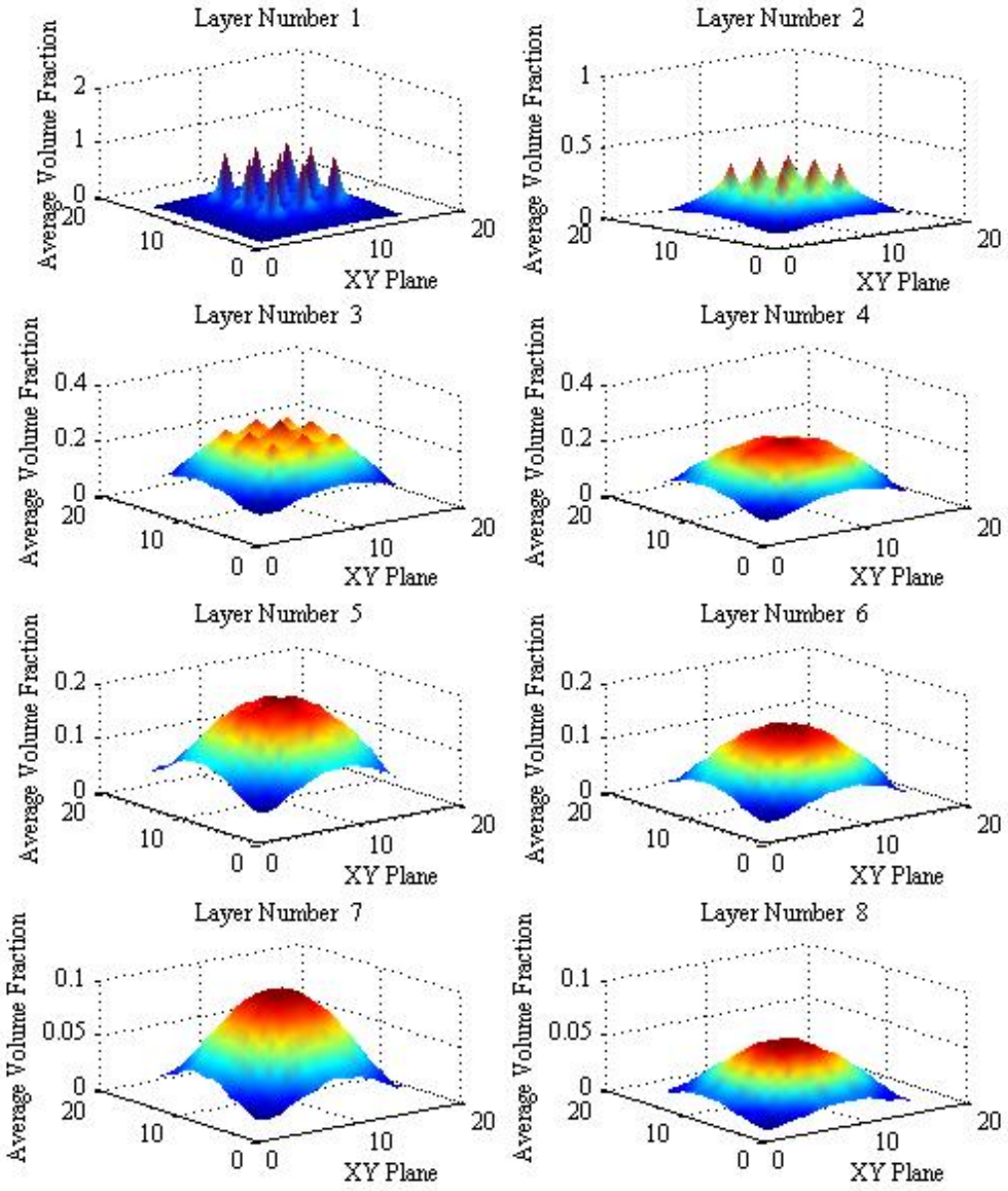

Figure 3.18: The average volume fraction of polymer segments at layers (1-8) in the system at separation distance $d = 3$ and $K_BT = 2$.

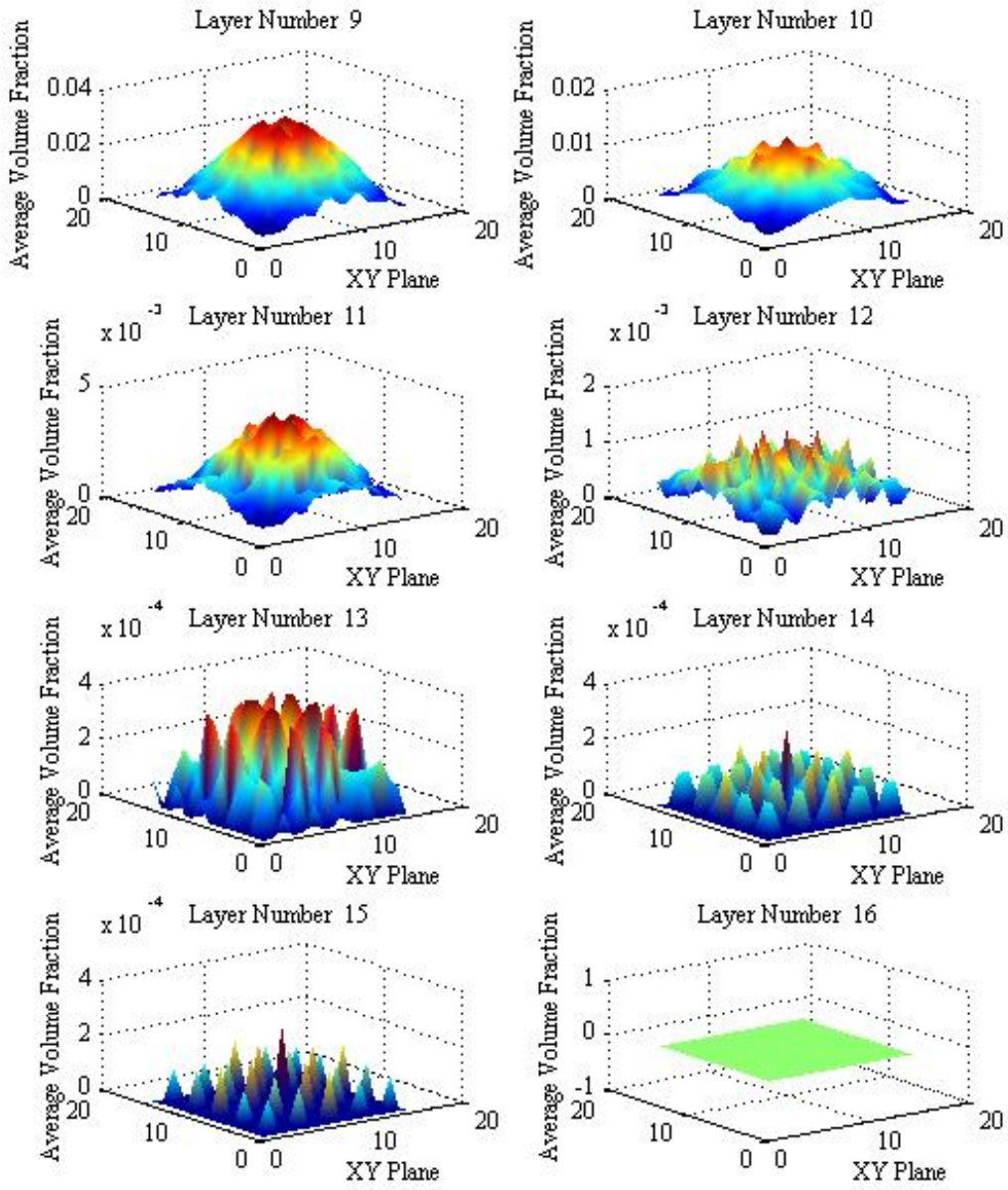

Figure 3.19: The average volume fraction of polymer segments at layers (9-16) in the system at separation distance $d = 3$ and $K_BT = 2$.

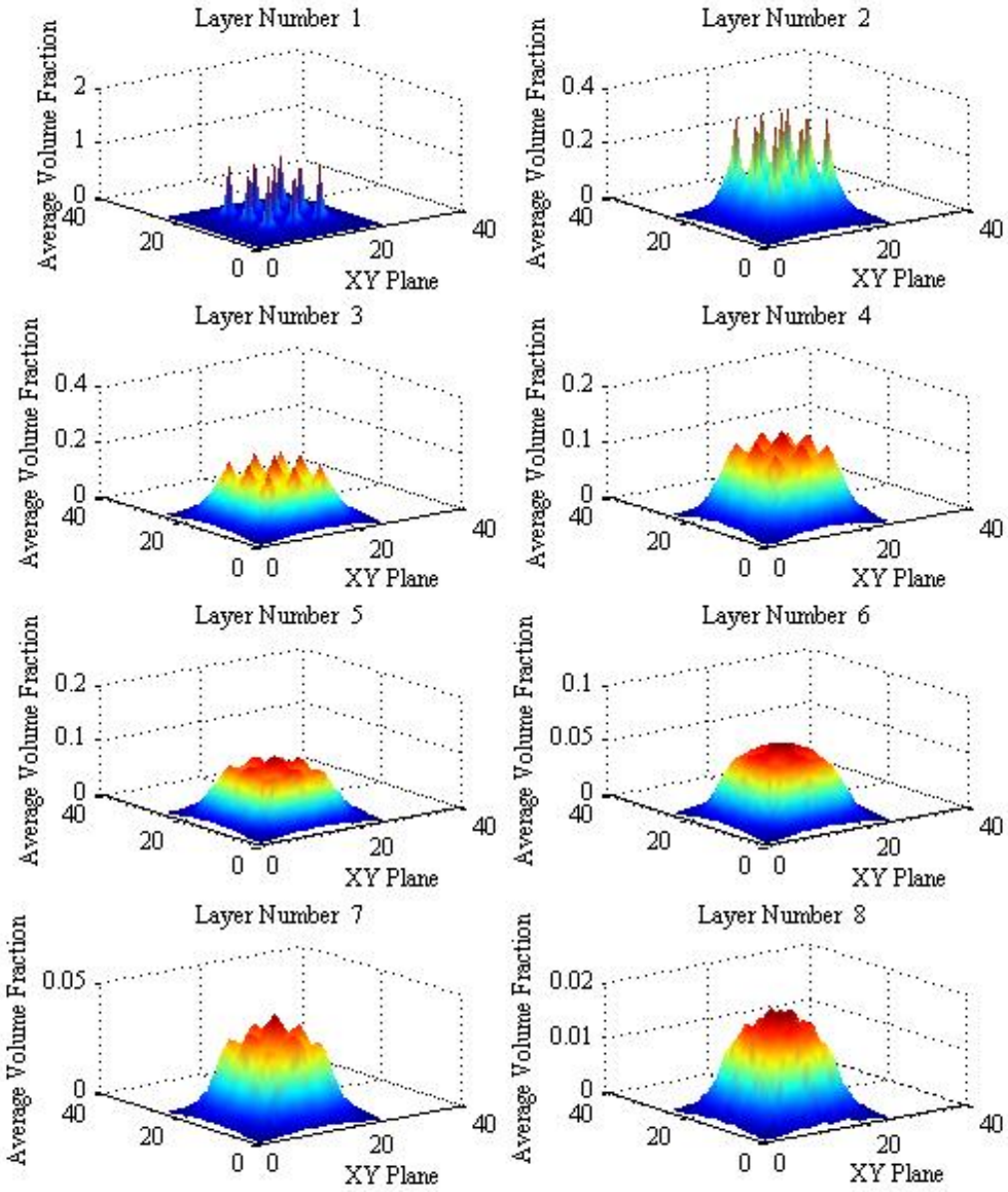

Figure 3.20: The average volume fraction of polymer segments at layers (1-8) in the system at separation distance $d = 5$ and $K_BT = 2$.

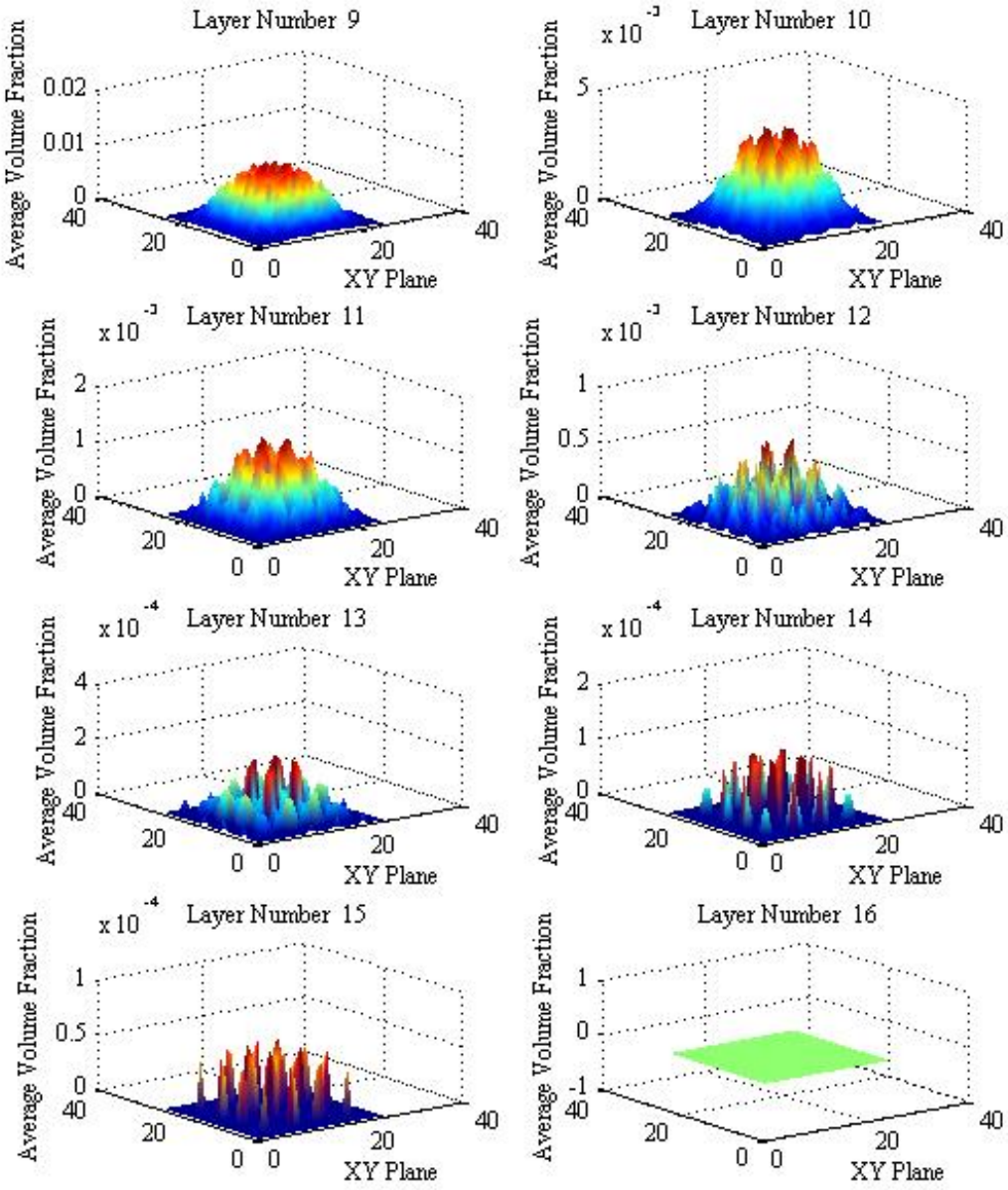

Figure 3.21: The average volume fraction of polymer segments at layers (9-16) in the system at separation distance $d = 5$ and $K_BT = 2$.

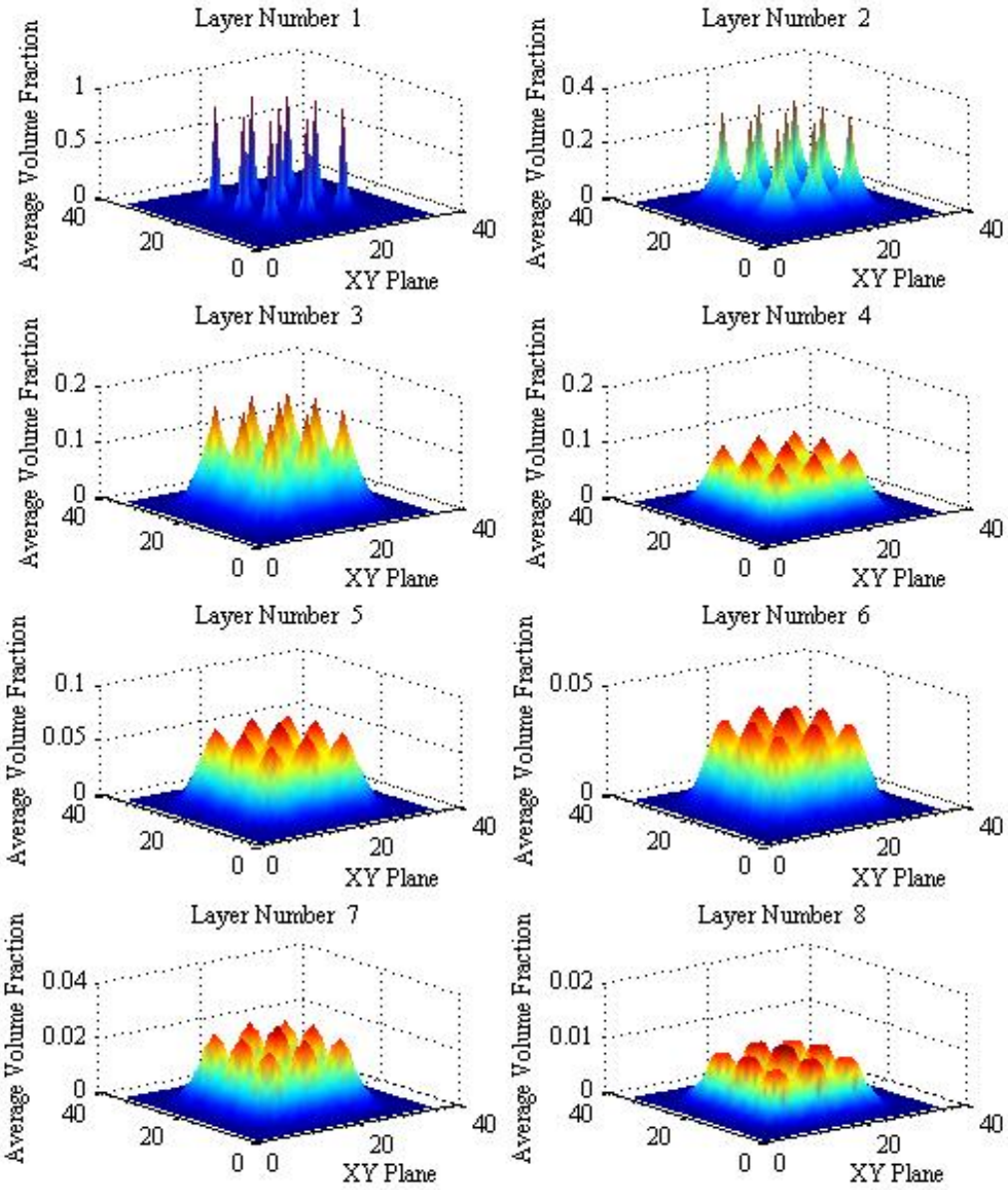

Figure 3.22: The average volume fraction of polymer segments at layers (1-8) in the system at separation distance $d = 7$ and $K_BT = 2$.

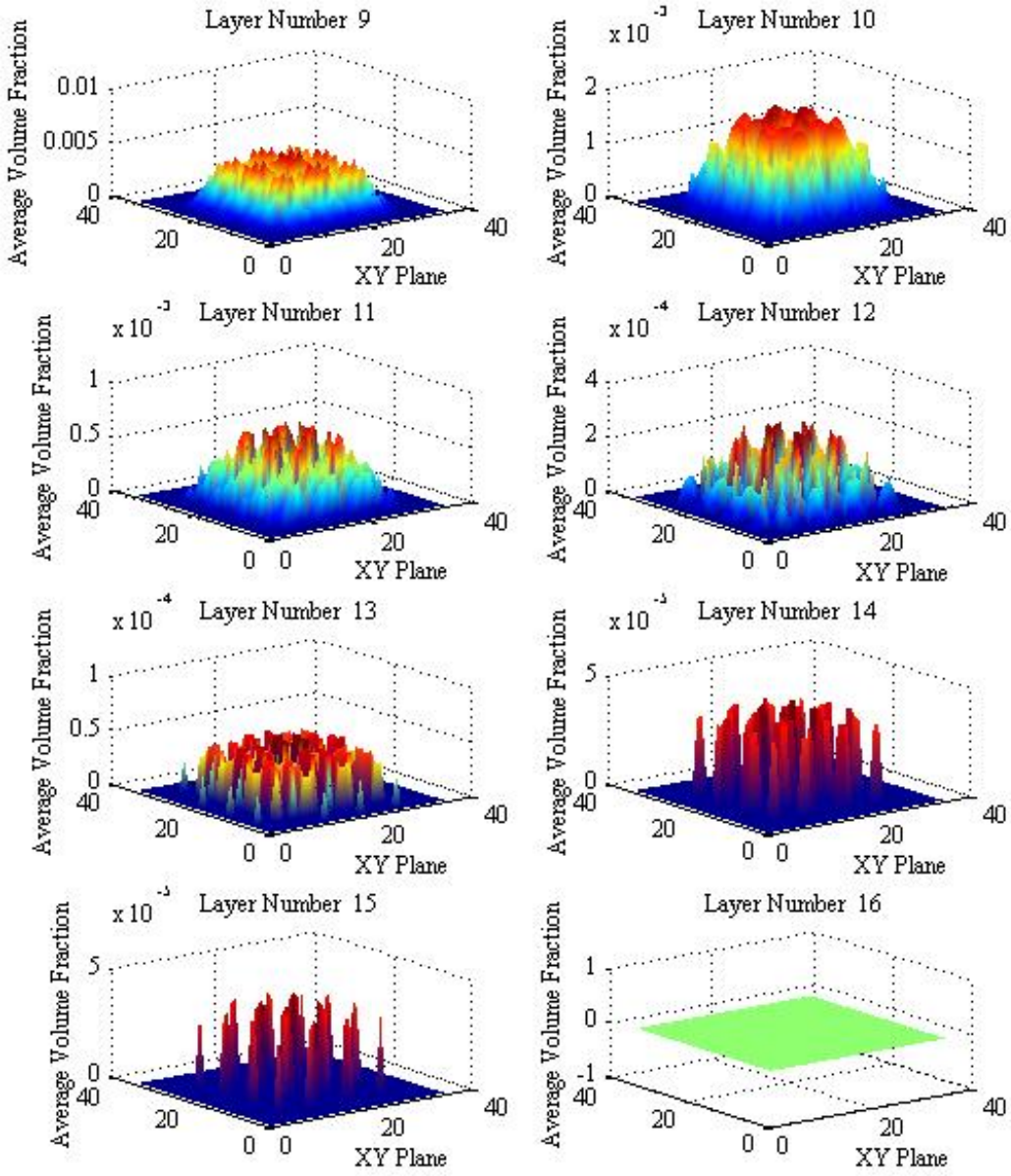

Figure 3.23: The average volume fraction of polymer segments at layers (9-16) in the system at separation distance $d = 7$ and $K_BT = 2$.

Chapter 4

Modeling Ligand-Receptors Binding Between Micelles and Cancer Cells

A variety of interactions between drug delivery devices and local cells and tissues impact clinical outcomes in terms of both therapeutic action and biological response. The further development of design objective micelles for drug delivery applications is associated with understanding the competition of interactions in the system. In this chapter, we use the mean-field approximation to generalize molecular theories that determine the competition between electrostatic, van der Waals and steric interactions, thus determining the ligand-receptor binding protocols between the micelle and the targeted cell.

The micelle is designed to target cancer cells primarily through pH sensitivity and electrostatic binding. This is made possible by using pH-sensitive polyelectrolytes that contain functional groups that can dissociate to become positively charged at low pH [22]. The positive groups on those polymers become attracted to the negative surface of cancer cell, where the electrostatic binding takes place [11, 6, 10]. At Jilin University in China, Huang and colleagues have used the previous two principles to prepare a smart drug delivery system that should enhance tumor therapy and tunable drug release [21].

Cancer cells and healthy cells have the same kinds of receptors, however some of these receptors are over-expressed in cancer cells, such as epidermal growth factor receptors (EGFR) and folate receptors (FR). The developed theories consider the

influence of different receptor densities on the ligand-receptor binding, however the molecular reorganization on the surface of the micelle is a design variable that needs to be considered for enhanced targeting. Micellar size (curvature) is strongly coupled to the way polymers express ligands to the surface. Several systems of ligand-receptor binding are modeled to achieve the optimum binding that allows the therapeutic micelle to release the drug inside the cancer cell through endocytosis (see Figure 4.1). The molecular theory platform for each system is uniquely suited to address specific subjects.

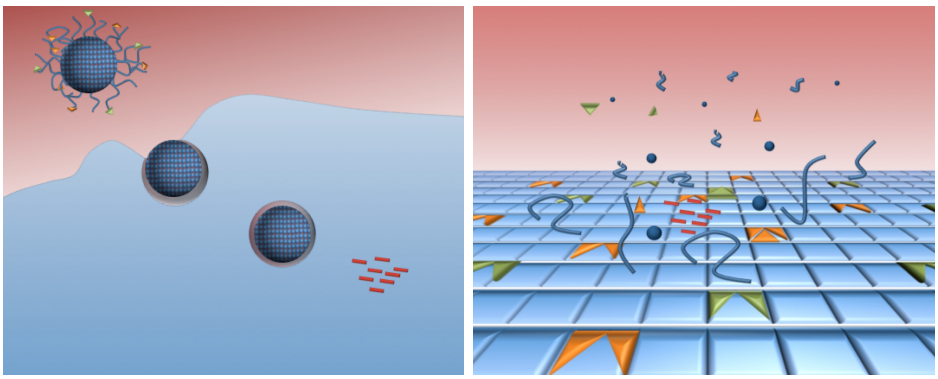

(a) Endocytosis Release (b) Degradation Release

Figure 4.1: An illustration of two paths for micellar drug release.

This chapter covers two models of the outer structure of a micelle. Both models have grafted PEGs as spacers, however, one model has a ligand that is attached to free end-grafted polybases, and the other model has two ligands that are attached to free end-grafted polybases (see Figure 4.2). The polybases, or pH sensitive polymers, should increase the attraction energy between the micelle and the cancer cell, which has a negatively charge surface. The theory predicts that the competition between all forces in the system leads to two significant therapeutic states. The *shield state* in which collapsed polybases protect the ligands from binding to healthy cells when the micelle is separated from the cancer cell by distance. The *expose state*, in which stretched polybases expose the ligands to bind to specific receptors on the malignant

cells. The transition between the two states depends on the length and surface coverage of the spacers and the polybase-ligands. The ligand-receptor binding is affected by the receptors density on the cell.

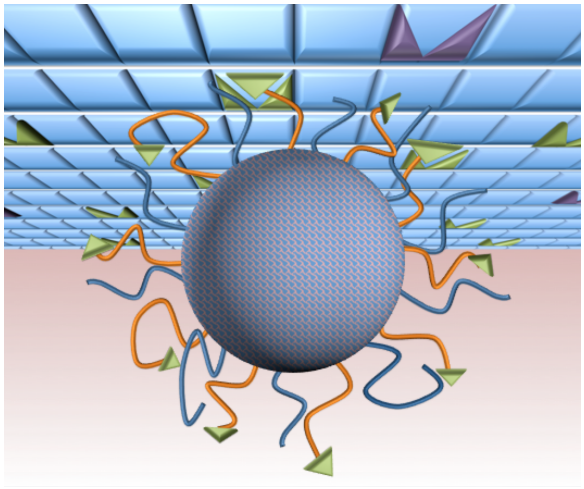

Figure 4.2: An illustration of a micelle with spacers (blue lines) and polybases (orange lines) that are attached to ligands (green rectangles) which are designed to bind to specific receptors.

4.1 Micelles applications

Nanomedicine technology depends extensively on the creation of smart nanoparticles, such as micelles. Micelles are fabricated from amphiphilic surfactant [1] molecules that aggregate in water into spherical vesicles with a hydrophobic core and a hydrophilic surface. Thus, micelles are usually used to protect hydrophobic drugs, such as doxorubicin (DOX) [2], and release them under specific mechanisms. Smart micelles can respond to external stimuli, such as small changes in temperature, pH, salt concentra-

[1]Surfactant or surface-active agents are amphiphilic compounds. They contain both hydrophilic (heads) and hydrophobic (tails) groups, which make them ideal vehicles to protect hydrophobic drugs.

[2]DOX is a drug used in chemotherapy to treat cancer. It has very serious side effects leading to it becoming known as the "red devil".

tion, or magnetic and electrostatic field [15, 7, 27, 40]. The micellar response to these external stimuli appears as a change in the conformational structure. This change in structure causes the micelle to attach to the targeted cell or to release its contents at the site of action. Smart micelles are developed for drug delivery applications as well as for biosensing and as molecular imaging tenders [38]. Micelles can be created from different kinds of polymers to protect their contents from the external environment, and to increase their capability of binding to the targeted cells [8, 2, 38].

The hydrophobicity of the micellar core combined with the high toxicity of the hydrophobic anticancer drugs, has inspired biomedical engineers to design micelles as anticancer drug delivery systems. The micellar design prevents drug leakage and ensures the delivery to the cancerous cells. In one study published in the PNAS journal, a group of researchers report a unique micellar design that delivers an anticancer drug (cisplatin) to prostate cancer cells[8]. The nanoparticle is made of poly(D,L-lactic-co-glycolic acid) (PLGA)-poly(ethylene glycol) (PEG) that are attached to prostate-specific membrane antigen (PSMA) targeting aptamers. The specific design ensured the binding to prostate cancer cells only, and the release of the drug inside the cells through endocytosis. Another recent study that appears in the Biomaterial journal reported the usage of antibody-drug congregates (ADCs) for targeted delivery [2]. The ADCs ligands are attached to micelles that are loaded with cytotoxic platinum drugs for treatment of pancreatic tumors. The study results show an efficient delivery of the anti-cancer drug, and accordingly a significant suppression in the growth of the pancreatic malignant cells. A multifunctional micelle has also been developed by a group of researchers at the University of Texas, Southwestern Medical Center, at Dallas to target αvβ3-expressing cancer cells, and deliver doxorubicin (DOX) and MRI-ultrasensitive particles to the tumor [38].

Refining micelles that can target malignant cells at very high concentration compared to the healthy cells in the blood stream, is sufficient motivation for the further

research and development of smart micelles. However, improving the targeting proficiency of smart micelles is governed by the choice of polymers that are attracted to malignant cells only, and ligands that bind to cancer cells through the molecular recognition of specific cancer markers [35]. Many theoretical works have been done to understand the ligand-receptor binding properties through the consideration of the molecular interaction in the biological system [17, 32]. In a recent study published in the Biomaterials Science journal, Nap and Szleifer found that attaching desired ligands to polybases in a micelle has improved the ligand-overexpressed receptor binding in cancer cells [37]. The control of the positive charges on the polybases in acidic environments should improve the targeting of the over-expressed receptors on the negatively charged cancer cell's surface [21, 6].

This study uniquely addresses the size of the therapeutic micelle to improve the targeting to malignant cells. Most malignant treating micelles are synthesized with ligands that bind to over-expressed receptors on cancer cells such as epidermal growth factor receptors (EGFR) [35]. EGFRs also exist on healthy cells, however they are overexposed on cancerous cells, where they are critical for proliferation and survival of the cell. Controlling the size of the therapeutic micelle is essential to ensure the binding to the cancer cells while screening the healthy cells. The design of the size of the therapeutic micelle should take into account the density of the EGFR, or any other targeted receptor on the targeted cells. In this study, we calculated the optimum size of micelles created to treat human glioblastoma cells based on the EGFRs density on those cells [57].

4.2 The Size of The Therapeutic Micelle

The density of the targeted receptors differs significantly between the healthy and the malignant cells, for example, the density of epidermal growth factor receptors (EGFR) in malignant cells can be 100 times higher than in normal cells [57]. Figure

(4.3) (a) illustrates a large micelle that could bind to several EGFRs on a healthy cell. These several bonds could stabilize the micelle on the healthy cell against the washing effect of the blood stream. Figure 4.3 (b) illustrates the binding of small micelles to EGFR on healthy cells. In the case of small micelles, one ligand-receptor bond could be enough to stabilize the micelle. In this study, we design an efficient therapeutic micelle with a precise size that allows it to bind to a minimum of two over-expressed receptors on the cancerous cell (see Figure 4.3 (c)). Increasing the ligand-receptor attractive binding forces by moderating the size of the micelle triggers an increase of the binding between micelles and cancer cells. Moderating the micellar size, leads to an increase of the binding forces that in turn increases the stability of the micelle on the cancerous cell surface. Thus, the optimum choice of the size of the therapeutic micelle is critical for efficient treatment.

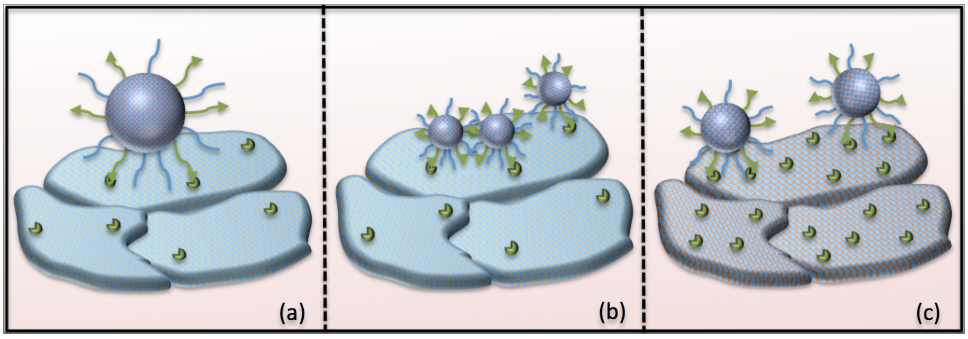

Figure 4.3: An illustration shows the dependency between the micellar size and the receptor density on healthy and malignant cells.

a. Large micelle binds to a healthy cell.
b. Small micelles bind to a healthy cell.
c. Therapeutic micelles bind to cancerous cell efficiently.

The proper size of the therapeutic micelle should depend on the density of the targeted receptors. Consequently, there should be precise therapeutic micelles for a specific treatment. As an example, epidermal growth factor receptors (EGFR) are targeted in most cancer treatments [33, 35, 39, 57]. EGFRs are over-expressed on malignant cells to support the growth and spread of the cancerous cells. The density

of EGFRs differs on different types of cancerous cells. In Lab on a Chip Journal, a group of researchers from the University of Texas at Arlington, found experimentally that human glioblastoma cells (h-GBM) carry a minimum of 1 EGFR per $100nm^2$ [57]. Accordingly, to design a therapeutic micelle that targets EGFR on h-GBM cells, the interaction surface area between the micelle and the h-GBM cell should not be less $100nm^2$ in size. Doubling the size of the interaction surface area should allow a minimum of two EGFRs to bind to the therapeutic micelle, which causes an increase in the binding energy. Increasing the binding energy between the therapeutic micelles and the cancer cells is favorable to stabilize the micelle on the cancer cell surface, thus avoiding the washing of these micelles away with the blood stream.

Our innovative design is based on an evaluation of the size of the interaction surface area between the micelle and the cancerous cell. The size of that interaction surface area should be equal to double the area that holds one of the targeted receptors, such as EGFR on the cancerous cell. Doubling the size of the interaction area allows a minimum of two ligands on the micelle to bind to receptors on the malignant cell. Thus, if the density of our targeted receptors is d/nm^2, then the interaction surface area, A_{ins}, is given as $A_{int} = 2/dnm^2$.

Once the interaction surface area has been determined, the radius of the required micelle can be calculated. A cross-sectional view of a therapeutic micelle, such as that shown in figure 4.4, gives us a circular shape. Considering the length of the perimeter of the computed interaction area (the red line), $S = \sqrt{A_{int}}$, this circular shape can be approximated by different polygon shapes. Pentagon, hexagon, and heptagon shapes were fitted around the micellar cross-section area as shown in Figure (4.4). However, the side of the pentagon and hexagon shapes were found to be a best fit to describe a circle with an interaction area equal to S. The radius (yellow line) of a circle inside a polygon is given by $R = \frac{S}{2\tan(\frac{180}{n})}$, where n is the number of polygon sides. Using the previous relation, we found that the average radius calculated by fitting both

pentagon and hexagon shapes is given by the following relation:

$$R = 0.777S \tag{4.1}$$

Correspondingly, the optimum size of the therapeutic micelles for h-GBM cells that have a minimum of 1 EGFR per $100nm^2$, and accordingly $S \approx 14nm$, is approximately $20nm$ in diameter.

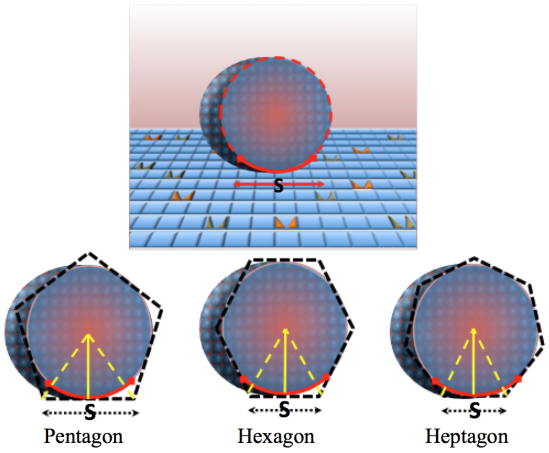

Figure 4.4: Calculating the size of the therapeutic micelle from the size of the interaction area with the targeted cell.

4.3 Modeling The Binding of One Ligand to One Receptor

This model focuses on the micelle-cell interaction surface. Figure 4.5 presents one side of the therapeutic micelle, which interacts with a cell surface. The micellar surface carries two different kinds of polymers with a total density of σ_p, and N_m number of monomers for each. The polyelectrolyte polymers (represented by the orange lines in Figure 4.5) are attached to ligands (L) (represented by the green shapes in Figure 4.5). The expression "ligand complexes" is used here to refer to polyelectrolytes that are attached to ligands. In order to design micelles that target cancer cells only, weak polyelectrolytes with basic groups were chosen. The basic groups (B) on the ligand

complexes are able to protonate at low pH in the biological aqueous environment into positively charged ions (BH^+) as follows:

$$B + H^+ \overset{K_d}{\rightleftharpoons} BH^+ \tag{4.2}$$

where K_d is the equilibrium dissociation constant for for the chemical interaction, which is given by Equation 3.4.1. For weak polyelectrolytes, this dissociation constant is not fixed, but is affected by the external pH through the following relation:

$$pK_a \equiv -\log K_d = \log\left(\frac{[BH^+]}{[B]}\right) + pH \tag{4.3}$$

Using a modified form of Henderson-Hasselbalch equation that takes into account the electrostatic interaction along the chain by an empirical parameter n, one can write the following equation [5]:

$$pK_{a(app)} = n\log\left(\frac{1-\alpha}{\alpha}\right) + pH \tag{4.4}$$

where, $\alpha = \left(\frac{[B]}{[B]+[BH^+]}\right)$. The apparent dissociation constant, $pK_{a(app)}$, relates the hydrogen ion activity to the molar concentrations of the species involved in the dissociation reaction.

The positive monomers get attracted to the negatively charged surface of the cancerous cells, allowing the ligand complexes to stretch [21, 1, 6]. The stretched ligand complexes expose their ligands to the receptors (R) on the cell surface causing an increase in the binding probability. The ligand-receptor (LR) binding interaction can be described by the relation $L + R \overset{K_{LR}}{\rightleftharpoons} LR$, and a binding association constant $K_{LR} = \frac{[LR]}{[L][R]} = C\exp(-\beta(\mu^\circ_{LR} - \mu^\circ_L - \mu^\circ_R))$. $[L], [R]$ and $[LR]$ denote the concentration of the respective molecule, and μ° is the standard chemical potential for the corresponding molecule.

The poly(ethylene glycol) (PEG) polymers that are attached to the micellar surface are used as spacers (represented with blue lines in figure 4.5). The role of these

spacers is to protect the ligands until they reach the cancerous cells. PEGs are well known as highly hydrophilic-biocompatible polymers that have also been used as a non-inflammatory modifier for drugs [23]. The choice of PEG served to increase the solubility and improve the biocompatibility of the therapeutic micelle.

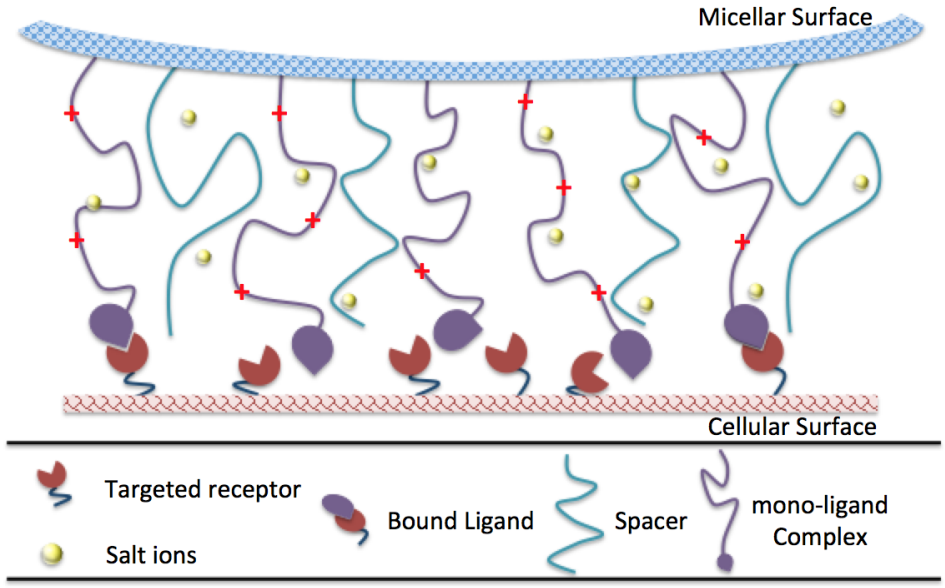

Figure 4.5: A model illustrating the interaction between the micellar surface and the targeted cellular surface. The ligand complexes (poly-electrolytes + ligands) are represented by orange lines, and the spacers are represented by blue lines.

The cellular surface, which is opposite to the micellar surface (see figure 4.5), has a density (σ_R) of the targeted receptors. The fraction of ligands in the system is given by $X_L = \frac{N_L}{N_L+N_s}$, where N_L and N_S refers to the number of ligands and spacers respectively. The fraction of bound ligands is $f_{LR} = \frac{[\mathrm{LR}]}{[\mathrm{LR}]+[\mathrm{L}]}$, where $[LR]$ and $[L]$ are the concentrations of bound and free ligands respectively [32]. Accordingly, the concentration per unit area (or the density) of the molecules in the system is as follows:

- Spacers: $\frac{[S]}{A} = \sigma_s = \sigma_p(1 - X_L)$
- Free ligand-complexes: $\frac{[L]}{A} = \sigma_L = \sigma_p X_L(1 - f_{LR})$

- Bound ligand-complexes: $\frac{[LR]}{A} = \sigma_{LR} = \sigma_p X_L f_{LR}$
- Free receptors: $(\sigma_R - \sigma_p X_L f_{LR})$

The system is modeled in a cubic lattice structure, where each polymer segment or receptor occupies a single cubic lattice site. The polymers configurational structures (α) are built randomly using self avoiding random walk (SAW) with Rosenbluth weighting technique to improve the statistics [43]. The remaining cubic sites are filled randomly with water and salt ion molecules. All molecules in the system are subject to different kinds of forces, such as steric, van der Waals and electrostatic forces.

The cubic lattice model has an incompressibility constraint that maintain the repulsive steric interactions between all molecules in the system. The mathematical representation of the constraint is as follows:

$$\langle\phi_s(z)\rangle+\langle\phi_L(z)\rangle+\langle\phi_{LR}(z)\rangle+\phi_w(z)+\phi_{\mathrm{H^+}}(z)+\phi_{\mathrm{OH^-}}(z)+\phi_+(z)+\phi_-(z)+\phi_R = 1 \quad (4.5)$$

Note that the system studies three different polymers: spacers (s), free ligand-complexes (L), and ligand-complexes that are bound to receptors (LR). Thus, $\langle\phi_p(z)\rangle$ is the average volume fraction of polymer p, and $\phi_x(z)$ is the volume fraction of specie x.

The van der Waals interactions are accounted for in each configuration (α) through the intra-molecular interactions ($E_{intra}(\alpha)$) between segments of one polymer, and the inter-molecular interactions ($E_{inter}(\alpha)$) between polymer segments from different polymers. Below is the mathematical representation for van der Waals interactions per unit area for all kinds of polymers in the system:

$$\begin{aligned}\langle E_{intra}(\alpha)\rangle &= \sum_p \sigma_p \sum_\alpha P_p(\alpha) E_{intra,p}(\alpha) \\ \langle E_{inter}(\alpha)\rangle &= -\frac{\varepsilon_{inter}}{2} \sum_p \sigma_p \sum_z \langle\phi_p(z)\rangle\langle\eta_p(z)\rangle\end{aligned} \quad (4.6)$$

where $P_p(\alpha)$ is the probability of polymer kind p to be at configuration α, and $E_{intra,p}(\alpha)$ is the intra molecular interactions of that polymer. $\langle\phi_p(z)\rangle$ is the average volume fraction of polymer p segments at layer z, and $\langle\eta_p(z)\rangle$ is the fraction of its possible intermolecular interactions at layer z [1].The average volume fraction of polymer kind p is defined as follows:

$$\langle\phi_p(z)\rangle = \sigma_p \sum_{\alpha} P_p(\alpha) n_p(\alpha, z) v_{sol} \tag{4.7}$$

where $n_p(\alpha, z)$ is the number of polymer segments at layer z, and v_{sol} is the volume of solvent molecule ($v_{water} = 0.03nm^2$), which is set to be the volume of each cubic lattice site with the assumption that all molecules in the system have the same volume (notice that $v_p(\alpha, z) = n_p(\alpha, z)v_{sol}$). The values of the elementary short-ranged molecular-attractive interactions, (ε_{intra} and ε_{inter}), are chosen carefully so as not to effect the solubility of the solvent.

The electrostatic interactions between two charged molecules in the system are influenced by several variables, such as the polymer density (σ_p), the surface charge coverage on the cell (σ_q), the bulk pH, and the local temperature through (K_BT). These interactions can be noticed on the extension of the ligand complexes. Different electrostatic interactions cause different configurations and accordingly, different intra and inter-molecular interactions. The model demonstrates the complexity of the chemical equilibrium and the physical interactions between all molecules in the system on the ligand-receptors binding probabilities.

---

[1]Notice that here we don't use the sympol ($*$) that we used in Chapter 3 to calculate the inter-molecular interactions. The $1D$ system considers the volume fraction and the inter-molecular interactions of one polymer at different configurations, while the $3D$ accounts for the volume fraction and the inter-molecular interactions of a polymer with respect to several grafted polymers at different configurations.

[2]We show how we got this number in Appendix (E).

4.3.1 Theoretical Approach

The system between the micellar and the cell surfaces is discretized into discrete layers at the XY plane with thickness dz. The model assumes that the system is homogeneous in planes parallel to the cell surface and the micelle surface (XY), and inhomogeneous in the norm direction (Z). The mean field approximation is used to describe the molecular interactions in the system [50]. The system Helmholtz free energy per unit area is calculated by taking into account the polymers, electrostatics, chemical interactions, ion formation and mixture of free energies ($F = F_{pol} + F_{elc} + F_{chem} + F_{if} + F_{mix}$).

The polymers free energy is expressed by its self-energy due to the intra and intermolecular interactions between the three kinds of polymers, as well as their conformational entropy (S) [1]. The polymers free energy can be expressed mathematically as follows:

$$\begin{aligned} F_{pol} &= U_{pol} + \frac{S_p}{K_B} \\ &= \sum_p \left[\langle E_{intra} \rangle_p + \langle E_{inter} \rangle_p + \sigma_p \sum_\alpha P_p(\alpha) \ln P_p(\alpha) \right] \end{aligned} \tag{4.8}$$

where $p = \{s, L, LR\}$.

The second term of the system free energy is the electrostatic free energy, which is defined as follows;

$$F_{elec} = \int \left[\langle \rho_q(z) \rangle \psi(z) - \frac{1}{2} \epsilon \left(\frac{\partial \psi(z)}{\partial z} \right)^2 dz \right] \tag{4.9}$$

where:

- $\langle \rho_q(z) \rangle = f_{\mathrm{H}^+}(z) q_p \Big(\langle \rho_L(z) \rangle + \langle \rho_{LR}(z) \rangle \Big) + \sum_m q_m \rho_m(z)$, where q_p is the charge on the dissociated functional groups of the polyelectrolytes.

[1] Note that polymers conformational entropy increases dramatically by increasing their polymerization number N (number of monomers

- $\langle\rho_L(z)\rangle + \langle\rho_{LR}(z)\rangle = \sigma_p X_L(1-f_{LR})\sum_\alpha P_L(\alpha)v_L(\alpha,z) + \sigma_p X_L f_{LR}\sum_\alpha P_{LR}(\alpha)v_{LR}(\alpha,z)$
- $q_m\rho_m$ represents the charge and the volume fraction of the molecular species other than polymers in the system ($H^+ - OH^- - Na^+ - Cl^-$).

The third term in the system free energy accounts for the chemical interactions of all molecules in the system including the ligand-receptor binding interaction, which can be represented as follows:

$$\begin{aligned} F_{chem} =& \frac{1}{\beta}\int(\langle\rho_L(z)\rangle + \langle\rho_{LR}(z)\rangle)\Big\{f_{H^+}(z)[\ln f_{H^+}(z) + \beta\mu^\circ_{BH^+}] \\ &+ (1-f_{H^+}(z))[\ln(1-f_{H^+}(z)) + \beta\mu^\circ_{B}]\Big\}dz \\ &+ \frac{1}{\beta}\Big\{\sigma_p X_L(1-f_{LR})\beta\mu^\circ_L + \sigma_p X_L f_{LR}\beta\mu^\circ_{LR} + (\sigma_R - \sigma_p X_L f_{LR})\beta\mu^\circ_R\Big\} \end{aligned} \tag{4.10}$$

where μ°_m is the standard chemical potential for molecule m, which accounts for the molecule self-energy. Terms that have the following form ($\langle\rho_m(z)\rangle f_n(z)[\ln f_n(z)$) denote the translational entropy of molecule m due to the chemical interaction n.

The fourth term is the ion formation free energy that is produced due to the ion's translational entropy. This term is defined as follows:

$$F_{ion} = \int(\rho_{H^+}(z)\mu^\circ_{H^+} + \rho_{OH^-}(z)\mu^\circ_{OH^-})\,dz \tag{4.11}$$

The last term accounts for the mixture free energy. This term represents the translational (mixing) entropy for the water molecules, the ions, charged monomers, ligands, receptors, and bound ligand-receptors. The mixture free energy is represented

mathematically as follows:

$$\begin{aligned} F_{mix} = -TS_{mix} =& \frac{1}{\beta}\int \Big\{[\rho_w(z)(\ln\rho_w(z)-1)] + [\rho_{\mathrm{H}^+}(z)(\ln\rho_{\mathrm{H}^+}(z)-1)] \\ &+[\rho_{\mathrm{OH}^-}(z)(\ln\rho_{\mathrm{OH}^-}((z)-1)] + [\rho_+((z)(\ln\rho_+(z)-1)] \\ &+[\rho_-(z)(\ln\rho_-(z)-1)]\Big\}dz \\ &+\frac{1}{\beta}\Big\{\sigma_p(1-X_L)\ln(1-X_L) + \sigma_p X_L(1-f_{LR})\ln(1-f_{LR}) \\ &+\sigma_p X_L f_{LR}\ln f_{LR} + (\sigma_R - \sigma_p X_L f_{LR})\ln\left(1-\frac{\sigma_p X_L f_{LR}}{\sigma_R}\right)\Big\} \end{aligned} \tag{4.12}$$

By summing all the above free energies in the system, one gets the total free energy for a semi-grand canonical ensemble as follows:

$$\begin{aligned} \Omega =& \frac{\beta F}{A} - \beta\sum_m \rho_m\mu_m \\ =& -\beta\Bigg[\Big[\sigma_p(1-X_L)P_s(\alpha) + \sigma_p X_L(1-f_{LR})P_L(\alpha) + \sigma_p X_L f_{LR}P_{LR}(\alpha)\Big]E_{intra}(\alpha) \\ &+ \frac{\varepsilon_{inter}}{2}\int_z \Big(\langle\phi_s(z)\rangle\langle\eta_s(z)\rangle + \langle\phi_L(z)\rangle\langle\eta_L(z)\rangle + \langle\phi_{LR}(z)\rangle\langle\eta_{LR}(z)\rangle\Big)dz\Bigg] \\ &+ \sigma_p(1-X_L)\sum_\alpha P_s(\alpha)\ln P_s(\alpha) + \sigma_p X_L(1-f_{LR})\sum_\alpha P_L(\alpha)\ln P_L(\alpha) \\ &+ \sigma_p X_L(f_{LR})\sum_\alpha P_{LR}(\alpha)\ln P_{LR}(\alpha) \\ &+ \beta\int\left[\left(f_{H^+}(z)q_p\Big(\langle\rho_L(z)\rangle + \langle\rho_{LR}(z)\rangle\Big) + \sum_m q_m\rho_m(z)\right)\psi(z) - \frac{1}{2}\epsilon\left(\frac{\partial\psi(z)}{\partial z}\right)^2\right]dz \\ &+ \int\Big(\langle\rho_L(z)\rangle + \langle\rho_{LR}(z)\rangle\Big)\Big\{f_{H^+}(z)[\ln f_{H^+}(z) + \beta\mu^\circ_{BH^+}] \\ &+ (1-f_{H^+}(z))[\ln(1-f_{H^+}(z)) + \beta\mu^\circ_{\mathrm{B}}]\Big\}\,dz \\ &+ \Big\{\sigma_p(1-X_L)\ln(1-X_L) + \sigma_p X_L(1-f_{LR})[\ln(1-f_{LR}) + \beta\mu^\circ_L] \\ &+ \sigma_p X_L f_{LR}[\ln(f_{LR}) + \beta\mu^\circ_{LR}] + (\sigma_R - \sigma_p X_L f_{LR})[\ln(1-\frac{\sigma_p X_L f_{LR}}{\sigma_R}) + \beta\mu^\circ_R]\Big\} \\ &+ \int\Big\{[\rho_w(z)(\ln\rho_w(z)-1)] + [\rho_{\mathrm{H}^+}(z)(\ln\rho_{\mathrm{H}^+}(z) - 1 + \beta\mu^\circ_{\mathrm{H}^+})] \\ &+ [\rho_{\mathrm{OH}^-}(z)(\ln\rho_{\mathrm{OH}^-}(z) - 1 + \beta\mu^\circ_{\mathrm{OH}^-})] \\ &+ [\rho_+(z)(\ln\rho_+(z) - 1 - \beta\mu_+)] + [\rho_-(z)(\ln\rho_-(z) - 1 - \beta\mu_-)]\Big\}\,dz \end{aligned} \tag{4.13}$$

The theory describes the system by calculating the most probable configurations of spacers, free ligand complexes and bound ligand complexes. Note that the fraction of binding f_{LR} equals *zero* at all layers accept the final layer on the cell surface, where the receptors are present. Thus, all terms in the free energy that include σ_R and/or f_{LR} are constant, and are not included in the integral over all layers z.

Introducing Lagrange multipliers $\pi(z)$ with the incompressibility constraint and minimizing the free energy allows the calculation of the three different probabilities that describe the system:

- The probability of having a spacer (P_s) at configuration (α).
- The probability of having a free ligand complex (P_L) at configuration (α).
- The probability of having a bound ligand complex (P_{LR}) at configuration (α).

These probabilities are given by the following relations:

$$P_s(\alpha) = \frac{W_R}{q_s} \exp\left(-\beta\Big[E_{intra}(\alpha) + E_{inter}(\alpha)\Big] - \beta \int \pi(z) v_s(\alpha, z)\ dz \right) \tag{4.14}$$

$$\begin{aligned} P_{ii}(\alpha) = & \frac{W_R}{q_{ii}} \exp\left(-\beta\Big[E_{intra}(\alpha) + E_{inter}(\alpha)\Big] - \beta \int \pi(z) v_{ii}(\alpha, z)\ dz \right. \\ & \left. - \beta \int q_p \psi(z) v_{ii}(\alpha, z)\ dz - \int \ln f_{H^+}(z) v_{ii}(\alpha, z)\ dz \right) \end{aligned} \tag{4.15}$$

where, q is the partition function of the corresponding polymer, which satisfies the condition that $\sum_\alpha P(\alpha) = 1$. The Rosenbluth weighting function (W_R) is used to improve the statistics of all possible polymer configurational structures [43]. The first two terms in all probabilities account for the intra and inter-molecular interactions between polymer segments [1], where $\beta = \frac{1}{K_B T}$ is the inverse thermodynamic temperature. In the third term of Equation (4.14), $v_s(\alpha, z)$ is the volume fraction

[1] We use the decoupled mean-field approach that we discussed in Chapter 3 to calculate the intra and the inter-molecular interactions.

of a spacer that occupies layer z. Similarly, in the third term of Equation (4.15), $v_{ii}(\alpha, z)$ is the volume fraction of a free or a bound ligand that occupies layer z. The extra two terms in Equation (4.15), account for the electrostatic interactions as this equation describes the probability of the free and bound ligand complexes that are made of polybases (see section 4.3). In Equation (4.15), q_p is the amount of charge on a dissolved monomer (see Equation (4.2)), and $n_{ii}(\alpha, z)$ is a Kronecker delta function that equals *one* if there is a monomer of polymer ii at layer z, and *zero* otherwise. $\psi(z)$ is the electric potential at layer z. In the last term of equation (4.15), f_{H^+} is the protonation fraction, which is given by the following:

$$\frac{f_{H^+}(z)}{(1 - f_{H^+}(z))} = \frac{\phi_{\mathrm{H^+}}(z)}{K_d^{\circ}\phi_w(z)} \tag{4.16}$$

The volume fraction profile of all molecular species in the system is given by the following relations:

$$\begin{aligned}
\phi_w(z) &= \exp(-\beta\pi(z)v_w) \\
\phi_{\mathrm{H^+}}(z) &= \exp(-\beta\mu^{\circ}_{\mathrm{H^+}} - \beta\pi(z)v_w - \beta q_{\mathrm{H^+}}\psi(z)) \\
\phi_{\mathrm{OH^-}}(z) &= \exp(-\beta\mu^{\circ}_{\mathrm{OH^-}} - \beta\pi(z)v_w - \beta q_{\mathrm{OH^-}}\psi(z)) \\
\phi_+(z) &= \exp(\beta\mu_+ - \beta\pi(z)v_w - \beta q_+\psi(z)) \\
\phi_-(z) &= \exp(\beta\mu_- - \beta\pi(z)v_w - \beta q_-\psi(z))
\end{aligned} \tag{4.17}$$

where, μ^0_{jj}, and q_{jj} are the standard chemical potential, and the amount of charge for specie jj respectively. In this system, we assume that all molecules have the volume of the solvent molecule (water molecule).

The fraction of ligand-receptor binding is given by the following relation:

$$\frac{f_{LR}}{(1 - f_{LR})} = \frac{C\ K_{LR}\ q_{LR}\ e}{q_L\phi_R}\left(1 - \frac{\sigma_p X_L f_{LR}}{\sigma_R}\right) \tag{4.18}$$

where, q_L and q_{LR} are the partition functions for free and bound ligand complexes. C is the constant in the association constant equation $\mathrm{K_{LR}}$=$\mathrm{C}\exp(-\beta(\mu^{\circ}_{\mathrm{LR}} - \mu^{\circ}_{\mathrm{L}} - \mu^{\circ}_{\mathrm{R}}))$, $\phi_R(z)$) is the volume fraction of receptors on the interacting cell surface at specific

microstate, which can be calculated from the receptor density and the cell-surface interaction area, and e is the base of the natural logarithm.

We discretize the system into z number of layers with a thickness value around the third root of the volume of a water molecule [1]. The complex non-linear system is composed of seven sets of unknowns. Three of these unknowns are the average volume fractions: for spacers, complex ligands, and bound complex ligands $\Big(\langle \phi_s(z) \rangle, \langle \phi_L(z) \rangle, \langle \phi_{LR}(z) \rangle \Big)$. Another three unknowns are the fraction of inter-molecular interactions: for spacers, complex ligands, and bound complex ligands $\Big(\langle \eta_s(z) \rangle, \langle \eta_L(z) \rangle, \langle \eta_{LR}(z) \rangle \Big)$. The final unknown is the electric potential profile ($\psi(z)$). We use the minimized free energy Equations (eqs. (4.14) to (4.17)), and Poisson equation to solve for the seven sets of unknowns. Exterminimizing the free energy with respect to the electric potential gives Poisson equation in the following form:

$$\frac{\partial^2 \psi(z)}{\partial z^2} = -\frac{\langle \rho_q(z) \rangle}{\epsilon} \tag{4.19}$$

where ϵ is the permittivity constant of the medium, which we assume to be water. $\langle \rho_q(z) \rangle$ is the density of charges in the system, which is given by $\langle \rho_q(z) \rangle = f_{H^+}(z))\ q_p\ (\langle \rho_L(z) \rangle + \langle \rho_{LR}(z) \rangle) + \sum_{jj} q_{jj} \rho_{jj}(z)$, where q_p is the amount of charge on a charged polymer segment, while q_{jj} is the amount of charge on a specie jj that has a density of $\rho_{jj}(z)$ at layer z. The electric potential profile is subject to two boundaries: the charge density on the cell surface $\sigma_{q_{cell}}$ and the charges on the micellar surface $\sigma_{q_{micelle}}$, which depends on the number of charged polymer segments that are attached to that surface.

$$\frac{\partial \psi(z)}{\partial z} = \begin{cases} \frac{-\sigma_{q_{micelle}}}{\epsilon}, & \text{at } z = 1 \\ \frac{-\sigma_{q_{cell}}}{\epsilon}, & \text{at } z = L \end{cases}$$

That can be translated into:

$$\frac{\psi(2) - \psi(1)}{\Delta} = \frac{-\sigma_{q_{micelle}}}{\epsilon}$$

[1] That value is calculated in Appendix E.

$$\frac{\psi(L-1)-\psi(L)}{\Delta}=\frac{-\sigma_{q_{cell}}}{\epsilon}$$

where, $z=1$ and $z=L$ are our boundaries, and $z=2$ and $z=L-1$ are the first layers encountered as we move toward the middle of the system.

We solve the Poisson equation by calculating the number of charged monomers on both the micellar surface and the cell surface. The cell surface has additional charge due to the density of charge on the cell. The system is solved twice. Firstly, to find the number of monomers on the cell, and secondly to use these inputs to solve for the Poisson equation.

4.4 Modeling The Binding of A Dual Ligand

The dual ligand technique has been used to enhance nanocarrier targeting and to spare healthy cells [45, 53, 28]. Tumor and healthy cells have the same receptors on their surfaces, but some of these receptors are over-expressed in cancer cells, such as epidermal growth factor receptors (EGFR) and folate receptors (FR). Designing a drug nanocarrier (micelle) with a ligand that binds to two or more kinds of over-expressed receptors should improve tumor cells targeting.

This section covers the model of one ligand binding to two different receptors. Figure 4.6 shows the interaction area between the micelle and the targeted cell. The cell surface has two over-expressed targeted receptors (R_1, R_2), with densities of σ_{R_1}, and σ_{R_2}) respectively. The micellar surface has two different kinds of polymers with N_m number of monomers for each and a total density of σ_p. Spacer polymers are represented by the blue lines in Figure 4.6. Basic polyelectrolytes have two attached ligands to target two different receptors and are represented by purple lines in Figure (4.6).

The expression "ligand complex" will be used here to represent the polyelectrolyte that is attached to a dual-ligand. Similar to the previous model, the basic groups on the ligand complexes are able to dissolve in the biological aqueous environment to

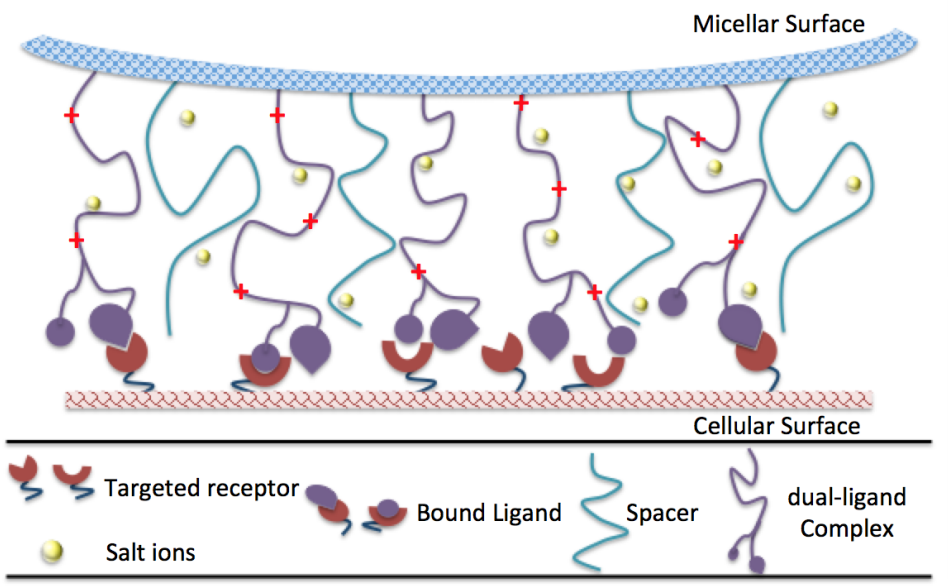

Figure 4.6: A model illustrating the interaction between dual-ligand complexes (polyelectrolytes + dual-ligand) at the micellar surface and the targeted receptors on the cellular surface.

form positively charged ions $\mathrm{B} + \mathrm{H}^+ \overset{K_d}{\rightleftharpoons} \mathrm{BH}^+$ where $\mathrm{K_d}$ is the dissociation constant for the chemical interaction. As the ligand complexes stretch they expose their ligands to the two different receptors (R_1, R_2) on the cell surface causing an increase in the binding probability. The ligands-receptors (LR_1, LR_2) binding interaction can be described by the following relations:

$$\mathrm{L} + \mathrm{R}_1 \overset{K_{LR_1}}{\rightleftharpoons} \mathrm{LR}_1 \qquad \text{and} \qquad \mathrm{L} + \mathrm{R}_2 \overset{K_{LR_2}}{\rightleftharpoons} \mathrm{LR}_2$$

where $\mathrm{K_{LR_1}}$ and $\mathrm{K_{LR_2}}$ are the association constants for these chemical reactions. The two association constants are defined as follows:

$$\begin{aligned} \mathrm{K_{LR_1}} &= \frac{[\mathrm{LR_1}]}{[\mathrm{L}][\mathrm{R_1}]} = C \exp(-\beta(\mu^\circ_{LR_1} - \mu^\circ_L - \mu^\circ_{R_1})) \\ \mathrm{K_{LR_2}} &= \frac{[\mathrm{LR_2}]}{[\mathrm{L}][\mathrm{R_2}]} = C \exp(-\beta(\mu^\circ_{LR_2} - \mu^\circ_L - \mu^\circ_{R_2})) \end{aligned} \tag{4.20}$$

The fraction of ligands in the system is given by $X_L = \frac{N_L}{N_L + N_s}$, where N_L and N_S refer to the number of ligands and spacers respectively. The fraction of bound

dual-ligands to receptors R_1 and R_2 is given by the following relations:

$$f_{LR_1} = \frac{[\mathrm{LR_1}]}{[\mathrm{LR_1}] + [\mathrm{LR_2}] + [\mathrm{L}]} \qquad \text{and} \qquad f_{LR_2} = \frac{[\mathrm{LR_2}]}{[\mathrm{LR_1}] + [\mathrm{LR_2}] + [\mathrm{L}]}$$

where $[LR_1]$, $[LR_2]$ and $[L]$ are the concentrations of bound ligand to receptors (R_1, R_2), and free ligands respectively. The density of all molecules in the system is given as follows:

- Spacers: $\sigma_s = \sigma_p(1 - X_L)$
- Free ligands: $\sigma_L = X_L\sigma_p(1 - f_{LR_1} - f_{LR_2})$
- Bound ligands, or bound receptors: $\sigma_{LR_1} + \sigma_{LR_2} = \sigma_p X_L(f_{LR_1} + f_{LR_2})$
- Unbound receptors: $(\sigma_{R_1} - \sigma_p X_L f_{LR_1}) + (\sigma_{R_2} - \sigma_p X_L f_{LR_2})$

Similar to the previous model, this system is modeled in a cubic lattice structure with a coordination number of six. Each polymer segment or receptor molecule occupies a single cubic lattice site. Polymer conformational structures (α) are built randomly using a self avoiding random walk (SAW) with the Rosenbluths weighting technique to improve the statistics (see Chapter 2). The remaining cubic sites are filled randomly with water and salt ion molecules. All molecules in the system are subject to different kinds of forces, such as steric, van der Waals and electrostatic forces.

An incompressibility constraint is applied to maintain the repulsive steric interactions between all molecules in the system. The mathematical representation of the constraint is as follows:

$$\begin{aligned} &\langle\phi_s(z)\rangle + \langle\phi_L(z)\rangle + \langle\phi_{LR_1}(z)\rangle + \langle\phi_{LR_2}(z)\rangle \\ &\qquad + \phi_w(z) + \phi_{\mathrm{H^+}}(z) + \phi_{\mathrm{OH^-}}(z) + \phi_+(z) + \phi_-(z) + \phi_R = 1 \end{aligned} \tag{4.21}$$

Note that the system studies four different polymers; spacers (s), free ligand-complexes (L), and ligand-complexes that are bound to receptors (LR_1 and LR_1). Thus, $\langle\phi_p(z)\rangle$

is the average volume fraction of polymer p, and $\phi_x(z)$ is the volume fraction of specie x.

The van der Waals interactions are accounted for in each configuration (α) through the intra-molecular interactions ($E_{intra}(\alpha)$) between segments of one polymer, and the inter-molecular interactions ($E_{inter}(\alpha)$) between polymer segments from different polymers. The values of these two short-ranged molecular-attractive interactions, (ε_{intra} and ε_{inter}), depend on the choice of polymers in the system and their interaction with the solvent. Moreover, the electrostatic interactions between two charged molecules in the system are influenced by several variables, such as: the polymer density (σ_p), the surface charge coverage on the cell (σ_q), the bulk pH, and the local temperature through (K_BT). We study the effect of those variables on the extension of the ligands complexes. Different electrostatic interactions cause different configurations and accordingly, different intra and inter-molecular interactions. The model demonstrates the complexity of the chemical equilibrium and the physical interactions between all molecules in the system on the two different ligand-receptor bindings probabilities (P_{LR_1} and P_{LR_2}).

4.4.1 Theoretical Approach

Similar to the previous model, the space between the micelle and the cell surfaces is discretized into discrete layers in the XY plane with thickness dz. The system is assumed to be homogeneous in planes parallel to the cell surface and the micelle surface (XY), and inhomogeneous in the norm direction (Z). The molecular interactions are described in the system through the mean field approximation. The Helmholtz free energy per unit area for the system has a similar form to the Helmholtz free energy in the previous model.

$$(F = F_{pol} + F_{elc} + F_{chem} + F_{if} + F_{mix})$$

The system Helmholtz free energy considers the polymer, electrostatic, chemical interaction, ion formation and mixture free energies. However, the chemical and the mixture free energies in this system account for the standard chemical potential (self-energy) for the two kinds of ligand- receptor bindings ($\mu^{\circ}_{LR_1}, \mu^{\circ}_{LR_2}$), as well as the translational entropy due to those two interactions.

Polymers self-energy due to the intra and inter-molecular interactions between the three kinds of polymers, as well as their conformational entropy (S) are added to calculate the polymers free energy. Polymers free energy mathematical expression is given in Equation 4.8 but in this case $p = \{s, L, LR1, LR2\}$.

The second term of the system free energy is the electrostatic free energy (see Equation 4.9), where in this model:

- $\langle \rho_q(z) \rangle = f_{H^+}(z) q_p (\langle \rho_L(z) \rangle + \langle \rho_{LR_1}(z) \rangle) + \langle \rho_{LR_2}(z) \rangle) + \sum_m q_m \rho_m(z)$, where q_p is the charge on the dissociated functional groups of the polyelectrolytes.

- $\Big(\langle \rho_L(z) \rangle + \langle \rho_{LR_1}(z) \rangle + \langle \rho_{LR_2}(z) \rangle \Big) = \sigma_p X_L (1 - f_{LR_1} - f_{LR_2}) \sum_\alpha P_L(\alpha) v_L(\alpha, z)$
  $+ \sigma_p X_L f_{LR_1} \sum_\alpha P_{LR_1}(\alpha) v_{LR_1}(\alpha, z) + \sigma_p X_L f_{LR_2} \sum_\alpha P_{LR_2}(\alpha) v_{LR_2}(\alpha, z)$

- $q_m \rho_m$ represents the charge and the volume fraction of the molecular species other than polymers in the system ($\mathrm{H^+ - OH^- - Na^+ - Cl^-}$).

The third term in the system free energy accounts for the chemical interactions of all molecules in the system including the two kinds of ligand-receptor binding interactions, which can be represented as follows:

$$
\begin{aligned}
F_{chem} =& \frac{1}{\beta} \int (\langle \rho_L(z) \rangle + \langle \rho_{LR}(z) \rangle) \Big\{ f_{H^+}(z) [\ln f_{H^+}(z) + \beta \mu^{\circ}_{BH^+}] \\
& + (1 - f_{H^+}(z)) [\ln(1 - f_{H^+}(z)) + \beta \mu^{\circ}_{\mathrm{B}}] \Big\} dz \\
& + \frac{1}{\beta} \Big\{ \sigma_p X_L (1 - f_{LR_1} - f_{LR_2}) \beta \mu^{\circ}_L + \sigma_p X_L f_{LR_1} \beta \mu^{\circ}_{LR_1} + \sigma_p X_L f_{LR_2} \beta \mu^{\circ}_{LR_2} \\
& + (\sigma_{R_1} - \sigma_p X_L f_{LR_1}) \beta \mu^{\circ}_{R_1} + (\sigma_{R_2} - \sigma_p X_L f_{LR_2}) \beta \mu^{\circ}_{R_2} \Big\}
\end{aligned}
\tag{4.22}
$$

where μ_m° is the standard chemical potential for molecule m, which accounts for the molecule self-energy. Terms that have the following form $(\langle\rho_m(z)\rangle f_n(z)[\ln f_n(z))$ denote the translational entropy of molecule m due to the chemical interaction n.

The ion formation free energy term in this system is exactly the same as in the previous system (see Equation (4.11)). The last free energy term accounts for the mixture free energy. This term represents the translational (mixing) entropy for all molecules in the system, and it is represented mathematically as follows:

$$\begin{aligned}
F_{mix} = -TS_{mix} =& \frac{1}{\beta}\int\Big\{[\rho_w(z)(\ln\rho_w(z)-1)] + [\rho_{\mathrm{H}^+}(z)(\ln\rho_{\mathrm{H}^+}(z)-1)] \\
&+[\rho_{\mathrm{OH}^-}(z)(\ln\rho_{\mathrm{OH}^-}((z)-1)] + [\rho_+((z)(\ln\rho_+(z)-1)] \\
&+[\rho_-(z)(\ln\rho_-(z)-1)]\Big\}dz \\
&+\frac{1}{\beta}\Big\{\sigma_p(1-X_L)\ln(1-X_L) \\
&+\sigma_p X_L(1-f_{LR_1}-f_{LR_2})\ln(1-f_{LR_1}-f_{LR_2}) \\
&+\sigma_p X_L f_{LR_1}\ln f_{LR_1} + (\sigma_{R_1}-\sigma_p X_L f_{LR_1})\ln\left(1-\frac{\sigma_p X_L f_{LR_1}}{\sigma_{R_1}}\right) \\
&+\sigma_p X_L f_{LR_2}\ln f_{LR_2} + (\sigma_{R_2}-\sigma_p X_L f_{LR_2})\ln\left(1-\frac{\sigma_p X_L f_{LR_2}}{\sigma_{R_2}}\right)\Big\}
\end{aligned} \tag{4.23}$$

By summing all the above free energies in the system, one gets the total free energy for a semi-grand canonical ensemble as follows:

$$\begin{aligned}
\Omega =& \frac{\beta F}{A} - \beta\sum_m \rho_m\mu_m \\
=& -\beta\Bigg[\Bigg[\sigma_p(1-X_L)P_s(\alpha) + \sigma_p X_L(1-\sum_{i=1}^{2} f_{LR_i})P_L(\alpha) \\
&+ \sigma_p X_L\Big(\sum_{i=1}^{2} f_{LR_i}P_{LR_i}(\alpha)\Big)\Bigg]E_{intra}(\alpha) \\
&+ \frac{\varepsilon_{inter}}{2}\int_z\Big(\langle\phi_s(z)\rangle\langle\eta_s(z)\rangle + \langle\phi_L(z)\rangle\langle\eta_L(z)\rangle + \sum_{i=1}^{2}\langle\phi_{LR_i}(z)\rangle\langle\eta_{LR_i}(z)\rangle\Big)dz\Bigg] \\
&+ \sigma_p(1-X_L)\sum_\alpha P_s(\alpha)\ln P_s(\alpha) + \sigma_p X_L(1-\sum_{i=1}^{2} f_{LR_i})\sum_\alpha P_L(\alpha)\ln P_L(\alpha)
\end{aligned}$$

$$
\begin{aligned}
&+ \sigma_p X_L \Big(\sum_{i=1}^{2} f_{LR_i} \sum_{\alpha} P_{LR_i}(\alpha) \ln P_{LR_i}(\alpha) \Big) \\
&+ \beta \int \Bigg[\Bigg(f_{+H}(z) q_p \Big(\langle \rho_L(z) \rangle + \Big(\sum_{i=1}^{2} f_{LR_i} \langle \rho_{LR_i}(z) \rangle \Big) \Big) + \sum_{m} q_m \rho_m(z) \Bigg) \psi(z) \\
&- \frac{1}{2} \epsilon \left(\frac{\partial \psi(z)}{\partial z} \right)^2 \Bigg] \, dz \\
&+ \int \Big(\langle \rho_L(z) \rangle + \sum_{i=1}^{2} f_{LR_i} \langle \rho_{LR_i}(z) \rangle \Big) \Big\{ f_{H^+}(z) [\ln f_{H^+}(z) + \beta \mu^{\circ}_{BH^+}] \\
&+ (1 - f_{H^+}(z)) [\ln(1 - f_{H^+}(z)) + \beta \mu^{\circ}_{\mathrm{B}}] \Big\} \, dz \\
&+ \Big\{ \sigma_p (1 - X_L) \ln(1 - X_L) + \sigma_p X_L (1 - \sum_{i=1}^{2} f_{LR_i}) [\ln(1 - \sum_{i=1}^{2} f_{LR_i}) + \beta \mu^{\circ}_{L}] \\
&+ \sum_{i=1}^{2} \sigma_p X_L f_{LR_i} [\ln(f_{LR_i}) + \beta \mu^{\circ}_{LR_i}] \\
&+ \sum_{i=1}^{2} (\sigma_{R_i} - \sigma_p X_L f_{LR_i}) [\ln(1 - \frac{\sigma_p X_L f_{LR_i}}{\sigma_{R_i}}) + \beta \mu^{\circ}_{R_i}] \Big\} \\
&+ \int \Big\{ [\rho_w(z)(\ln \rho_w(z) - 1)] + [\rho_{\mathrm{H}^+}(z)(\ln \rho_{\mathrm{H}^+}(z) - 1 + \beta \mu^{\circ}_{\mathrm{H}^+})] \\
&+ [\rho_{\mathrm{OH}^-}(z)(\ln \rho_{\mathrm{OH}^-}(z) - 1 + \beta \mu^{\circ}_{\mathrm{OH}^-})] \\
&+ [\rho_+(z)(\ln \rho_+(z) - 1 - \beta \mu_+)] + [\rho_-(z)(\ln \rho_-(z) - 1 - \beta \mu_-)] \Big\} \, dz
\end{aligned}
\tag{4.24}
$$

The developed theory describes the interaction between the micelle and the cell surface with a single, dual, or even treble and higher ligand functionality. In this model, the constant term increases as the number of ligand functionality increases. Having a dual ligand with two fractions of binding to two different receptors causes an increase in the attractive energy. However, this increase on the binding energy should not affect the probability of having a specific polymer at a specific configuration as you will see below.

The system is described by calculating the most probable configurations of spacers, free ligand complexes and any set of bound ligand complexes. Introducing Lagrange multipliers $\pi(z)$ with the incompressibility constraint, then minimizing the free energy allows calculation of the three different probabilities that describes the system:

- The probability of having a spacer (P_s) at specific configuration (α) [1].
- The probability of having a free ligand complex (P_L) at configuration (α).
- The probability of having any set of bound ligand complex (P_{LR_i}) at configuration (α), where i represents the number of the ligand receptor set.

The probabilities are given by the same relations as described in the single ligand model through equations 4.14 and 4.15, where in this case, $ii = \{L, LR_i\}$, and q is the partition function of the corresponding polymer, which satisfies that $\sum_\alpha P(\alpha) = 1$.

Notice that the probabilities in this system look similar to the probabilities in the previous system (see Equations (4.14), (4.15)), however the number of probabilities that are needed to describe the system should increase as the set of ligand-receptors increases in the model. This shows that the probability of having a spacer, ligand or bound ligand complex at a specific configuration is only effected by the steric, van der Waals, and electrostatic interactions, which are treated similarly in both systems. The only difference in this system, compared to the previous model, is that the binding energy increases dramatically at the last layer near the cell surface. This increase on the binding energy should effect the cell surface curvature, which should increase the probability of endocytosis. This could be a future topic in studying micelles as drug delivery devices.

The protonation fraction, and the volume fraction of all molecular species in the system are exactly as described in equations 4.16 and 4.17.

The general equation for the fraction of set of ligand-receptor binding is given by the following relation:

$$\frac{f_{LR_i}}{(1-\sum_{i=1}^{2} f_{LR_i})} = \frac{C\ K_{LR_i}\ q_{LR_i}\ e}{q_L \phi_{R_i}} \left(1 - \frac{\sigma_p X_L f_{LR_i}}{\sigma_{R_i}}\right) \tag{4.25}$$

[1]Notice that the spacers probability in this system is similar to P_s in the previous system since this probability is not effected by the fraction of binding.

where, q_L is the partition function for free ligand complexes and q_{LR_i} is the partition function for the set i of bound ligand complexes. C is the association constant in the equation $\mathrm{K_{LR_i}}$=Cexp$(-\beta(\mu^{\circ}_{\mathrm{LR_i}} - \mu^{\circ}_{\mathrm{L}} - \mu^{\circ}_{\mathrm{R_i}}))$, ϕ_{R_i} is the volume fraction of receptors on the interacting cell surface at a specific microstate, which can be calculated by knowing the receptor density and the cell-surface interaction area, and e is the base of the natural logarithm.

The system is solved numerically by discretizing the system into z number of layers with thickness of $0.33nm$. This complex non-linear system is composed of nine sets of unknowns. There are four unknown average volume fractions: for spacers, complex ligands, and two sets of bound complex ligands $\Big(\langle\phi_s(z)\rangle$, $\langle\phi_L(z)\rangle$, $\langle\phi_{LR_1}(z)\rangle$, $\langle\phi_{LR_2}(z)\rangle \Big)$. Another four unknowns are the fraction of inter-molecular interactions: for spacers, complex ligands, and two sets of bound complex ligands $\Big(\langle\eta_s(z)\rangle$, $\langle\eta_L(z)\rangle$, $\langle\eta_{LR_1}(z)\rangle$, $\langle\eta_{LR_2}(z)\rangle \Big)$. The electric potential profile $(\psi(z))$ is the last unknown. We use the minimized free energy equations (eqs. (4.14) to (4.17)), and Poisson's equation to solve for the nine sets of unknowns. We exterminimize the free energy with respect to the electric potential to solve for the electric potential $\psi(z)$ with the same boundary conditions as in the previous model. The same assumptions of different charge densities on the cell surface, and precise charge on the micellar surface are used to solve for the electric potential.

4.5 Results and Discussion

This section will be divided into two sections to discuss the previous two models:

4.5.1 The Results of The Binding of One Ligand to One Receptor

We design our model in a cubic lattice system and discretize the space into layers in the XY plane and set the thickness of the layers to be equal to $0.33nm$ for all calculations. The system contains three different kinds of polymer chains, each con-

sisting of 25 monomers. The salt concentration is maintained at $0.1 molar$ during all calculations. We started by testing the incompressibility constraint of the system where the cell surface is far away from the micellar surface. At this state the fraction of ligands bound to receptors is *zero*. For this test we set the system $pH = 7$, $\sigma_p = 0.3/nm^2$, $X_L = 0.4$, and the number of layers between the micellar surface and the cell ($L = 30$). Figure (4.7) shows the volume fraction of water molecules, spacers and complex ligand segments at each layer of the system. The sum of all molecules at each layer is equal to *one*. At layers that are far away from the micellar surface, we see that the volume fraction of water molecules is always equal to *one*.

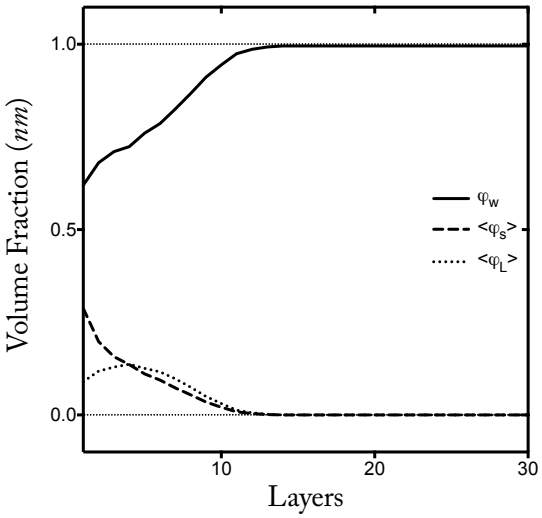

Figure 4.7: An illustration of the incompressibility constraint.

We studied the electric potential profile for the system ($\psi(z)$). Figure (4.8) shows the electric potential profile in three different criterial. The first criterion is when there is no charge on the surface of the cell. We notice that the electric potential profile decreases smoothly from a positive electric potential value due to the positively charged polyelectrolyte segments on the micellar surface to reach zero at the cell. This criterion is similar to the electric potential profile in the limit of $z \to \infty$, where it converged asymptotically to zero.

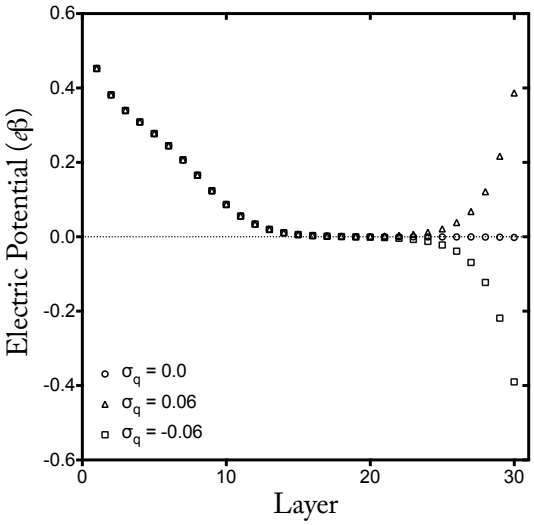

Figure 4.8: The electric potential profile for the same density of grafted polyelectrolytes and different charges on the surface of the targeted cell.

The second and the third criterial illustrate a positive and a negative charge on the cell surface respectively. In both cases, the electric potential profile shows at first an asymptotic converge to zero at the middle layers where there are no polyelectrolyte segments (ligand-complexes), and where the charge on the cell surface has no effect at these layers. This zero domain represents the bulk in the system and is affected by the distance between the micelle surface and the cell surface (see figure (4.9)). In the case of the positively charged cell surface, the electric potential passes the zero domain to increase as it approaches the cell surface. In the other case, where the cell surface is negatively charged, we see that the zero domain is followed by a decrease in the electric potential as it approaches the negatively charged cell surface.

Notice that when the separation distance between the micelle surface and the cell surface is about ten layers, there is no zero domain. Meaning that at this distance there is no bulk in the system. The ten layers distance is the distance at which the ligand-receptor bindings appear, which is the system understudy. It is important to realize that the system under study has no bulk properties. Thus, the pH bulk

value and the values of the standard chemical potentials in the system will always be affected by the pK_a of the ligand-complexes, the salt concentration as well as the charge on the cell surface.

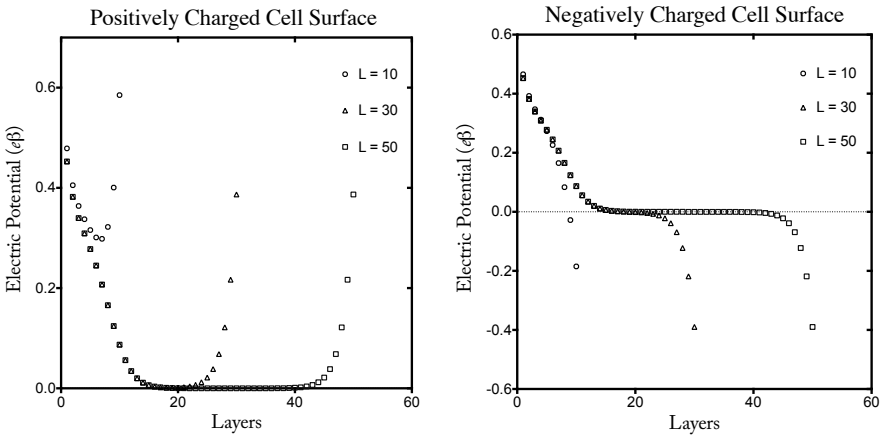

Figure 4.9: The zero domain at the electric potential profile for both negatively and positively charged cell surface is effected by the distance between the micelle and the cell.

The ligand-receptor binding is effected by several environmental parameters, such as the local temperature, local pH, the cell surface charge and the density of receptors on the cell. The ligand-receptor binding is also affected by several engineered parameters, such as the density of ligands on the micelle, the choice of polyelectrolytes, which is influenced by the pKa value and the elementary attractive molecular energy ($\varepsilon_{intra}, \varepsilon_{inter}$). We will study the effect of each parameter on the elongation of the ligand complexes (polyelectrolytes that are attached to ligands) or their average volume.

Local temperature: To design polymers that stretch at high temperature, we choose UCST polymers. Both spacers (thermo-responsive polymers) and ligand complexes (polyelectrolytes) stretch at high local temperatures. We vary the K_BT values between 4 and 1, while keeping the elementary molecular attractive interaction ($\varepsilon_{intra}, \varepsilon_{inter}$) at -1 value. Notice that the change in K_BT value causes a

change in the elementary molecular attractive interaction values. Figure(4.10) shows the effect of increasing the temperature, by increasing the K_BT values, on the end-to-end distance of the polymer. Notice that ligand length is slightly above the length of the spacers. The charged polymer segments on the ligand create repulsive interactions between them, which causes the polymer to expand in length.

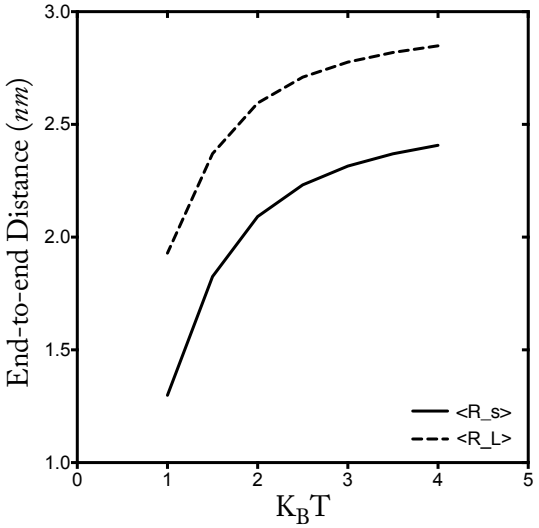

Figure 4.10: The effect of the temperature on the length of micelle spacers and ligands.

Local pH: The effect of local pH on the polymer length is subject to the polyelectrolyte's pKa value. We calculate the end-to-end distance of the ligands at different pK_as while keeping the cell away from the micelle ($L = 25$). Accordingly, we neglect the charge on the cell surface ($q_{cell} = 0$). In these calculations, we set the polymers' density ($\sigma_p = 0.3/nm^2$), the fraction of ligands ($X_L = 0.4$), $KT = 3$ and $T = 37°C$.

Figure (4.11) shows the behavior of polyelectrolytes with different pK_as at several local pH values. This plot can be used as a design guideline to choose specific polyelectrolytes that can target cells with precise local pH as well as

the cases at which the chemical potential values differ from the bulk chemical potential. Changing the polymer density can shift this plot. Figure (4.12) shows the influence of changing the polymer's density on the length of ligand complexes at local $pH = 7$ and cell surface charge. At $\sigma_p = 0.2$ the system couldn't solve for polyelectrolytes with pK_a above *nine*.

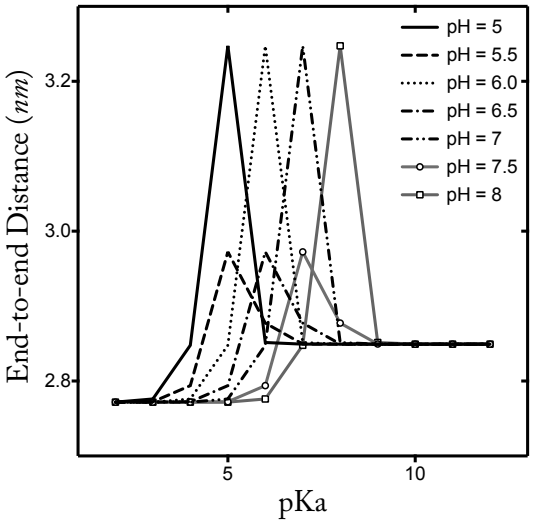

Figure 4.11: The effect of both the local pH and the polyelectrolyte pK_a on the ligands length.

Cell surface charge: The effect of cell charge on the length of ligands is tested at a distance of 10 layers between the micellar surface and the cell surface ($L = 10$). We vary the charges on the cell between (-0.12 - 0.12), choose ($\sigma_p = 0.1$) and ($X_L = 0.4$). Figure (4.13) shows different elongation behaviors at different local pH values. There is almost no charge effect on weak base-polyelectrolyte end-to-end distance. These weak polybases have a $pK_a = 3$ and 5. However, in strong polybases with $pK_a = 9$ and 11, we see a slight increase in the ligand's end-to-end distance. Polybases with $pK_a = 7$ shows an interesting behavior. Their end-to-end distance increases dramatically at negative cell surface charge, and decreases rapidly at cell charge above $+0.09e/nm^2$.

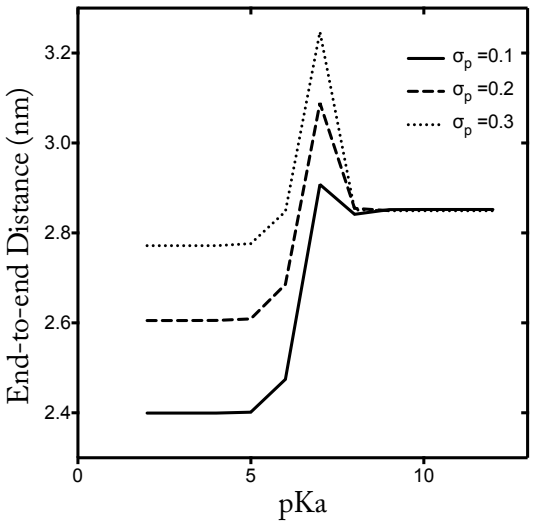

Figure 4.12: Different polymers density can shift the pK_a - pH plots.

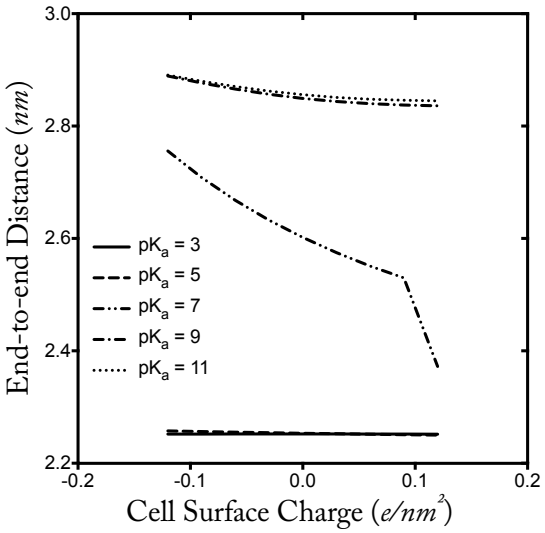

Figure 4.13: The effect of both the local pH and the polyelectrolyte pK_a on the ligands length.

We plot the volume fraction of spacers $\langle\phi_s(z)\rangle$, ligands $\langle\phi_L(z)\rangle$, charged ligands $\langle\phi_{L^+}(z)\rangle$, sodium ions $\langle\phi_{Na}(z)\rangle$, and chloride ions $\langle\phi_{Cl}(z)\rangle$ at three cell surface charge values $(-0.12, 0.0, +0.12)$ and three pK_a values $(3, 7, 11)$, to understand the system's behavior (see Figure (4.14)). At $pK_a = 3$, the number of chloride

ions is very low at the micellar surface at all three different charges. It increases slightly when it reaches the positively charged cell surface. Conversely, the sodium ions show the opposite behavior. In this environment, the amount of charged ligands is almost *zero*.

At $pK_a = 7$, we see an increase in the number of chloride ions at the micellar surface. This number decreases rapidly near the cell surface. The number of chloride ions slightly decreases or increases at the negatively charged surface and the positively charged surface respectively. The uncharged cell surface shows no change in the number of chloride ions near the cell. In this environment, the number of charged ligand complexes at the middle layer is about 25% the total amount of ligands. Some charged and uncharged ligand complexes extend to reach the cell surface. The present of the extended ligand complexes near the cell surface increases the chance of ligand-receptor bindings. In this system, the sodium ions don't show significant behavior.

At $pK_a = 11$, the three plots for the different cell surface charge show a sharp decrease in the total average volume fraction of monomers in the system. The total average volume fraction of monomers in the system is a conserved value that is giving by the following relation:

$$\sum_z \langle \phi_s(z) \rangle = \sigma_p * N_{mon} * \Delta_z$$

where, σ_p is in $1/nm^2$ units, and Δ_z is the thickness of each layer z in nm units. The sharp decrease in the number of monomers in the system is a sign of a significant problem on the inputs. One of the most important inputs that could effect the average volume fraction values is the chemical potential values (see Equation (4.17)). While discussing Figure (4.8) and Figure (4.9), we mentioned that at ten layers separation distance between the micelle and the cell there is no

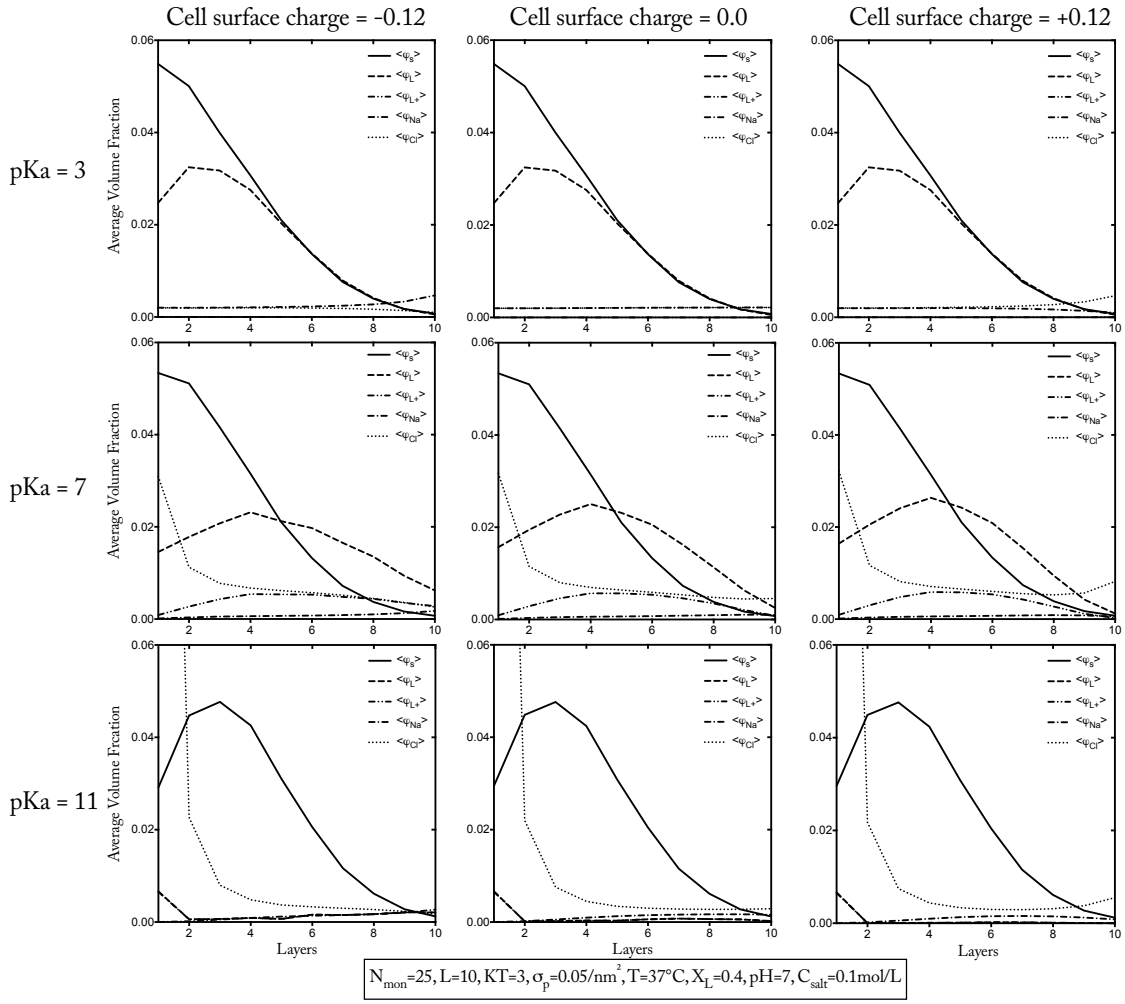

Figure 4.14: The average volume fraction of all molecules in the system at several cell surface charge values.

bulk behavior. Thus, the chemical potential values for the salt ions, hydrogen ions and the hydroxyl ions are different than what is calculated at the bulk.

The chemical potential values are effected by the system pH as well as the pK_a values of the ligand complexes. Figure (4.14) shows that $pK_a = 11$ have a significant effect on the chemical potential values. Thus, we changed the chemical potential values until we reached the values at which the average volume fraction of monomers is conserved in the system. At $pH = 7$, we found the the average volume fraction of monomers is conserved at $exp(-\beta\mu_-) = exp(-\beta\mu_+) = 0.075$ and $exp(-\beta\mu_{H^+}) = exp(-\beta\mu_{OH^-}) = 1 \times 10^{-9}$.

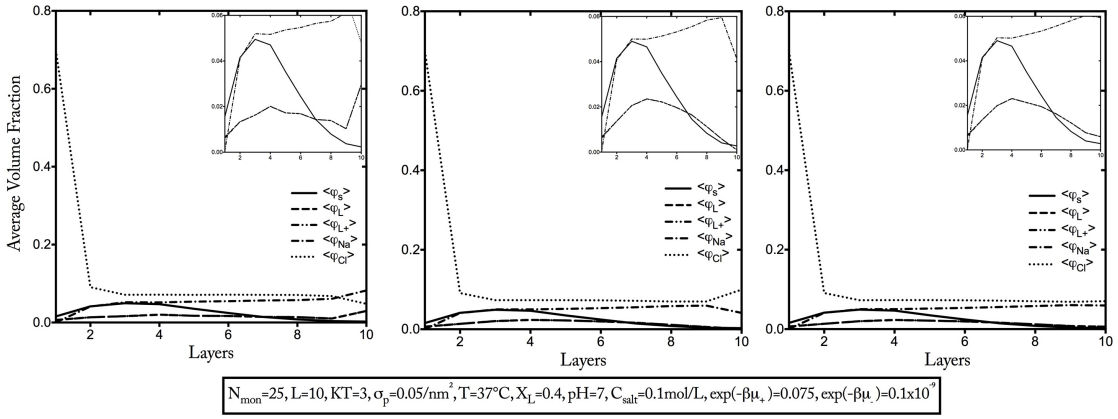

Figure 4.15: Choosing the right chemical potential values to represent the average volume fraction of all molecules in the system at several cell surface charge values for $pK_a = 11$.

Figure (4.15) shows that the chloride ions reach a very high average volume fraction ($\langle\phi_{Cl}(z)\rangle \approx 0.7$). This huge accumulation of the chloride ions adjusts for the extremely positively charged ligand complexes. Chloride ions show the same previous behavior near the cell surface. Interestingly, the system has almost no uncharged ligand complexes. The fraction of charged monomers is about 0.999 at all layers. The charged ligand complexes accumulate on the negatively charged cell surface to increase the probability of binding. The average volume fraction of ligand complexes at the uncharged and the positively charged cell surface is less than what we see near the negatively charged cell surface. At the positively charged cell surface we see an accumulation of the negatively chloride ions to neutralize the charge on the cell and to allow the positively charged ligand complexes to bind to the cell receptors.

Fraction of binding: Our theory indicates that the fraction of binding is affected by the density of receptors in the cell. We study the volume fraction of ligands complexes with $pK_a = 5$ at local $pH = 5.5$, polymers density$= 0.1/nm^2$, $X_L = 0.4$, $KT = 3$, $T = 39°$ C and cell surface charge $= 0$. The fraction of binding (f_{LR}) is chosen to vary between (0.1, 0.5, 0.9). Figure (4.16) represents the

decrease in the amount of ligands as it reaches the cell surface and and increase on the amount of bound ligands. As expected, when the amount of receptors increases, which leads to an increase on the fraction of binding, the number of bound ligands increases.

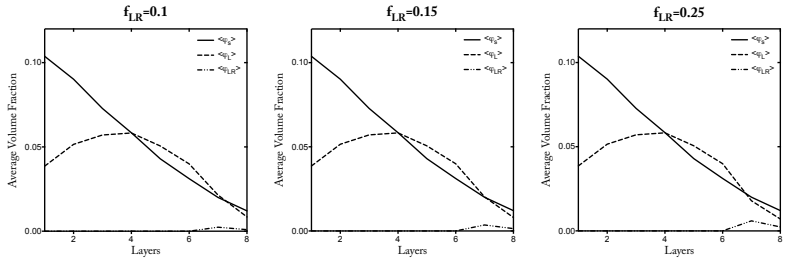

Figure 4.16: The effect of the fraction of binding on the volume fraction of ligands and bound ligands.

Density of ligands: Here we study the effect of ligand density on the number of bound ligands. We set the parameters as they were for studying the effect of the fraction of binding, and set the fraction of binding to be equal to 0.7. Then, we vary the fraction of receptors X_L between $(0.2, 0.4, 0.8)$. Figure (4.17) shows that increasing the fraction of ligands on the micelle, increases the amount of bound ligands. However, this should effect the amount of receptors on the cell. One should be careful with decreasing the amount of receptors as their biocompatible properties help with releasing the drug inside the cell. They also can protect the charged ligand complexes.

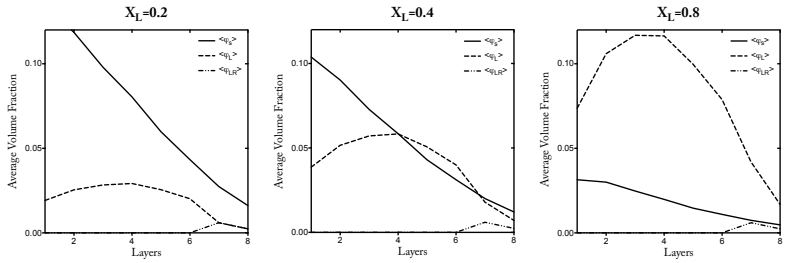

Figure 4.17: The effect of the fraction of ligands on the volume fraction of ligands and bound ligands.

Finally, the developed theory considers van der Waals, steric, and electrostatic interactions between all molecules at each layer of our dense system. These interactions could vary due to different stimuli in the system, such as pH, pK_B, T and charge density, as well as different micellar designs, such as the choice of polyelectrolytes pK_a, elementary molecular interactions ($\varepsilon_{intra}, \varepsilon_{inter}$), the fraction of ligands and the density of polymers. The coupling between these different interactions optimizes different structures of the ligand complexes, and different molecular volume fractions. The system reduces the attractive and the repulsive interactions through several mechanisms. Ligand receptors elongation helps in stabilizing the system in some cases. However, chloride ions play a significant role in neutralizing the system. Also, our theory shows the effect of receptor density on the number fraction of complex ligands that bind to the targeted receptors on the cell.

4.5.2 The Results of The Dual-Ligand Binding Technique

The system is modeled in a cubic lattice structure and discretized into layers in the XY plane. The thickness of the layers is set to be equal to $0.33nm$ for all calculations. The system contains four different kinds of polymer chains each consisting of 25 monomers. The salt concentration is maintained at 0.1molar during all calculations. As mentioned in the previous section, this system composed of *nine* sets of unknowns. The nonlinear system is solved using KINSOL solver from the SUNDIALS library with SPGMR interface.

The system's solution is tested first by plotting the incompressibility constraint, and Figure (4.18) illustrates the validation of the constraint. The plot shows that summing the volume fraction of all molecules in the system at each layer z goes to *one*. Notice that at a distance from the cell, the average volume fraction of all free ions in the system ($\phi_+, \phi_-, \phi_{H^+}, \phi_{OH^-}$) approaches *zero*. The incompressibility is tested at the following dependent variables: the polymer density ($\sigma_p = 0.3/nm^2$),

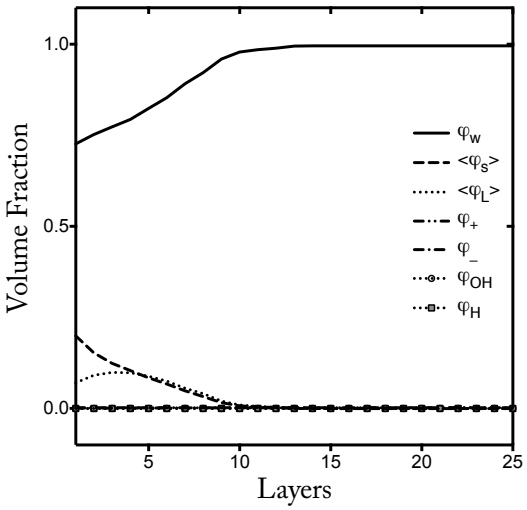

Figure 4.18: An illustration of the incompressibility constraint.

the separation distance ($L = 25$), the fraction of ligand complexes ($X_L = 0.4$), their $pK_a = 6$, $K_BT = 3.0$, the local temperature ($T = 37°C$) and the local $pH = 7$.

Because of the complexity of the system and the large number of unknowns, we also tested the solver by looking at the electric potential profile. Here we tested the system with previous inputs in two cases. When the micelle is at a distance from the charged cell surface ($\sigma_{q_{Cell}} = -0.12, and + 0.12$) at which we expect the electric potential to reach a zero domain between the two charged surfaces (the micellar surface is charged due to the charged grafted monomers on its surface). The second case is when the charged cell surface is close to the micellar surface ($L = 10$) at which we don't see the zero domain in the middle of the system. Figure (4.19) validated the expected behavior for the electric potential profile.

The dual-ligand technique is expected to improve the binding efficiency and selectivity. Here we will compare the number of bound ligands in the case of two different mono-ligands and a dual-ligand. In Figure (4.20), we see the average volume fraction of: bound receptors to mono-ligand (L_1), bound receptors to mono-ligand (L_2), total bound receptors to both mono-ligands ($L_1 + L_2$), and those bound to dual-ligand (L_{12}) at two different pK_a values (3 and 5). The dependent parameter for these re-

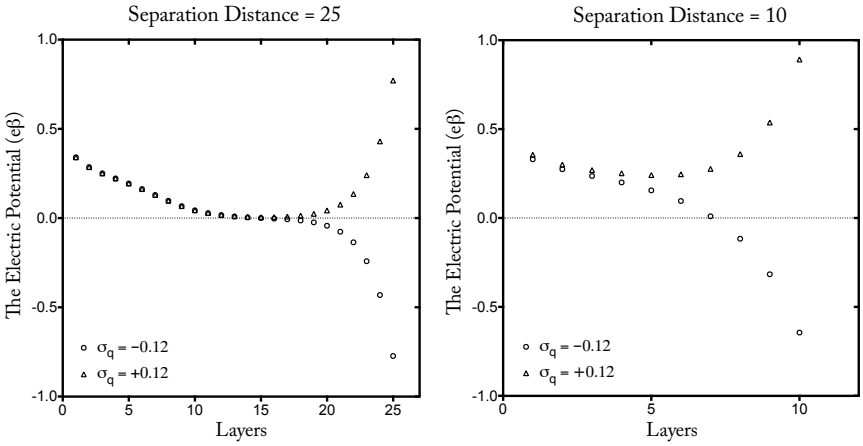

Figure 4.19: The effect of the distance between the micellar surface and the cell surface on the electric potential profile.

sults are chosen to be as follows: $(\sigma_p = 0.3/nm^2, X_L = 0.4, L = 8, \sigma_q = -0.06, pH = 5.5, K_BT = 3.5, T = 39°C)$. These parameters are chosen carefully depending on the cancer cell properties and the system behavior that we learned from our previous mono-ligand micelle model (see section4.5.1). According to Equation (4.4.1) there is a precise range of the fraction of ligand-receptor binding for different choices of polymer density and fraction of ligands at which the $\left(1 - \frac{\sigma_p X_L f_{LR_i}}{\sigma_{R_i}}\right)$ value has to be positive. For this system, and with receptors density reaches up to 0.01[1], the maximum fraction of bound receptors is 0.08.

Figure (4.20) has three diagrams each representing two different fractions of binding for two pK_a groups. In the first diagram, and for each group: the first column is the average volume fraction of a mono-ligand with $f_{LR} = 0.03$, the second is the average volume fraction of a mono-ligand with $f_{LR} = 0.05$, the third column is the sum of the average volume fractions of the two previous columns, and the last is the average volume fraction of a dual-bound ligand that has a fraction of binding of 0.03 to the first targeted receptor and 0.05 to the second targeted receptor. The same applied to the other two diagrams with different fraction of binding values.

[1]As a group of researchers from the University of Texas at Arlington found experimentally that human glioblastoma cells (h-GBM) carry a minimum of 1 EGFR per 100nm2 [57]

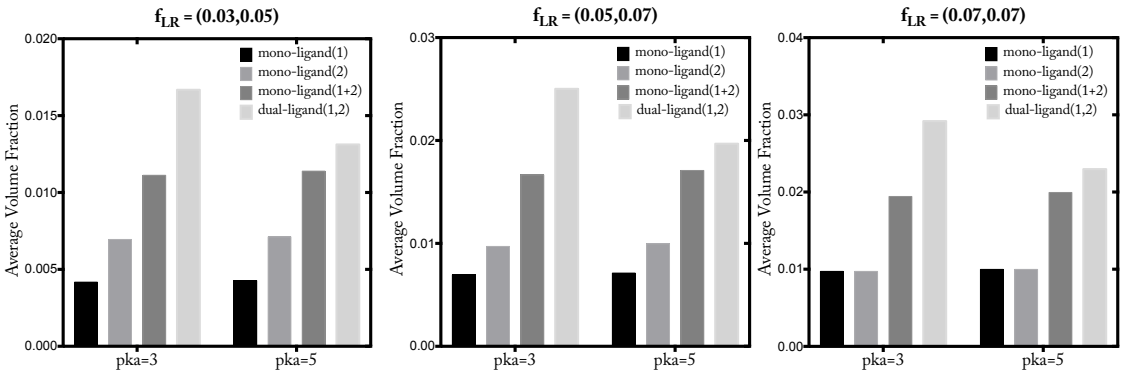

Figure 4.20: The efficiency of the dual-ligand technique and the effect of the pK_a values on the average volume fraction of binding.

Notice that the average volume fraction of a dual-ligand always exceeds the sum of the average volume fraction values of two mono-ligands that have the same fractions of binding as the dual-ligand. Since the dual-ligand has the affinity to bind to two receptors on the cell surface, its chance of binding should be higher than a mono-ligand that has an affinity to only one receptor on the cell surface. Thus, the dual-ligand technique seems to improve the binding efficiency. Figure (4.20) shows that the binding efficiency depends on the polyelectrolyte pK_a value. We see more binding at $pK_a = 3$ than at $pK_a = 5$. However, we know from the previous results (see Figure (4.14) and Figure (4.15)) that the ligand complexes should stretch at higher pK_a values, when the local pH of the system is at seven and the separation distance is about ten layers.

$$pK_a \downarrow \rightarrow BH^+ \downarrow \xRightarrow[10\ layers]{pH=7} \text{Collapsed chains}$$

$$pK_a \uparrow \rightarrow BH^+ \uparrow \xRightarrow[10\ layers]{pH=7} \text{Steretch chains}$$

We also know that these results are effected by the choice of the local pH and the separation distance, which both are effecting the chemical potential values in the system.

To study the dual-ligand design selectivity, we set the micelle dependent parameters at: $(\sigma_p = 0.3/nm^2, X_L = 0.4, L = 8, pK_a = 3, 4, 5, 6)$. For each pK_a value we

calculated the average volume fraction of bound dual-ligands for three different cases: cancerous cell with dependent parameters ($\sigma_q = -0.06, pH = 5.5, K_BT = 3.5, T = 39°C, \sigma_{R1} = \sigma_{R2} = 0.01$) [1], healthy cell with the same density of receptors as the cancer cell ($\sigma_q = -0.02, pH = 7, K_BT = 3.0, T = 37°C, \sigma_{R1} = \sigma_{R2} = 0.01$), and healthy cell with 10% lower receptor density than the cancer cell ($\sigma_q = -0.02, pH = 7, K_BT = 3.0, T = 37°C, \sigma_{R1} = \sigma_{R2} = 0.001$).

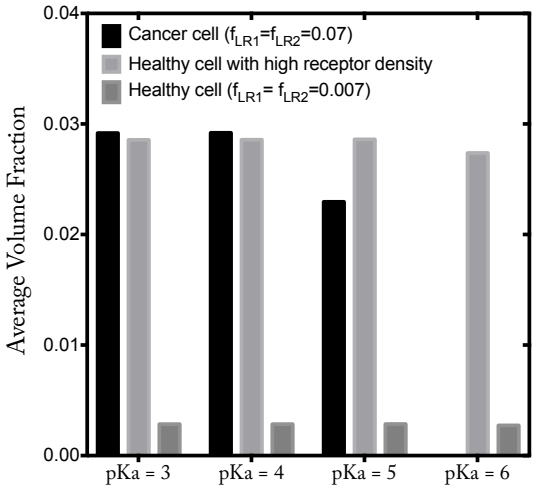

Figure 4.21: The digram shows that the dual-ligand selectivity depends on the density of receptors on the surface of the cell.

Figure(4.21) shows that at low pK_a values ($pK_a = 3, 4$), changing the local environment from cancerous to healthy cell environment decreases the average volume fraction of bound dual-ligands slightly if the amount of receptors on both cells are the same. The case of low pK_a values and separation distance of eight layers can be represented as follows:

$$\text{At cancer cell: } pH \downarrow \rightarrow H^+ \uparrow \Rightarrow BH^+ \uparrow \Rightarrow \text{Steretched chains}$$

$$\text{At healthy cell: } pH \uparrow \rightarrow H^+ \downarrow \Rightarrow BH^+ \downarrow \Rightarrow \text{Collapseed chains}$$

However, increasing the pK_a values showing an unexpected results. At $pK_a = 5$ the average volume fraction of bound dual-ligands increases at healthy cell environ-

[1]The maximum fraction of binding for these inputs and according to Equation (4.4.1) is $f_{LR1} = f_{LR2} = 0.08$, and we choose it to be equal to 0.07

ment. At pK_a values higher than 6, we see no binding to receptors on cancer cells, while dual-ligands bind to a good number of receptors on healthy cells. At pK_a values above 5, the plot shows that base-polyelectrolytes collapse at low pH values (cancer cell environment) prohibiting the dual-ligands from reaching the cell surface and stretch at higher pH values (Healthy cell environment) allowing more ligand receptor binding behavior. This unexpected effect is influenced by the change on the chemical potential values that are effected strongly by the pK_a values, the local pH as well as the separation distance between the micelle and the cell.

In the case of healthy cells with 10% less receptors on their surface than cancer cells, the average volume fraction of bound dual-ligands deceases dramatically. Although the dual-ligand can stretch at the healthy cell environment, the density of the targeted receptor on the healthy cell surface is significant to control the ligand-receptor binding. Thus, the dual-ligand technique seems to improve the selectivity, if the density of the targeted receptors is chosen carefully to be much higher in the cancer cell than in the healthy cell.

The selectivity in both the mono and the dual-ligand techniques can be improved by limiting the stability of the micelle on the cell with the requirement of having more than one ligand to bind to the cell. In other words, the binding to one receptor on the cell shouldn't be enough to stabilize the micelle against the blood stream. Previously, we mentioned the importance of the size of the therapeutic micelle in improving the selectivity 4.2. We calculated the size of the therapeutic micelle depending on the density of receptors of the targeted cell. Using the dual-ligand technique with a micelle that has the right therapeutic size should improve both: the selectivity and the efficiency.

In conclusion, herein we generalize a molecular theory that accounts for steric, van der Waals, and electrostatic interactions in a biological system to study the dual-ligand binding protocols. We used a decoupled mean-field approach to improve the

van der Waals inter-molecular interaction efficiency. Different stimuli in the system affected the dual-ligand binding, however we found that the system local pH, the polyelectrolytes pK_a values and the chemical potential values are the driving parameters in the system. That could be highly related to the way the polyelectrolytes get ionized in the system. In our system we choose polyelectrolytes that bind to hydrogen ions to become positively charged. The system behavior could change if in the case of polybases that dissociate to hydroxide groups and positively charged ions, which we may consider as a future work. We found that the dual-ligand technique should improve the binding efficiency and selectivity to cancer cells that have over-expressed receptors. The technique can be farther improved by using the optimum therapeutic micellar size.

Chapter 5

Future Work

Several drugs in existence today are producing the anticipated results on diseased cell cultures or tissues, however most of these drugs have side effects on other healthy cells or tissues. It is therefore essential to ensure delivery of the drug directly to the site of action and the designing of a drug delivery vehicle has become an imperative topic. The material used to design drug delivery devices must have several properties: it must be nontoxic, it must be biocompatible so the cell can absorb the drug and the material has to have an on/off switch that responds to some external stimulus so that the drug is protected until it reaches the site of action. Several synthesized polymers can be manipulated to meet the requirements for a specific application. In the previous two chapters we have covered some of these applications. There are still abundant designs that can be further explored to improve the targeted drug delivery devices. In this chapter we will highlight certain polymeric drug delivery device designs, where their physical behavior can be studied in the future.

5.1 Modeling Micelles with pH-Sensitive Charge-Conversion Polyelectrolytes

In the previous two models in Chapter 4, we have used pH-sensitive polyelectrolytes as ligand-complexes. We have studied the effect of the low pH in the cancer environment, which raises the positive charges on the polybases. This raised charge leads to an attractive interaction between the micelle and the cancer cell. The Macromolecular Bioscience journal presented an interesting synthesis of a smart micelle that has

pH-sensitive charge converting behavior [21]. The synthesized polymers are slightly negatively charged at neutral or basic pH but become positively charged at low pH. Such a design reduces the interaction between the micelle and the negatively charged surface of the healthy cells.

The model of the dual pH-sensitive polyelectrolytes undergoes two different interactions as follows:

- At neutral and basic pH:

$$AH \rightleftharpoons A^- + H^+$$

- At low pH:

$$B + H^+ \rightleftharpoons BH^+$$

The first chemical interaction represents the dissolving of the acid groups along the polymer chain. The dissociation constant for this interaction is ($K_a = \frac{[A-][H+]}{[AH]}$). The second interaction is identical to the interaction discussed in Chapter 3 and Chapter 4, where the dissociation constant is ($K_b = \frac{[BH+]}{[B][H+]}$). Looking at the two dissociation constants, one can determine the effect of one reaction on the other, and how these reactions could effect the pH of the surrounding environment. The study of the competition between the different forces in the system could improve the stability and the targeted delivery.

5.2 Modeling Microgels that Release Hydrophobic-Hydrophilic Drugs

In Chapter 3 we have discussed the behavior of thermo-responsive polymers. LCST polymers have been used to control drug release, due to their swilling behavior at low temperature. Cross-linked gels can be made of thermo-responsive polymers with LCST around 32°. The gel swills at this temperature but starts to shrink when it reaches the higher temperature of the body. This shrinkage behavior allows the drug to escape from the holes within the cross-linked gel.

In 2015, the Materials Letters journal published a paper studying the simultaneous release of aspirin and probucol, as hydrophilic and hydrophobic drugs respectively, to treat restenosis [1] [31]. This shows that designing microgels that can protect and control the release of hydrophobic and hydrophilic drugs at the same time is significant for medical applications. One can design different microgel models to meet specific desired rates of drug release. A spherical model of hydrophilic and hydrophobic gels that protect the hydrophobic and the hydrophilic drugs respectively can be used for different rates of release (see Figure 5.1). In this model, the two layers of LCST gels shrink at body temperature, which is above the LCST point, allowing the drugs to leave the gels. Controlling the size of the outer shell gel and the inside spherical gel has a significant impact on the rate of the drugs' release..

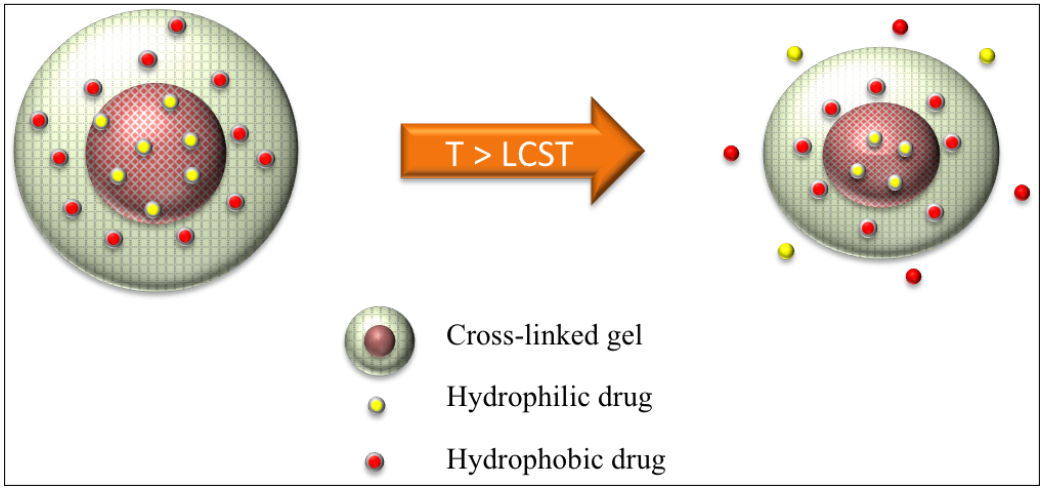

Figure 5.1: A spherical microgel model to release hydrophilic and hydrophobic drugs.

In the case of thermo-degradable cross-linked gels, one can design a layer-by-layer microgel (see Figure 5.2). The two layers of hydrophilic and hydrophobic gels that contain the hydrophobic and the hydrophilic drugs respectively, can be protected with a biocompatible coating material. The coat prevents the drug from being released

[1]Restenosis is the recurrence of stenosis, a narrowing of a blood vessel, leading to restricted blood flow [59].

until it is dissolved in the biological solution. The time for the coat to dissolve can be regulated through the design. The thickness of the hydrophilic and the hydrophobic layer-by-layer gel can also be modified to control the release rate of both drugs.

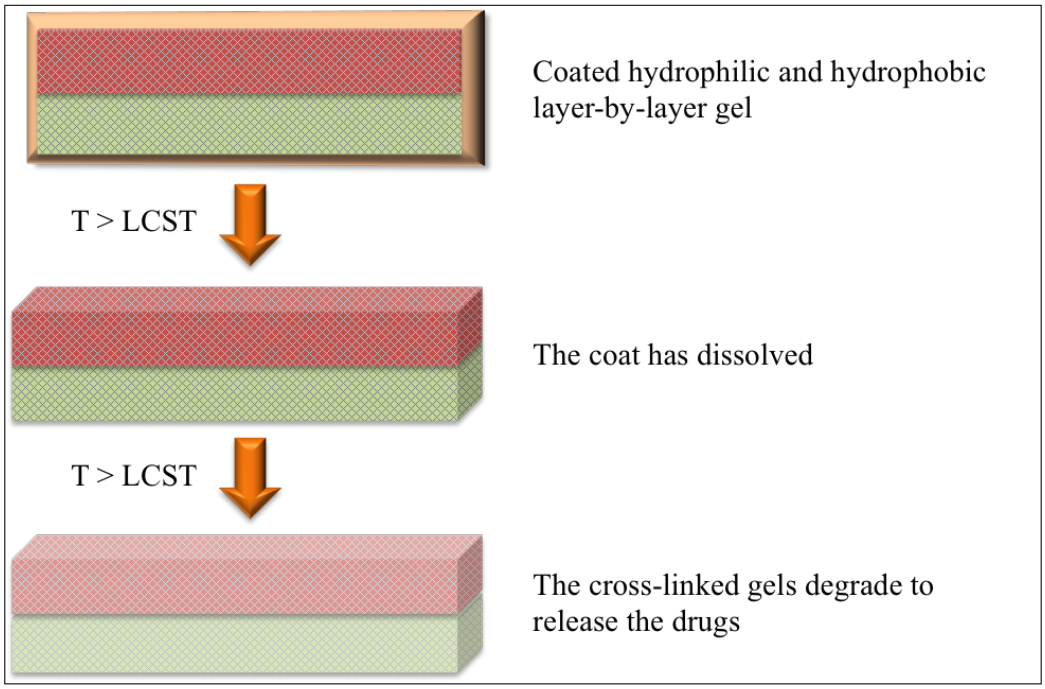

Figure 5.2: A layer-by-layer microgel model to release hydrophilic and hydrophobic drugs.

5.3 Calculating The Micelle-Cell Binding Energy That Enhance Endocytosis

As mentioned earlier, most drugs have side effects on healthy cells. Thus, the ability of releasing the drug inside the cell through endocytosis is essential for an efficient treatment. Our goal is to allow the cell to swallow the micelle that is loaded with the needed drug. To do this, we need to understand the cell's endocytosis behavior, including: the molecules that could undergo endocytosis, the size and weight of these molecules and if there is any kind of binding between the cell and these molecules before the endocytosis mechanism.

Understanding the physical interactions between the cell and the loaded micelle is critical to achieve the desired endocytosis behavior. We need to study all the forces between the micelle and the cell. Once we compare these forces with the weight and the binding forces of the proteins that are inserted into the cell through endocytosis, we can mimic the natural endocytosis behavior of the cell. Figure (5.3) represents the effect of the strength of the binding energy in increasing the curvature on the cell that enhance endocytosis.

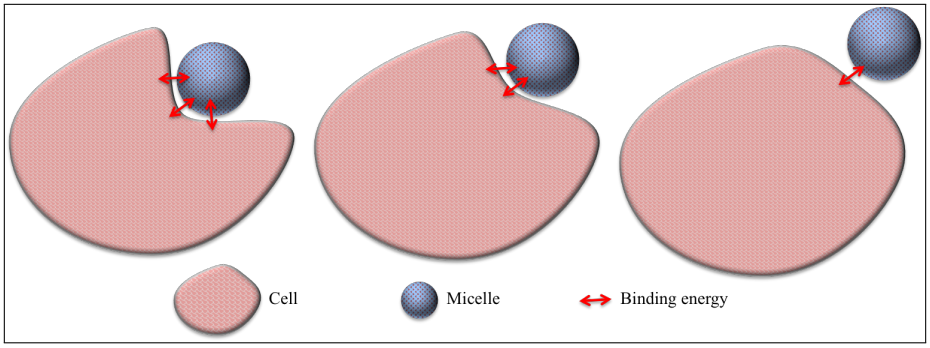

Figure 5.3: An illustration represents the effect of the binding energy between the micelle and the cell in increasing the cell Curvature.

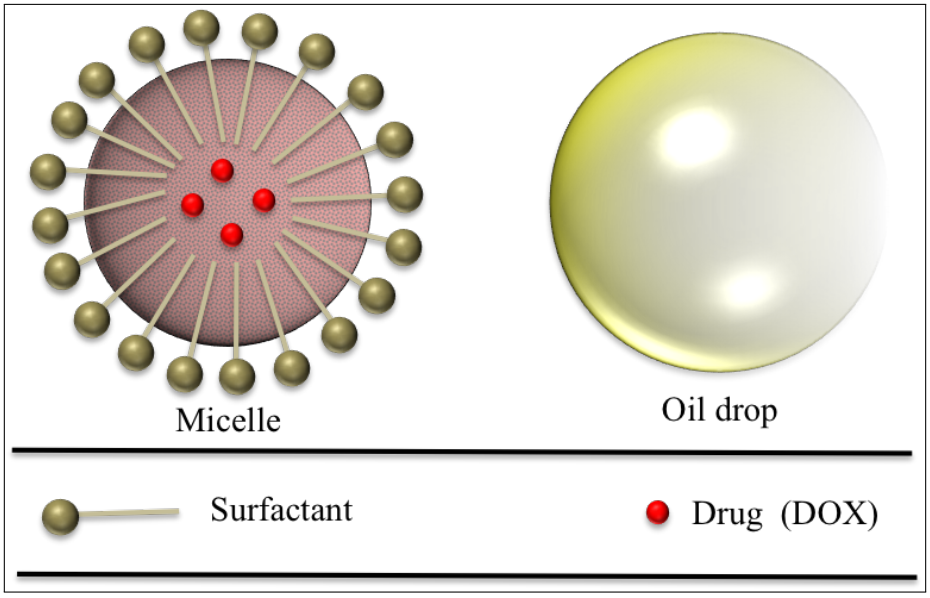

Figure 5.4: Using the oil drop model to study the micelle stability.

5.4 Calculating The Micelle's Self-Assembly Energy to Diminish Drug Leakage

For this model we need to study polymers' self-assembly in a spherical coordinates system (see Appendix C). In this study, we can use the oil drop model to determine the force needed to stabilize the micellar shape (see Figure (5.4)). This force should be determined by the size of the micelle, the density of the micelle, and the density of the surrounding solution. Thomas Russell and colleagues have published papers in the use of the oil drop model to study nanoparticles self-assembly [4, 30, 29]. One, can use these models to design stable micelles at several biological conditions.

Bibliography

[1] M Abercrombie and EJ Ambrose. "The surface properties of cancer cells: a review". In: *Cancer research* 22.5 Part 1 (1962), pp. 525–548.

[2] Jooyeon Ahn et al. "Antibody fragment-conjugated polymeric micelles incorporating platinum drugs for targeted therapy of pancreatic cancer". In: *Biomaterials* 39.C (Jan. 2015), pp. 23–30.

[3] Carolina de las Heras Alarc n, Sivanand Pennadam, and Cameron Alexander. "Stimuli responsive polymers for biomedical applications". In: *Chemical Society Reviews* 34.3 (2005), pp. 276–10.

[4] Alexander Böker et al. "Self-assembly of nanoparticles at interfaces". In: *Soft Matter* 3.10 (2007), pp. 1231–19.

[5] Susan E. Burke and Christopher J. Barrett. "Controlling the physicochemical properties of weak polyelectrolyte multilayer films through acid/base equilibria". In: *Pure and Applied Chemistry* 76 (7-8 Jan. 2009), pp. 1387–1398.

[6] Pranjal Chandra, Hui-Bog Noh, and Yoon-Bo Shim. "Cancer cell detection based on the interaction between an anticancer drug and cell membrane components". In: *Chemical Communications* 49.19 (2013), pp. 1900–4.

[7] Guoping Chen, Yoshihiro Ito, and Yukio Imanishi. "Regulation of growth and adhesion of cultured cells by insulin conjugated with thermoresponsive polymers". In: *Biotechnology and bioengineering* 53.3 (1997), pp. 339–344.

[8] Shanta Dhar et al. "Targeted delivery of cisplatin to prostate cancer cells by aptamer functionalized Pt (IV) prodrug-PLGA– PEG nanoparticles". In: *Proceedings of the National Academy of Sciences* 105.45 (2008), pp. 17356–17361.

[9] Ken A. Dill and Sarina Bromberg. *Molecular Driving Forces Statistical Thermodynamics in Biology, Chemistry, Physics, and Nanoscience*. 2nd. New York: Garland Science, 2011. ISBN: 978-0-8153-4430-8.

[10] Izabela Dobrzyńska, Elżbieta Skrzydlewska, and Zbigniew A Figaszewski. “Changes in Electric Properties of Human Breast Cancer Cells”. In: *The Journal of Membrane Biology* 246.2 (Nov. 2012), pp. 161–166.

[11] Izabela Dobrzyńska et al. “Characterization of Human Bladder Cell Membrane During Cancer Transformation”. In: *The Journal of Membrane Biology* 248.2 (Jan. 2015), pp. 301–307.

[12] C Domb. “Excluded-Volume Effect for Two- and Three-Dimensional Lattice Models”. In: *The Journal of Chemical Physics* 38.12 (1963), pp. 2957–8.

[13] Glenn H. Fredrickson. *The Equilibrium Theory of Inhomogeneous Polymers*. 1st. Oxford: Oxford Science Publication, 2006. ISBN: 978-0-19-856729-5.

[14] Igor Y Galaev and Bo Mattiasson. “Smart polymers and what they could do in biotechnology and medicine”. In: *Trends in Biotechnology* 17.8 (1999), pp. 335 –340. ISSN: 0167-7799. DOI: http://dx.doi.org/10.1016/S0167-7799(99)01345-1. URL: http://www.sciencedirect.com/science/article/pii/S0167779999013451.

[15] Igor Y Galaev and Bo Mattiasson. “âĂŸSmartâĂŹ polymers and what they could do in biotechnology and medicine”. In: *Trends in Biotechnology* 17.8 (1999), pp. 335 –340. ISSN: 0167-7799.

[16] Pierre-Gilles de Gennes. *Scaling Concepts in Polymer Physics*. 1st. Ithaca and London: Cornell University Press, 1979. ISBN: 978-0-8014-1203-5.

[17] Matthew C Hagy, Shihu Wang, and Elena E Dormidontova. “Optimization of Functionalized Polymer Layers for Specific Targeting of Mobile Receptors on Cell Surfaces”. In: *Langmuir* 24.22 (Nov. 2008), pp. 13037–13047.

[18] J A Hickey et al. “Simultaneous Release of a Hydroxy-Methylglutaryl Coenzyme A Reductase Inhibitor and a Glycoprotein IIb/IIIa Antagonist from a Thermoresponsive NiPAAm/NtBAAm Copolymer System”. In: *Journal of Biomaterials and Nanobiotechnology* 02.01 (2011), pp. 18–27.

[19] M Hrubý et al. “Thermoresponsive polymers as promising new materials for local radiotherapy”. In: *Applied Radiation and Isotopes* 63.4 (2005), pp. 423–431.

[20] Gang Huang et al. “Self-assembled UCST-Type Micelles as Potential Drug Carriers for Cancer Therapeutics”. In: *Macromolecular Chemistry and Physics* 216.9 (Feb. 2015), pp. 1014–1023.

[21] Hailong Huang et al. “A Smart Drug Delivery System from Charge-Conversion Polymer-Drug Conjugate for Enhancing Tumor Therapy and Tunable Drug Release”. In: *Macromolecular Bioscience* 14.4 (Apr. 2014), pp. 485–490.

[22] Kang Moo Huh et al. “pH-sensitive polymers for drug delivery”. In: *Macromolecular Research* 20.3 (Mar. 2012), pp. 224–233.

[23] Tomoki Ito, Chikara Yoshida, and Yoshihiko Murakami. “Design of novel sheet-shaped chitosan hydrogel for wound healing: A hybrid biomaterial consisting of both PEG-grafted chitosan and crosslinkable polymeric micelles acting as drug containers”. In: *Materials Science & Engineering C* 33.7 (Oct. 2013), pp. 3697–3703.

[24] Tianyue Jiang et al. “Furin-Mediated Sequential Delivery of Anticancer Cytokine and Small-Molecule Drug Shuttled by Graphene”. In: *Advanced Materials* 27.6 (Dec. 2014), pp. 1021–1028.

[25] Joseph W. KANE and Morton M. STERNHEIM. *Physics*. 3rd. John Wiley and Sons, 1988. ISBN: 0-471-63845-5.

[26] Yu.A. Kuznetsov. *Newton method. Encyclopedia of Mathematics.* 2011. URL: `http://www.encyclopediaofmath.org/index.php?title=Newton_method&oldid=12312`.

[27] Eun Seong Lee et al. “Super pH-sensitive multifunctional polymeric micelle for tumor pHe specific TAT exposure and multidrug resistance”. In: *Journal of Controlled Release* 129.3 (Aug. 2008), pp. 228–236.

[28] Xi Li et al. “Enhancement of cell recognition in vitro by dual-ligand cancer targeting gold nanoparticles”. In: *Biomaterials* 32.10 (2011), pp. 2540–2545.

[29] Yao Lin et al. “Nanoparticle Assembly at Fluid Interfaces: Structure and Dynamics”. In: *Langmuir* 21.1 (Jan. 2005), pp. 191–194.

[30] Yao Lin et al. “Ultrathin Cross-Linked Nanoparticle Membranes”. In: *Journal of the American Chemical Society* 125.42 (Oct. 2003), pp. 12690–12691.

[31] Hui Liu and Jie He. “Simultaneous release of hydrophilic and hydrophobic drugs from modified chitosan nanoparticles”. In: *Materials Letters* 161.C (Dec. 2015), pp. 415–418.

[32] Gabriel Longo and I Szleifer. “Ligand-Receptor Interactions in Tethered Polymer Layers”. In: *Langmuir* 21.24 (Nov. 2005), pp. 11342–11351.

[33] Haitao Ma et al. “Nucleic acid aptamers in cancer research, diagnosis and therapy”. In: *Chemical Society Reviews* (Jan. 2015), pp. 1–17.

[34] D MacDonald et al. “Self-avoiding walks on the simple cubic lattice”. In: *Journal of Physics A: Mathematical and General* 33.34 (2000), pp. 5973–5983.

[35] E Martinelli et al. “Anti-epidermal growth factor receptor monoclonal antibodies in cancer therapy”. In: *Clinical Experimental Immunology* 158.1 (Oct. 2009), pp. 1–9.

[36] Atsushi Mori et al. “SEMIGRAND CANONICAL MONTE CARLO SIMULATION WITH GIBBS-DUHEM INTEGRATION TECHNIQUE FOR ALLOY PHASE DIAGRAMS”. In: *Mater.Phys.Mech.* 6 (2003), pp. 49–57.

[37] R J Nap and I Szleifer. “How to optimize binding of coated nanoparticles: coupling of physical interactions, molecular organization and chemical state”. In: *Biomaterials Science* 1.8 (2013), pp. 814–11.

[38] Norased Nasongkla et al. “Multifunctional Polymeric Micelles as Cancer-Targeted, MRI-Ultrasensitive Drug Delivery Systems”. In: *Nano Letters* 6.11 (Nov. 2006), pp. 2427–2430.

[39] Taiho Noh et al. “Block copolymer micelles conjugated with anti-EGFR antibody for targeted delivery of anticancer drug”. In: *Journal of Polymer Science Part A: Polymer Chemistry* 46.22 (Nov. 2008), pp. 7321–7331.

[40] Motoi Oishi et al. “Endosomal release and intracellular delivery of anticancer drugs using pH-sensitive PEGylated nanogels”. In: *Journal of Materials Chemistry* 17.35 (2007), pp. 3720–6.

[41] S M Oversteegen et al. “On the Pressure in Mean-Field Lattice Models”. In: *Langmuir* 15.25 (1999), pp. 8609–8617.

[42] Bart R Postmus, Frans A M Leermakers, and Martien A Cohen Stuart. “Self-Consistent Field Modeling of Adsorption from Polymer/Surfactant Mixtures”. In: *Langmuir* 24.13 (2008), pp. 6712–6720.

[43] Marshall N. Rosenbluth and Arianna W. Rosenbluth. “Monte Carlo Calculation of the Average Extension of Molecular Chains”. In: *The Journal of Chemical Physics* 23.2 (1955), pp. 356–5.

[44] Michael Rubinstein and Ralph H. Colby. *Polymer Physics*. 1st. Oxford: Oxford University Press, 2003. ISBN: 978-0-19-852059-7.

[45] Justin M Saul, Ananth V Annapragada, and Ravi V Bellamkonda. “A dual-ligand approach for enhancing targeting selectivity of therapeutic nanocarriers”. In: *Journal of Controlled Release* 114.3 (2006), pp. 277–287.

[46] S M Scheinhardt-Engels, F A M Leermakers, and G J Fleer. “Lattice mean-field method for stationary polymer diffusion”. In: *Physical Review E* 68.1 (2003), pp. 011802–15.

[47] Julian Schwinger et al. *Classical Electrodynamics*. 1st. Boulder: Westview Press, 1988. ISBN: 0-7382-0056-5.

[48] Martien A Cohen Stuart et al. “Emerging applications of stimuli-responsive polymer materials”. In: *Nature Materials* 9.2 (Jan. 2010), pp. 101–113.

[49] *SUNDIALS*. URL: `https://computation.llnl.gov/casc/sundials/main.html`.

[50] I Szleifer and M A Carignano. “Tethered Polymer Layers”. In: *Advances in Chemical Physics*. Hoboken, NJ, USA: John Wiley & Sons, Inc., Jan. 1996, pp. 165–260.

[51] Igal Szleifer, Eamonn M O’Toole, and Athanassios Z Panagiotopoulos. “Monte Carlo simulation of the collapse-coil transition in homopolymers”. In: *The Journal of Chemical Physics* 97.9 (1992), pp. 6802–8.

[52] M Tagliazucchi, M O de la Cruz, and I Szleifer. “Self-organization of grafted polyelectrolyte layers via the coupling of chemical equilibrium and physical interactions”. In: *Proceedings of the National Academy of Sciences* 107.12 (Mar. 2010), pp. 5300–5305.

[53] Kazuhiro Takara et al. “Size-controlled, dual-ligand modified liposomes that target the tumor vasculature show promise for use in drug-resistant cancer therapy”. In: *Journal of Controlled Release* 162.1 (2012), pp. 225–232.

[54] Ian F. Tannock and Daniela Rotin. “Acid pH in Tumors and Its Potential for Therapeutic Exploitation1”. In: *Cancer Research* 49 (1989), pp. 4373–4384.

[55] B TWAITES et al. “Thermoresponsive polymers as gene delivery vectors: Cell viability, DNA transport and transfection studies”. In: *Journal of Controlled Release* 108.2-3 (2005), pp. 472–483.

[56] Mark J Uline, Yitzhak Rabin, and Igal Szleifer. “Effects of the Salt Concentration on Charge Regulation in Tethered Polyacid Monolayers”. In: *Langmuir* 27.8 (Apr. 2011), pp. 4679–4689.

[57] Yuan Wan et al. “Capture, isolation and release of cancer cells with aptamer-functionalized glass bead array”. In: *Lab on a Chip* 12.22 (2012), pp. 4693–10.

[58] Mark A Ward and Theoni K Georgiou. “Thermoresponsive Polymers for Biomedical Applications”. In: *Polymers* 3.4 (2011), pp. 1215–1242.

[59] Wikipedia. *Restenosis Wikipedia, The Free Encyclopedia*. [Online; accessed 30-March-2016]. 2016. URL: `https://en.wikipedia.org/wiki/Restenosis`.

Appendix A

Calculating the exclude volume parameter

Flory came with a brilliant and simple idea to calculate the excluded volume parameter ν. He computed the repulsive energy in the chain due to the interaction between two neighboring monomers. The repulsive energy per unit volume is giving by:

$$u_{rep} = \frac{1}{2}(1-2\chi)a^d c^2 K_B T$$

Where χ is Flory's interaction parameter, a is Kuhn length, d is an arbitrary dimensionality, and c is the local concentration number of monomers. Flory defined $\nu = (1-2\chi)a^d$. This definition indicates that for a good solvent ν should be positive, for which χ should be less than $\frac{1}{2}$.

Flory used a typical *mean field* approach; he ignored all correlations between monomers. Thus he assumed that the average of the local monomer concentration squared is equal to the average concentration squared [16]. Then he took that to be equivalent to the internal monomer concentration ($c_{int} \cong \frac{N}{R^d}$).

$$\left\langle c^2 \right\rangle \to \langle c \rangle^2 = c_{int}^2$$

Hence, the total repulsive interaction over the total volume R^d is:

$$u_{rep,tot} \cong \nu c_{int}^2 R^d K_B T = \nu \frac{N^2}{R^d} K_B T$$

Also, he includes an elastic energy term:

$$u_{els} \cong \frac{R^2}{Na^2} K_B T$$

Then we can write the total repulsive energy as:

$$\beta U_{rep} = \nu \frac{N^2}{R^d} + \frac{R^2}{Na^2}$$

By taking the minimum of the repulsive energy and neglecting all numerical coefficients, we get:

$$R^{d+2} \cong \nu N^3 a^2$$

and from:

$$R \sim N^{\nu}$$

that gives us:

$$\begin{cases} d+3 \to 3 \\ 1 \to \nu \end{cases}$$

Hence:

$$\nu = \frac{3}{d+2} \tag{A.1}$$

The previous equation gives the expected value for ν one dimensional coordinates, which is 1, and for higher dimensions it gives a very accurate value.

Appendix B

Calculating Flory's interaction parameter

p	p
s	s

For a polymer solution with n_s number of solvent molecules, n_p number of polymers each having a polymerization number N, the total number of molecules in the system $N_{tot} = n_s + Nn_p$. We define the volume fraction for each molecular species as:

$$\phi_p = \frac{Nn_p}{N_{tot}} = \phi$$

$$\phi_s = \frac{n_s}{N_{tot}} = (1 - \phi)$$

The total internal energy in the system is equal the sum of van der Waals interactions between all molecules in the system.

$$U_{int} = U_{pp} + U_{ss} + U_{sp}$$

$$U_{pp} = n_{pp}\varepsilon_{pp}$$

$$U_{ss} = n_{ss}\varepsilon_{ss}$$

$$U_{sp} = n_{sp}\varepsilon_{sp}$$

Where n_{pp}, n_{ss} and n_{sp} is the number of contacts or interactions between the molecular species, and ε_{pp}, ε_{ss} and ε_{sp} are the corresponding interaction energies. Note that

each free molecule should have z number possible interactions accept the monomers that are connected to each other. They should have $(z-2)$ interactions or at $(z-1)$ for the chain-end [9]. Then, from the conservation of number of sites we can write:

$$(z-2)Nn_p = 2n_{pp} + n_{sp} \Rightarrow n_{pp} = \frac{1}{2}\left((z-2)Nn_p - n_{sp}\right)$$

$$\approx \frac{1}{2(zNn_p - n_{sp}}$$

$$zn_s = 2n_{ss} + n_{sp} \Rightarrow n_{ss} = \frac{1}{2}(zn_s - n_{sp})$$

By summing n_{pp} and n_{ss}, we get:

$$U_{pp} = \frac{1}{2}(zNn_p - n_{sp})\varepsilon_{pp} = \frac{z}{2}Nn_p\varepsilon_{pp} - \frac{1}{2}n_{sp}\varepsilon_{pp}$$

$$U_{ss} = \frac{1}{2}(zn_s - n_{sp})\varepsilon_{ss} = \frac{z}{2}n_s\varepsilon_{ss} - \frac{1}{2}n_{sp}\varepsilon_{ss}$$

$$U_{sp} = n_{sp}\varepsilon_{sp}$$

Thus,

$$U_{int} = U_{pp} + U_{ss} + U_{sp}$$

$$U_{int} = \frac{z}{2}Nn_p\varepsilon_{pp} - \frac{1}{2}n_{sp}\varepsilon_{pp} + \frac{z}{2}n_s\varepsilon_{ss} - \frac{1}{2}n_{sp}\varepsilon_{ss} + n_{sp}\varepsilon_{sp}$$

$$U_{int} = \frac{z}{2}Nn_p\varepsilon_{pp} + \frac{z}{2}n_s\varepsilon_{ss} - \frac{1}{2}n_{sp}(\varepsilon_{pp} + \varepsilon_{ss} - 2\varepsilon_{sp})$$

Hence the internal energy per site is given by:

$$\bar{U}_{int} = \frac{z}{2}\phi\varepsilon_{pp} + \frac{z}{2}(1-\phi)\varepsilon_{ss} - \frac{1}{2}\frac{n_{sp}}{N_{tot}}(\varepsilon_{pp} + \varepsilon_{ss}) - \varepsilon_{sp})$$

To get the right χ parameter the following relation should be correct

$$n_{sp} = \frac{zNn_pn_s}{N_{tot}}$$

Then we can write:

$$\bar{U}_{int} = \frac{z}{2}\phi\varepsilon_{pp} + \frac{z}{2}(1-\phi)\varepsilon_{ss} - \frac{z}{2}\phi(1-\phi)(\varepsilon_{pp} + \varepsilon_{ss} - 2\varepsilon_{sp})$$

Where Flory's Chi Parameter is defined as:

$$\chi \equiv \frac{z}{2}\frac{(\varepsilon_{pp} + \varepsilon_{ss} - 2\varepsilon_{sp})}{K_B T} \tag{B.1}$$

Appendix C

Mathematical Relations

A. **Cartesian Coordinate**

For a function f of three-dimensional Cartesian coordinates x, y, and z, we can write the following:

Gradient of function f

$$\nabla f(x,y,z) = \left(\frac{\partial f}{\partial x}\hat{x} + \frac{\partial f}{\partial y}\hat{y} + \frac{\partial f}{\partial z}\hat{z}\right)$$

Where $\hat{x}$, $\hat{y}$ and $\hat{z}$ are unit vectors pointing along the coordinate directions.

Divergence of a vector function f

$$\nabla \cdot f(x,y,z) = \left(\frac{\partial f}{\partial x} + \frac{\partial f}{\partial y} + \frac{\partial f}{\partial z}\right)$$

Laplacian operator

$$\nabla^2 f(x,y,z) = \left(\frac{\partial^2 f}{\partial x^2} + \frac{\partial^2 f}{\partial y^2} + \frac{\partial^2 f}{\partial z^2}\right)$$

Note that in planner homogenous systems the first and the second terms are neglected and we will end up calculating the last term only.

B. **Polar Coordinate**

For a function f of three-dimensional Polar coordinates r, θ, and ϕ, we can write the following:

Gradient of function f

$$\nabla f(r,\theta,\phi) = \left(\frac{\partial f}{\partial r}\hat{r} + \frac{1}{r}\frac{\partial f}{\partial \theta}\hat{\theta} + \frac{1}{r\sin\theta}\frac{\partial f}{\partial \phi}\hat{\phi}\right)$$

Where $\hat{r}$, $\hat{\theta}$ and $\hat{\phi}$ are unit vectors pointing along the coordinate directions.

Divergence of a vector function f

$$\nabla \cdot f(r,\theta,\phi) = \left(\frac{1}{r^2}\frac{\partial}{\partial r}(r^2 f) + \frac{1}{r\sin\theta}\frac{\partial}{\partial\theta}(\sin\theta f) + \frac{1}{r\sin\theta}\frac{\partial f}{\partial\phi}\right)$$

Laplacian operator

$$\nabla^2 f(r,\theta,\phi) = \left(\frac{1}{r^2}\frac{\partial}{\partial r}\left(r^2\frac{\partial f}{\partial r}\right) + \frac{1}{r^2\sin\theta}\frac{\partial}{\partial\theta}\left(\sin\theta\frac{\partial f}{\partial\theta}\right) + \frac{1}{r^2\sin^2\theta}\frac{\partial^2 f}{\partial\phi^2}\right)$$

In the case of studying a spherical homogenous planner system, we take the derivative with respect to the change in the radius direction, r, only.

C. **CylindricalCoordinate**

For a function f of three-dimensional Cylindrical coordinates ρ, ϕ, and z, we can write:

Divergence of a vector function f

$$\nabla \cdot f(\rho,\phi,z) = \left(\frac{1}{\rho}\frac{\partial}{\partial\rho}(\rho f) + \frac{1}{\rho}\frac{\partial f}{\partial\phi} + \frac{\partial f}{\partial z}\right)$$

Laplacian operator

$$\nabla^2 f(\rho,\phi,z) = \left(\frac{1}{\rho}\frac{\partial}{\partial\rho}\left(\rho\frac{\partial f}{\partial\rho}\right) + \frac{1}{\rho^2}\frac{\partial^2 f}{\partial\phi^2} + \frac{\partial^2 f}{\partial z^2}\right)$$

We didn't consider the spherical and the cylindrical coordinate systems in our study, but we may consider it in future work.

Appendix D

Calculating Poisson-Boltzmann equation

A. For a planner surface

Poisson equation:

$$\frac{\partial}{\partial z}\left(\epsilon(z)\frac{\partial}{\partial z}\psi(x,y,z)\right) = -\rho_q(z)$$

$\psi(x,y,z)$: The electric potential at distance z.

$\rho(z)$: Charge density at distance z.

$\epsilon(z)$: Medium permittivity and it is held to be constant given by the bulk value.

Thus we can rewrite the following:

$$\nabla^2\psi(x,y,z) = -\frac{\rho_q(z)}{\epsilon}$$

In Cartesian coordinates we write:

$$\left(\frac{\partial^2}{\partial x^2} + \frac{\partial^2}{\partial y^2} + \frac{\partial^2}{\partial z^2}\right)\psi(x,y,z) = -\frac{\rho_q(z)}{\epsilon}$$

If the electric potential is homogeneous on the x and y dimensions, and changes only at the Z-direction, we can write:

$$\epsilon\left(\frac{\partial^2}{\partial z^2}\psi(z)\right) = -\rho_q(z)$$

Using **Boltzmann** distribution equation we can write the charge density as:

$$\rho_q(z) = \sum_i Z_i e C_i$$

z_i: The charge valance e: The elementary charge C_i: The ion concentration The sum is over all ion species in the system i, which follow Boltzmann distribution. The ions concentrations is given by:

$$C_i(z) = C_\infty e^{-\beta z_i e\psi(z)}$$

C_∞: is the bulk concentration. The resulting Poisson-Boltzmann equation is:

$$\epsilon\frac{\partial^2\psi(z)}{\partial z^2} = -\sum_i Z_i e C_\infty \exp[-\beta Z_i e\psi(z)]$$

$$Z_+ = +Z \qquad Z_- = -Z$$

$$\frac{\partial^2\psi(z)}{\partial z^2} = -\frac{eZC_\infty}{\epsilon}\left(\exp[-\beta Ze\psi(z)] - \exp[-\beta Ze\psi(z)]\right)$$

This equation can be expressed in terms of hyperbolic sine function, $\sinh(x) = \frac{e^x - e^{-x}}{2}$

$$\frac{\partial^2\psi(z)}{\partial z^2} = \frac{2eZC_\infty}{\epsilon}\sinh(\beta Ze\psi(z))$$

For very small potential $\beta Ze\psi(z) \ll 1$, which is our case, $\sinh\beta Ze\psi(z) \approx \beta Ze\psi(z)$

$$\frac{\partial^2\psi(z)}{\partial z^2} = \frac{2eZC_{infty}}{\epsilon}\beta Ze\epsilon(z) = \kappa^2\psi(z)$$

Where, this equation is called Poisson-Boltzmann (PB) or Debye-Huckle equation, and $\kappa^2 = \frac{2\beta e^2 Z^2 C_{infty}}{\epsilon}$, and $\frac{1}{\kappa} = \lambda_D$ is called **Debye** length. The solution for PB equation is as follows:

$$\psi(z) = Ae^{-z/\lambda_D} + Be^{z/\lambda_D}$$

Boundary conditions:

$$\psi(0) = \psi_0 \qquad \psi(\infty) \to 0$$

then,

$$\psi(z) = \psi_0 e^{-z/\lambda_D}$$

To find ψ_0, we do the following:

$$\nabla\psi(z) = -E(z) = -\frac{\sigma_q}{\epsilon}$$

By differentiating $\nabla\psi(z) = -\kappa\psi_0 e^{-\kappa z}$, and using the boundary conditions, we can calculate the constant ψ_0:

$$\psi_0 = \frac{\sigma_q}{\kappa\epsilon} = \frac{\sigma_q}{\epsilon}\lambda_D$$

The Analytical Solution

$$\boxed{\psi(z) = \frac{\sigma_q \lambda_D}{\epsilon}\exp(-\frac{z}{\lambda_D})} \tag{D.1}$$

B. For a spherical surface

Poisson equation:

$$\frac{\partial}{\partial r}\left(\epsilon(r)\frac{\partial}{\partial z}\psi(r,\theta,\phi)\right) = -\rho_q(r)$$

$\psi(r)$: The electric potential at distance r.

$\rho_q(r)$: Charge density at distance r.

$\epsilon(r)$: Medium permittivity and it is held to be constant given by the bulk value.

Thus we can rewrite the following:

$$\nabla^2\psi(r,\theta,\phi) = -\frac{\rho_q(r)}{\epsilon}$$

for spherical coordinates we can write:

$$\left(\frac{1}{r^2}\frac{\partial}{\partial r}r^2\frac{\partial}{\partial r} + \frac{1}{r^2\sin\theta}\frac{\partial}{\partial\theta}\sin\theta\frac{\partial}{\partial\theta} + \frac{1}{r^2\sin^2\theta}\frac{\partial^2}{\partial\phi^2}\right)\psi(r,\theta,\phi) = -\frac{\rho_q(r)}{\epsilon}$$

If the electric potential is homogeneous on the polar and azimuthal angles (θ,ϕ), and changes only at the r-direction, one can write the following:

$$\frac{1}{r}\left(\frac{\partial^2}{\partial r^2}[r\psi(r)]\right) = -\frac{\rho_q(r)}{\epsilon}$$

Using **Boltzmann** distribution equation, we can write the charge density as:

$$\rho_q(r) = \sum_i Z_i e C_i$$

Z_i: The charge valance.

e: The elementary charge.

C_i: The ion concentration.

The sum is over all ion species in the system i, which follow Boltzmann distribution. The ions concentrations is given by:

$$C_i(r) = C_\infty e^{-\beta Z_i e\psi(r)}$$

C_∞: is the bulk concentration.

The resulting Poisson-Boltzmann equation is:

$$\frac{1}{r}\left(\frac{\partial^2}{\partial r^2}[r\psi(r)]\right) = -\frac{1}{\epsilon}\sum_i Z_i e C_\infty e^{-\beta Z_i e\psi(r)}$$

$$Z_+ = +Z \qquad Z_- = -Z$$

$$\frac{\partial^2}{\partial r^2}[r\psi(r)] = -\frac{eZC_\infty}{\epsilon} r\left(\exp[-\beta Ze\psi(r)] - \exp[-\beta Ze\psi(r)]\right)$$

Similar to the planner surface case, this equation can be expressed in terms of hyperbolic sine function.

$$\frac{\partial^2}{\partial r^2}[r\psi(r)] = frac2eZC_\infty\epsilon r\sinh\left(\beta Ze\psi(r)\right])$$

For a very small potential $\beta Ze\psi(r) \ll 1$, we can write:

$$\frac{\partial^2}{\partial r^2}[r\psi(r)] = frac2eZC_\infty\epsilon\beta Ze[r\psi(r)] = \kappa^2[r\psi(r)]$$

where, this equation is called Poisson-Boltzmann (PB) or Debye-Huckle equation, $1/\kappa = \lambda_D$ is **Debye** length.

The solution for PB equation is as follows:

$$r\psi(r) = Ae^{-r/\lambda_D} + Be^{r/\lambda_D}$$

The boundary conditions:

$$\psi(R) = \psi_0 \qquad \psi(\infty) \to 0$$

Then,

$$\psi(r) = \psi_0 \frac{e^{-r/\lambda_D}}{r}$$

To find ψ_0 we use the following relations:

$$\nabla\psi(r) = -E(r)$$

$$E(R) = \frac{1}{4\pi\epsilon}\frac{Q}{R^2}$$

By differentiating the following;

$$\nabla\psi(r) = -\frac{\psi_0}{\lambda_D}\frac{e^{-r/\lambda_D}}{r} - \psi_0\frac{e^{-r/\lambda_D}}{r^2} = -\psi_0\frac{e^{-r/\lambda_D}}{r}\left(\frac{1}{\lambda_D} + \frac{1}{r}\right)$$

Using the boundary conditions, we can calculate the constant ψ_0:

$$\psi_0 = \frac{1}{4\pi\epsilon}\frac{Q}{e^{-R/\lambda_D}}\left(\frac{\lambda_D}{R+\lambda_D} = \frac{Qe^{R/\lambda_D}}{4\pi\epsilon\left(1+\frac{R}{\lambda_D}\right)}\right)$$

The Analytical Solution

$$\boxed{\psi(r) = \frac{Qe^{R/\lambda_D}}{4\pi\epsilon\left(1+\frac{R}{\lambda_D}\right)}\frac{e^{-r/\lambda_D}}{r}} \tag{D.2}$$

Appendix E

Calculating The Volume of Water Molecule (H_2O) and Sodium Chloride Molecule (NaCl)

- The Volume of H_2O Molecule:

  The density of H_2O=1 g/cm^3

  The molar mass of H_2O=18.01528 g/mol

$$\frac{(18.01528\ g/mol)}{N_a} = \frac{(18.01528\ g/mol)}{(6.02 \times 10^{23}\ atom/mol)} = 2.9925 \times 10^{-23}\ g/atom$$

$$(2.9925 \times 10^{-23}\ g/atom) \div 1\ g/cm^3 = 2.9925 \times 10^{-23}\ cm^3/atom$$

$$(2.9925 \times 10^{-23}\ cm^3/atom) \times 10^{21} = 0.029925\ nm^3$$

  Volume of water molecule = 0.029925 nm^3

- The Volume of NaCl Molecule:

  The density of NaCl=2.16 g/cm^3

  The molar mass of NaCl=58.44 g/mol

$$\frac{(58.44\ g/mol)}{N_a} = \frac{(58.44\ g/mol)}{(6.02 \times 10^{23}\ atom/mol)} = 9.7 \times 10^{-23}\ g/atom$$

$$9.7 \times 10^{-23}\ g/atom \div 2.16\ g/cm^3 = 4.49074 \times 10^{-23}\ cm^3/atom$$

$$(4.49074 \times 10^{-23}\ cm^3/atom) \times 10^2 1 = 0.0449074\ nm^3$$

  Volume of (NaCl) salt molecule = 0.0449074 nm^3

- The Volume of NaCl Ions (Na^+Cl-):

  The physiological density of ionized NaCl (Na^+Cl-)=0.1 mol/L

$$0.1\ mol/L \times N_a = 0.1 \frac{mol}{1000\ cm^3} \times \frac{6.02 \times 10^{23}\ atom}{mol} = 0.602 \times 10^{20}\ atom/cm^3$$

$$0.602 \times 10^{20}\ atom/cm^3 \times 10^{-21} \frac{cm^3}{nm^3} = 0.602 \times 10^{-1}\ atom/nm^3$$

  Salt concentration (C_{salt}) = $0.0602\ atom/nm^3$

  The volume fraction of slat ions in the bulk = $C_{salt}(in\ atoms/nm^3)\times$ volume of water molecule

$$\phi_{+,Bulk} = \phi_{-,Bulk} = 0.0602\ atom/(nm^3) \times 0.03\ nm^3 = 0.001806$$

  Thus, the water volume fraction in the bulk, $\phi_{w,Bulk} = 1 - \phi_{+,Bulk} - \phi_{-,Bulk} = 1 - 2(0.001806) = 0.996388$

Appendix F

Supporting Information for The Ligand-Receptor Binding Theory

- The Chemical Interactions in The System:

  1. $\mathrm{B} + \mathrm{H}^+ \rightleftharpoons \mathrm{BH}^+$ with
  $$\begin{cases} \mathrm{K_b} = \frac{[\mathrm{BH+}]}{[\mathrm{B}][\mathrm{H+}]} = \exp(-\beta(\mu^\circ_{\mathrm{BH+}} - \mu^\circ_{\mathrm{B}} - \mu^\circ_{\mathrm{H+}})) \\ or \\ \mathrm{K_a} = \frac{[\mathrm{B}][\mathrm{H+}]}{[\mathrm{BH+}]} = \exp(-\beta(\mu^\circ_{\mathrm{B}} + \mu^\circ_{\mathrm{H+}} - \mu^\circ_{\mathrm{BH+}})) \end{cases}$$
  2. $\mathrm{L} + \mathrm{R} \rightleftharpoons \mathrm{LR}$ with $\mathrm{K_{LR}} = \frac{[\mathrm{LR}]}{[\mathrm{L}][\mathrm{R}]} = \exp(-\beta(\mu^\circ_{\mathrm{LR}} - \mu^\circ_{\mathrm{L}} - \mu^\circ_{\mathrm{R}}))$

- Calculating The Concentrations of Molecules in The System:

  Number of polymer(N_p) = Number of Ligands(N_L) + Number of Spacers(N_S)

  Density of all polymer = $\sigma_p = \frac{N_p}{A}$, where (A) is the area of the system

  Fraction of ligands (X_L) = $\frac{N_L}{N_L+N_S}$

  Fraction of bound ligands (f_{LR}) = $\frac{[LR]}{[LR]+[L]} \Rightarrow [LR] = f_{LR}([LR] + [L])$

  1. $\frac{[L_T]}{A} = X_L\sigma_p$ [1]
  2. $\frac{N_S}{A} = (1 - X_L)\sigma_p$
  3. $[L_T] = [L_u] + [LR] \Rightarrow [L_u] = [L_T] - [LR]$
     $\frac{[L_u]}{A} = X_L\sigma_p - X_L\sigma_p f_{LR} = X_L\sigma_p(1 - f_{LR})$
  4. $[R_T] = [R_u] + [LR] \Rightarrow [R_u] = [R_T] - [LR]$

     Using the fraction o bound ligands equation, we can write:

[1] Notice that $(_T)$ refers to total ans $(_u)$ to un-bound molecules

$[LR](1-f_{LR}) = f_{LR}[L] \Rightarrow [LR] = \frac{f_{LR}[L]}{(1-f_{LR})}$

Thus, $\frac{[R_u]}{A} = \sigma_R - \frac{f_{LR}X_L\sigma_p(1-f_{LR})}{(1-f_{LR})}$

$\frac{[R_u]}{A} = \sigma_R - f_{LR}X_L\sigma_p$

- Converting a Continuous System into 1D Cubic Lattice System:

$$\langle\phi(z)\rangle = \frac{N_p}{A}\sum_\alpha P(\alpha)\delta_z(z - z_p(\alpha))v_p$$

$$\int\langle\phi(z)\rangle dz = \sum_i\langle\phi(i)\rangle\Delta_z$$

$$\frac{N_p}{A}\int\sum_\alpha P(\alpha)\delta_z(z - z_p(\alpha))v_p dz = \frac{N_p}{A}\sum_i\sum_\alpha P(\alpha)n_p(\alpha,i)v_p\Delta_z$$

$$\sum_i\langle\phi(i)\langle\Delta_z = \frac{N_p}{A}\sum_i\sum_\alpha P(\alpha)n_p(\alpha,i)v_p\Delta_z$$

$$\text{Then, } \langle\phi(i)\rangle = \frac{N_p}{A}\sum_\alpha P(\alpha)n_p(\alpha,i)v_p$$

- Calculating The Probabilities:

  We add the incompressibility constraint of the system that is multiplied by the Lagrange multipliers (π) to the semi-grand canonical ensemble free energy equation and set that to be equal to zero. Then, we take the derivative of the free energy with respect to the probability. Below we calculate the probability for the mono-ligand system:

$$\frac{\partial}{\partial P_S(\alpha)}\Bigg(\Omega + \beta\sum_i\pi(i)\Bigg[\Big(\langle\rho_s(i)\rangle + \langle\rho_L(i)\rangle + \langle\rho_{LR}(i)\rangle\Big)v_s + \rho_w(i)v_s$$
$$+ \rho_{H^+}(i)v_s + \rho_{OH^-}(i)v_s + \rho_+(i)v_s + \rho_-(i)v_s + \rho_R v_s - 1\Bigg]\Bigg) = 0$$

  where, $\rho_R = (\sigma_R - \sigma_p X_L f_{LR})n_R$

$$\frac{\partial}{\partial P_S(\alpha)}\Bigg(-\Bigg[\sum_\alpha\sigma_p(1-X_L)P_S(\alpha)\varepsilon_{intra}\sum_{n=1}^{N_m}\sum_{m=n+3}^{N_m}\delta(r)$$
$$+ \frac{\varepsilon_{inter}}{2}\sum_i(\langle\phi_s(i)\rangle\sigma_p(1-X_L)P_S(\alpha)\eta_s(\alpha,i))$$
$$+ (\langle\eta_s(i)\rangle\sigma_p(1-X_L)P_S(\alpha)v_S(\alpha,i))\Bigg] + \sigma_p(1-X_L)\sum_\alpha P_S(\alpha)\ln P_S(\alpha)\Bigg)$$
$$+ \beta\frac{\partial}{\partial P_S(\alpha)}\sum_i\pi(i)\sigma_p(1-X_L)\sum_\alpha P_S(\alpha)v_S(\alpha,i) = 0$$

$$-\beta\Bigg[\sum_{\alpha}\sigma_p(1-X_L)\varepsilon_{intra}\sum_{n=1}^{N_m}\sum_{m=n+3}^{N_m}\delta(r)$$
$$+\frac{\varepsilon_{inter}}{2}\sum_i(\langle\phi_s(i)\rangle\sum_p(1-X_L)\eta_s(\alpha,i))+(\langle\eta_s(i)\rangle\sum_p(1-X_L)v_s(\alpha,i))\Bigg]$$
$$+\sigma_p(1-X_L)\ln P_S(\alpha)+\beta\sum_i\pi(i)\sum_p(1-X_L)\sum_\alpha v_s(\alpha,i)=0$$

Notice that $\sum_\alpha dP_S(\alpha)=0$. Dividing by $\sigma_p(1-X_L)$ gives us the following:

$$\sum_\alpha\ln P_S(\alpha)=-\beta\Bigg[\sum_\alpha\varepsilon_{intra}\sum_{n=1}^{N_m}\sum_{m=n+3}^{N_m}\delta(r)+\frac{\varepsilon_{inter}}{2}\sum_i\Bigg(\langle\phi_s(i)\rangle\eta_s(\alpha,i)\Bigg)$$
$$+\Bigg(\langle\eta_s(i)\rangle v_s(\alpha,i)\Bigg)\Bigg]-\beta\sum_i\pi(i)v_s(\alpha,i)$$

Thus,

$$P_S(\alpha)=\frac{1}{q_S}\exp\Bigg(-\beta\Bigg[\sum_\alpha\varepsilon_{intra}\sum_{n=1}^{N_m}\sum_{m=n+3}^{N_m}\delta(r)$$
$$+\frac{\varepsilon_{inter}}{2}\sum_i\Bigg(\langle\phi_s(i)\rangle\eta_s(\alpha,i)+\langle\eta_s(i)\rangle v_s(\alpha,i)\Bigg)\Bigg]-\beta\sum_i\pi(i)v_s(\alpha,i)\Bigg)$$

where,

$$q_S=\sum_\alpha\exp\Bigg(-\beta\Bigg[\sum_\alpha\varepsilon_{intra}\sum_{n=1]^{[N_m}}^{N_m}\sum_{m=n+3}^{N_m}\delta(r)$$
$$+\frac{\varepsilon_{inter}}{2}\sum_i\Bigg(\langle\phi_s(i)\rangle\eta_s(\alpha,i)+\langle\eta_s(i)\rangle v_s(\alpha,i)\Bigg)\Bigg]-\beta\sum_i\pi(i)v_s(\alpha,i)\Bigg)$$

Similarly, we calculate the probability of having a ligand complex.

$$P_L(\alpha)=\frac{1}{q_L}\exp\Bigg(-\beta\Bigg[\sum_\alpha\varepsilon_{intra}\sum_{n=1}^{N_m}\sum_{m=n+3}^{N_m}\delta(r)$$
$$+\frac{\varepsilon_{inter}}{2}\sum_i\Bigg(\langle\phi_L(i)\rangle\eta_L(\alpha,i)+\langle\eta_L(i)\rangle v_L(\alpha,i)\Bigg)\Bigg]$$
$$-\beta\sum_i f_{H^+}(i)q_p n_L(\alpha,i)\psi(i)-\sum_i n_L(\alpha,i)$$
$$\Bigg\{f_{H^+}(i)[\ln f_{H^+}(i)+\beta\mu^0_{BH^+}]+(1-f_{H^+}(i))[\ln(1-f_{H^+}(i))+\beta\mu^0_B]\Bigg\}$$
$$-\beta\sum_i\pi(i)v_L(\alpha,i)\Bigg)$$

We minimize the free energy with respect to the fraction of charge to get the following relation:

$$\beta \sum_i q_p \psi(i) + \sum_i \left\{ [\ln f_{H^+}(i) + \beta \mu^0_{BH^+}] - [\ln(1 - f_{H^+}(i)) + \beta \mu^0_B] \right\} = 0$$

We use the previous relation to get the simplified form of the ligand complex probability equation (see Equation 4.15).